DEVELOPMENT AND VALIDATION OF IMPROVED LIVE LOAD DISTRIBUTION FACTORS FOR MOMENT IN PRESS-BRAKE-FORMED STEEL TUB GIRDER BRIDGES

Karl Barth, Ph.D.
Gregory Michaelson, Ph.D.
Brook Teklu Woldegabriel

Volume VIII: **DEVELOPMENT AND VALIDATION OF LIVE LOAD DISTRIBUTION FACTORS FOR MOMENT IN PRESS-BRAKE-FORMED STEEL TUB GIRDER BRIDGES**

Submitted to the AISI Steel Market
Development Institute Short Span
Steel Bridge Alliance

ABSTRACT

DEVELOPMENT AND VALIDATION OF LIVE LOAD DISTRIBUTION FACTORS FOR MOMENT IN PRESS-BRAKE-FORMED STEEL TUB GIRDER BRIDGES

Press-brake-formed tub girders (PBFTGs) offer innovative solutions for short-span steel bridge applications, possessing efficiency, versatility, and sustainability. These girders are galvanized shallow trapezoidal boxes fabricated from cold-bent structural steel plates. Depending on the design requirements, a concrete deck or other deck options, such as a steel sandwich plate system, can be placed on the girders. The Short Span Steel Bridge Alliance (SSSBA) extensively researched the steel PBFTG bridge system. As a testament to its potential, the AASHTO Innovation Initiative (AII) recognized it as a 2021 Focus Technology. AII has shown commitment to promoting the adoption of PBFTG among its member associations, local agencies, and industry partners, aiming to enhance the U.S. infrastructure. Given the growing recognition and support from industry leaders and organizations, PBFTGs are poised to be crucial in addressing the U.S. infrastructure challenges.

This project aims to improve the design and analysis of PBFTGs regarding live load distribution factor (LLDF) prediction. Field testing performed on PBFTG bridges showed that the empirical equations found in the American Association of State Highway and Transportation Officials' Load and Resistance Factor Design Bridge Design Specifications (AASHTO LRFD BDS) are conservative when used for PBFTG bridges. Hence, there is a potential for improving and refining the AASHTO LRFD BDS provisions related to PBFTGs and their LLDFs. The live load distribution behavior of a matrix of 207,696 PBFTG bridges with varied parameters was analyzed using three-dimensional finite element analysis. From the analysis result, statistical models were employed to produce simplified and enhanced empirical equations that can better predict live load moment distribution in PBFTGs. The prediction power and accuracy of the simplified equations were assessed using a comprehensive statistical analysis. In addition, the impact of the improved LLDF predictions was examined by using design feasibility and applicability to commercially available shallow steel tub girder bridges, contrasting the AASHTO LRFD BDS's empirical formulas against the newly proposed ones.

This study demonstrated that the developed equations significantly improve the prediction of live load distribution of PBFTGs from a statistical perspective. Hence, they are recommended for adoption in AASHTO LRFD BDS. Integrating these proposed equations can substantially streamline the design process for shallow steel tub girder bridges, broadening their applicability.

TABLE OF CONTENTS

LIST OF TABLES

LIST OF FIGURES

CHAPTER 1: INTRODUCTION

1.1 BACKGROUND AND OVERVIEW

Press-brake-formed tub girders (PBFTGs) offer innovative solutions for short-span steel bridge applications, combining efficiency, versatility, and sustainability. These girders are galvanized shallow trapezoidal boxes fabricated from cold-bent structural steel plates. Depending on specific design requirements, various deck options, such as concrete or steel sandwich plate systems, can be integrated with these girders. The Short Span Steel Bridge Alliance (SSSBA) has extensively researched the steel PBFTG bridge system.

Figure 1.1 Valmont's UBEAM™ PBFTG Bridge being constructed in Lancaster County, Nebraska

Recognizing its groundbreaking potential, the AASHTO Innovation Initiative (AII) acknowledged it as a 2021 Focus Technology. The AII, demonstrating its dedication to infrastructure advancement, actively promotes the adoption of PBFTG among its member associations, local agencies, and industry affiliates. With increasing endorsements from leading industry figures and organizations, PBFTGs are set to play a pivotal role in addressing the challenges faced by the U.S. infrastructure. As the development and applicability of PBFTGs are

expanding, the governing specifications for capacity and analysis for this type of bridge in the American Association of State Highway and Transportation Officials Load and Resistance Factor Design Bridge Design Specifications (AASHTO LRFD BDS) are limited, with many specifications relating to large, long-span welded box girders applying to PBFTGs.

1.2 Project Scope and Objectives

The primary objective of this study is to refine the design and analysis methods associated with PBFTGs, focusing on the prediction of the live load distribution factor (LLDF). Through field tests on PBFTG bridges, it has been observed that the empirical equations provided by the AASHTO LRFD BDS lean towards being conservative for this type of bridge. Hence, a window of opportunity exists for refining the AASHTO LRFD BDS provisions on PBFTGs and their LLDFs.

This objective is achieved through three-dimensional finite element analysis by studying the live load distribution behavior of an extensive matrix of 205,128 PBFTG bridges with varied design parameters. The extensive data from this analysis warrants a facilitated use of advanced statistical models to formulate more straightforward and precise empirical equations predicting live load moment distribution in PBFTGs. A comprehensive statistical assessment is subsequently used to validate the equations' accuracy and predictive strength. A side-by-side comparison is also performed, contrasting the empirical formulas of AASHTO LRFD BDS against the new proposals, emphasizing their design feasibility and relevance to commercially available shallow steel tub girder bridges.

1.3 Organization

The organization of this project is as follows:

Chapter 2

- This chapter presents a literature review on the development and evaluation of PBFTGs and the current live load distribution factors found in the AASHTO LRFD BDS.

Chapter 3

- This chapter presents a summarized review of the AASHTO LRFD BDS related to the design and analysis of PBFTG bridges.

Chapter 4

- This chapter presents the analytical modeling techniques, load applications, and verification of models against field tests.

Chapter 5

- This chapter presents the development and statistical assessment of LLDFs for the moment in the interior girder of PBFTG bridges.

Chapter 6

- This chapter presents the development and statistical assessment of LLDFs for the moment in the exterior girder of PBFTG bridges and skewed PBFTG bridges.

Chapter 7

- This chapter presents the comparison of the proposed equations to the current AASHTO LRFD BDS equation and the validity assessment of the proposed LLDF equations to commercially available PBFTGs. It also discusses expanding the applicability of PBFTGs through extension of the span length.

Chapter 8

- This chapter presents a summary of the project and recommendations for future work and continued research.

CHAPTER 2: LITERATURE REVIEW

2.1 INTRODUCTION

Bridge engineering has witnessed significant advancements in recent years, simplifying the design and analysis of numerous types of bridges for Accelerated Bridge Construction (ABC). While PBFTGs have emerged as a promising solution for short-span steel bridge applications, the distribution of live loads remains a critical study area. Historically, the primary focus of research on LLDFs has been centered on straight beam slab bridges. However, with the changing dynamics of bridge construction and the introduction of innovative bridge systems, there is a shift in this focus.

This chapter provides a comprehensive literature review of research conducted on PBFTGs and load distribution to bridge the gap between historical knowledge and current practices. The influence of various parameters on lateral load distribution is discussed, offering insights into the processes of developing LLDFs. The adoption of the Load and Resistance Factor Design by AASHTO in 1994 marked a significant milestone in this regard. This adoption changed the computation of load distribution and highlighted the need for continuous research and adaptation of these specifications.

2.2 DEVELOPMENT AND EVALUATION OF PRESS-BRAKE-FORMED TUB GIRDERS

2.2.1 Development and Feasibility Assessment of Shallow Press-Brake-Formed Steel Tub Girders for Short-Span Bridge Applications

Michaelson (2014) developed the first comprehensive behavioral study and analysis of a modular design for PBFTGs with the SSSBA, as illustrated in Figure 1.1. This design replaced traditional concrete box beams in short-span bridges, accommodating lengths up to 90 feet. This technology involves cold-bending standard mill plate widths and thicknesses to fabricate a trapezoidal box girder. The steel plate used can either be economical weathering steel or galvanized steel. After the press-brake forming process, shear studs are welded onto the top flanges. Subsequently, a reinforced concrete deck is cast onto the girder within the fabrication shop and left to cure, transforming it into a composite modular unit. This composite tub girder is transported to the bridge construction site, facilitating accelerated construction and minimizing

traffic disruptions. Importantly, this proposed system is versatile and can accommodate various deck options, including cast-in-place decks and full-depth and partial-depth precast panels.

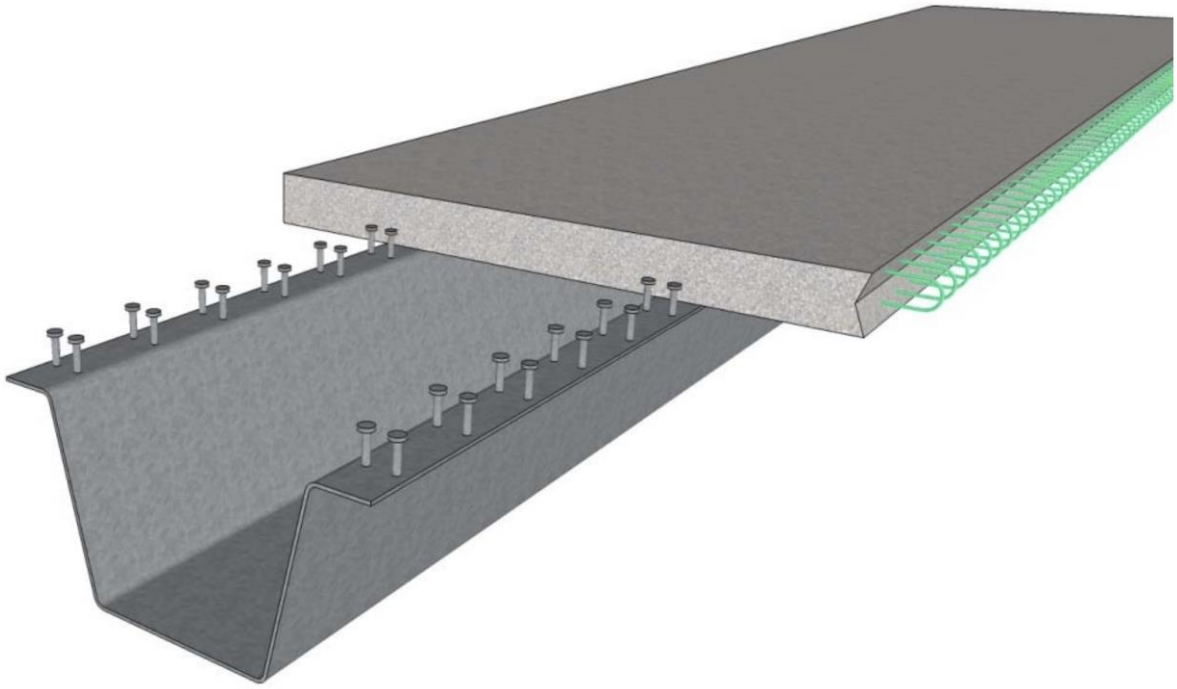

Figure 2.1 Proposed modular PBFTGs system (Michaelson, 2014)

The design methodology behind the press-brake steel tub girder system, specifically produced for short-span bridges, emerged from a rigorous process of iterative designs employing standard mill plates. Commercially available plate thicknesses and widths were examined, with certain design constants such as a 1:4 web slope and specific bend radii maintained for consistency. A tool was then developed to determine section properties for multiple tub girder configurations and plate sizes. Following this, a parametric study of design iterations was performed to determine the optimal depth for each plate, ensuring efficient design. Figure 2.1 shows a sample from the parametric study. For the 120-inch plate size, the optimal depth was approximately 34 inches. Each girder's noncomposite and composite section properties were also computed as part of the parametric study.

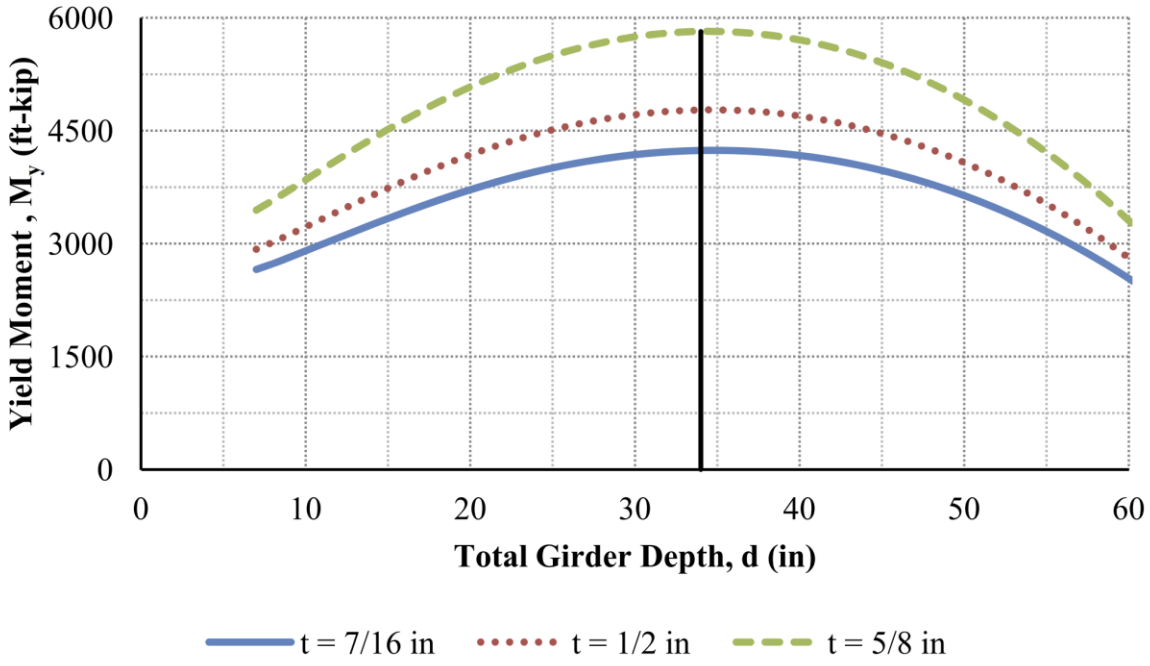

Figure 2.2 120" Wide standard mill plate design comparisons (Michaelson, 2014)

After the determination of the optimal configuration for the PBFTG, Michaelson performed a physical testing of both composite and non-composite PBFTGs. All tested girders shared identical dimensions, which were formed from an 84-inch wide, 7/16-inch thick, and 35-foot long plate. This specific plate was selected because it was the largest testing equipment an MTS 330-kip servo-hydraulic actuator could handle. Each girder underwent three-point bending tests. Composite modules failed at around 300 kips, resulting in concrete deck damage and loss of composite action, as depicted in Figure 2.3. The data obtained from these experiments was used to validate finite element analytical studies performed on this system. A three-dimensional nonlinear finite element model was generated to analyze the behavior of both composite and non-composite PBFTGs. The model accurately depicted the composite system's behavior up to its breaking point. This study also evaluated the suitability of the AASHTO LRFD BDS for the system.

The 3D nonlinear finite element modeling procedure aimed to capture the behavior and ultimate capacity of both noncomposite and composite press-brake tub girders. This modeling procedure employs the commercial finite element software package Abaqus/CAE, which provides

a comprehensive library of elements tailored for three-dimensional stress analysis. The S4R shell elements were identified as highly accurate for modeling the behavior of both noncomposite and composite steel plate girders. These elements are designed to offer robust solutions for both thin and thick shells, adapting to classical (Kirchhoff) shell theory for thinner shells and thick (Mindlin) shell theory as shell thickness increases. The elements account for finite membrane strains, rotations, and changes in shell thickness, making them suitable for large-strain analyses involving inelastic material deformation. The material modeling segment delves deep into the characteristics of both structural steel and reinforced concrete. Steel was modeled using an elastic-plastic constitutive law, capturing strain-hardening effects. In contrast, the reinforced concrete was represented using a smeared crack model, which does not track individual macro cracks but calculates the stress and material stiffness at each integration point. The modeling techniques were then verified against experimental data from previous laboratory experiments, showcasing their efficiency in capturing nonlinear behavior, as shown in Figure 2.3.

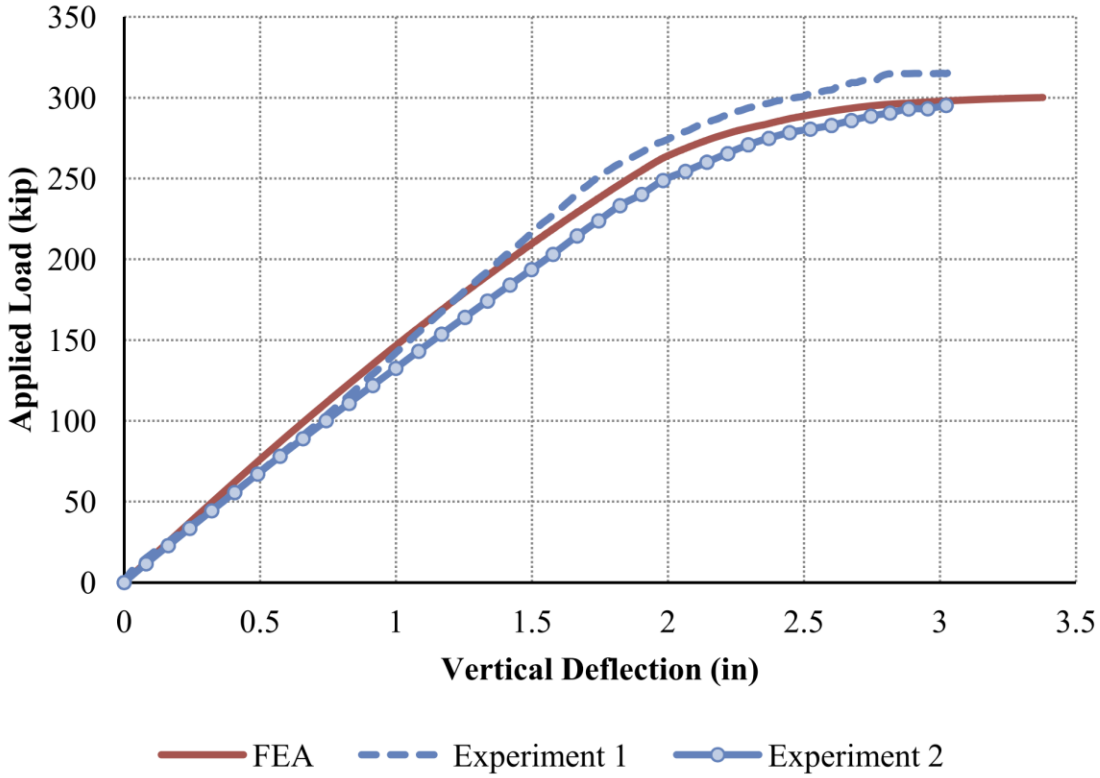

Figure 2.3 Comparison of experimental and analytical results for the composite tests (Michaelson, 2014)

After the behavioral studies, Michaelson evaluated the system's potential in the short-span bridge sector. An initial feasibility study was conducted to ascertain the maximum span length for each plate dimension, considering both the Strength I and Service II limit states and live load deflection. After examining various plate dimensions, three plate sizes were deemed suitable for widespread application. The most extensive system proposed utilized a 120-inch wide by 5/8-inch thick plate, suitable for spans up to 80 feet.

2.2.2 Experimental Evaluation of Noncomposite Shallow Press-Brake-Formed Steel Tub Girders

Kelly (2014) performed a comprehensive examination of the structural behavior of noncomposite PBFTGs, with a particular emphasis on their stability and torsional behavior. The research was on experimental tests carried out on two full-scale PBFTG specimens, as shown in Figure 2.4. To emulate real-world bridge conditions, the girders underwent three-point bending

tests. As part of the methodology, parameters such as deflection, strain, and rotations were recorded using a combination of precision level, strain gauges, and linear variable differential transformers (LVDTs). For this study, the system consisting of a cast-in-place deck was explored as opposed to a pre-cast concrete deck Michaelson (2014) proposed. The critical stage of the cast-in-place deck is during construction since the noncomposite section must resist the construction loads. The initial experiment displayed a linear load deflection curve reaching about 94 kips, equating to a 2.25-inch midspan vertical deflection. This led to an abrupt failure from lateral torsional buckling. A subsequent test on a galvanized sample showed resemblances to the first but ended earlier at roughly 33 kips because of excessive lateral deflections. This reduced capacity was linked to initial imperfections and their second-order effects.

Figure 2.4 Noncomposite test specimen setup (Kelly 2014)

To validate the experimental findings, Kelly employed a Finite Element Analysis (FEA) process. This technique was crucial in predicting the structural behavior of the PBFTGs under different load conditions. The FEA models were meticulously calibrated based on the physical properties and dimensions of the tested specimens. By simulating the same three-point bending

tests in the virtual environment, the researchers could closely study stress distribution, deformation patterns, and potential buckling zones in the girders. Comparisons between the experimental results and the FEA predictions revealed a high degree of correlation, affirming the accuracy of the modeling process. This similarity not only substantiated the validity of the experimental results but also highlighted the potential of FEA as a reliable tool for predicting the performance of PBFTGs in practical applications.

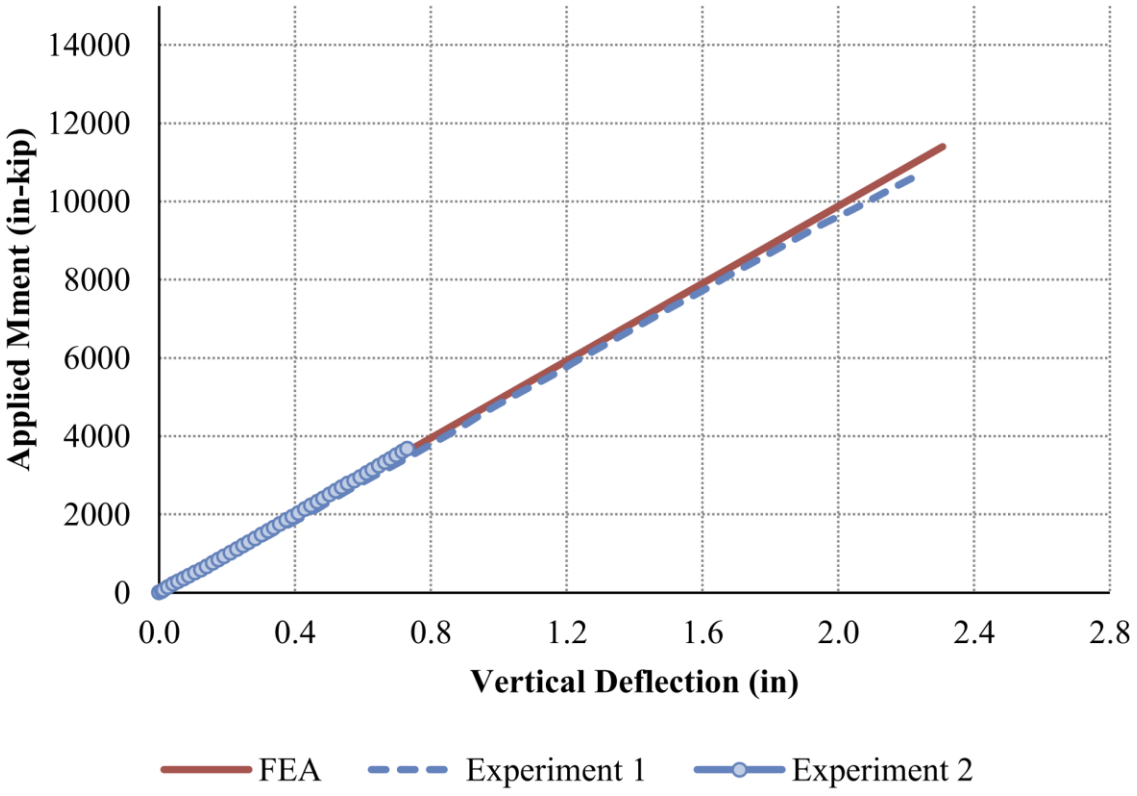

Figure 2.5 Mid-span moment comparison (Kelly, 2014)

2.2.3 Field Performance of Press-Brake-Formed Tub Girder Superstructures

Gibbs (2017) investigated the first on-field performance of a bridge constructed using PBFTGs. The subject of this study, the Amish Sawmill Bridge located in Buchanan County, Iowa (illustrated in Figure 2.6), consists of a design featuring four galvanized tub girders, each formed from a 96-inch wide by 1/2-inch thick plate. Th study's primary objective was to evaluate and validate live load field test results, with analysis from finite element modeling to understand the

live load distribution mechanism. The author instrumented the bridge with strain gauges to measure stresses. For the live load field test, Bridge Diagnostics, Inc.'s strain gauges were positioned on the bottom flange of each tub girder. Ensuring redundancy and accuracy, three gages were placed on each girder stationed at midspan.

Figure 2.6 Amish Sawmill bridge (Gibbs, 2017)

The axle weights and positioning of the loading vehicle were recorded, facilitating their subsequent replication in the FEA. The bridge's symmetric, non-skewed design streamlined the testing process, necessitating only five truck runs, as shown in Figure 2.7. These runs were strategically mapped out to maximize load placements on both interior and exterior girders under various scenarios. The LLDFs were derived by normalizing the strain in a specific girder against the cumulative strain across all girders – dividing the strain in the girder in question by the sum of strain in all girders. For multi-lane scenarios, strain values from two truck runs were superimposed to produce the LLDFs.

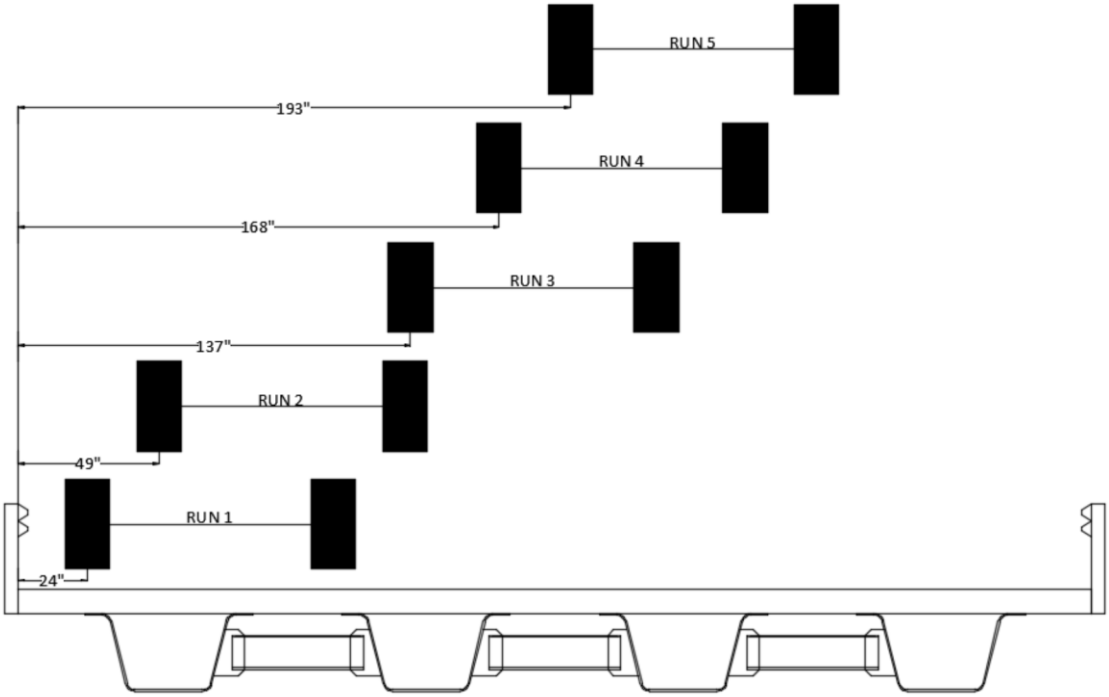

Figure 2.7 Live load truck placements for the Amish Sawmill bridge (Gibbs, 2017)

Although the analytical and experimental values agreed exceptionally, the bottom flange strains computed from FEA marginally surpassed those from on-site tests, as shown in Figure 2.9 below. This variance was attributed to the unique boundary conditions of the Amish Sawmill Bridge. Unlike traditional 'hinge-roller' supports, this bridge employed integral abutments, encasing each girder's ends in concrete, inducing stiffer support. However, the finite element model abstained from integrating these integral abutments due to the complexities and ambiguities associated with their modeling. A screenshot of the Abaqus strain distribution is provided in Figure 2.8. Further analytical exploration led to a comparative analysis of the derived LLDFs against those stipulated by the AASHTO LRFD BDS.

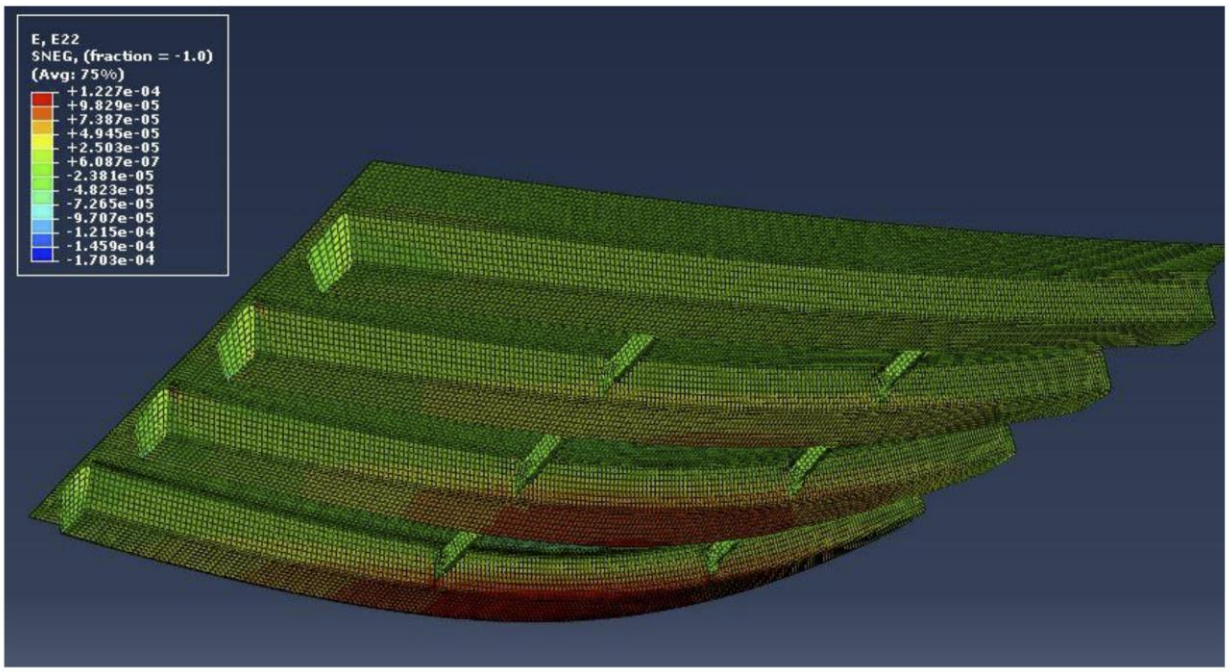

Figure 2.8 Deflected shape of Abaqus model - truck run 2, panel point 5 (Gibbs, 2017)

Figure 2.9 illustrates the comparison between analytical and experimental LLDFs while contrasting the significantly overestimated LLDFs obtained from the AASHTO LRFD BDS for single-lane scenarios. When it came to two-lane scenarios, while the analytical and experimental LLDFs still exhibited minor deviations from the AASHTO guidelines, they were less pronounced. Gibbs' exhaustive research underscored the consistent and reliable performance of PBFTGs. It also theorized that while the AASHTO LRFD BDS's LLDFs offer a conservative approach, there is room for refinement. Gibbs suggested the pursuit of further research, aiming to fine-tune the AASHTO LRFD BDS equations better to mirror the actual load distribution dynamics of PBFTGs.

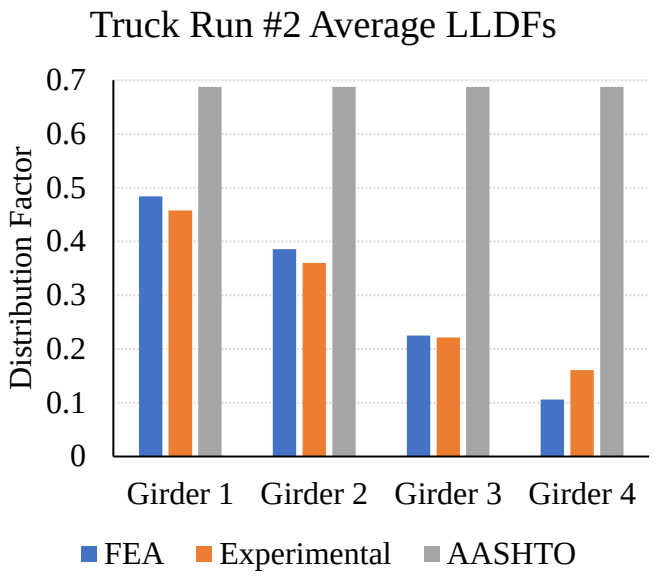

Figure 2.9 FEA vs. Experimental vs. AASHTO LLDFs for truck run 2 (Gibbs, 2017)

2.2.4 Field Evaluation of a Modular Press-Brake-Formed Steel Tub Girder in an Application that Includes Skew and Superelevation

Roh focused on the design, construction, and evaluation of the Fourteen Mile Bridge in Lincoln County, West Virginia, as shown in Figure 2.10. The 58-foot single-span bridge, carrying traffic over the Fourteen Mile Creek on State Route Number 37, incorporates a unique design with a skew angle of 10° and a superelevation of 8%. The bridge consisted of five modular composite units of PBFTGs that were pre-assembled offsite. These units, formed from 96-inch wide, 1/2-inch thick AASHTO M270 steel plates, were fabricated, incorporating shear studs, end-bearing diaphragms, and mounting angles for internal formwork. Galvanized for corrosion resistance, the units underwent subsequent procedures, including internal and external formwork creation, rebar placement, and concrete casting in a controlled environment.

The methodology employed for the bridge's construction highlighted ABC strategies, aiming to streamline the process and enhance the quality. By leveraging offsite fabrication, the research emphasized the benefits of a controlled environment, from consistent concrete application to optimized curing conditions, ensuring structural integrity. On-site, the precast modular units were lifted directly from transport trucks onto the bridge's abutments, eliminating the need for

additional staging yards. The utilization of ultra-high-performance concrete (UHPC) for closure pours further bolstered the bridge's resilience due to its superior compressive strength and rapid curing. No further exterior or interior bracing was required due to the high torsional stiffness of the composite PBFTG modules.

Figure 2.10 Placement of first composite module on-site (Roh, 2020)

The BDI STS Wi-Fi Data Acquisition System was central to the testing procedure, which facilitated the bridge's instrumentation and data recording. The bridge was instrumented with nineteen ed strain gauges, ensuring a comprehensive coverage of potential strain regions. Then, the bridge was delineated with a grid of panel points to guide the truck placements during the live load testing, ensuring strain was maximized on specific girders. Figure 2.11 shows the truck placement.

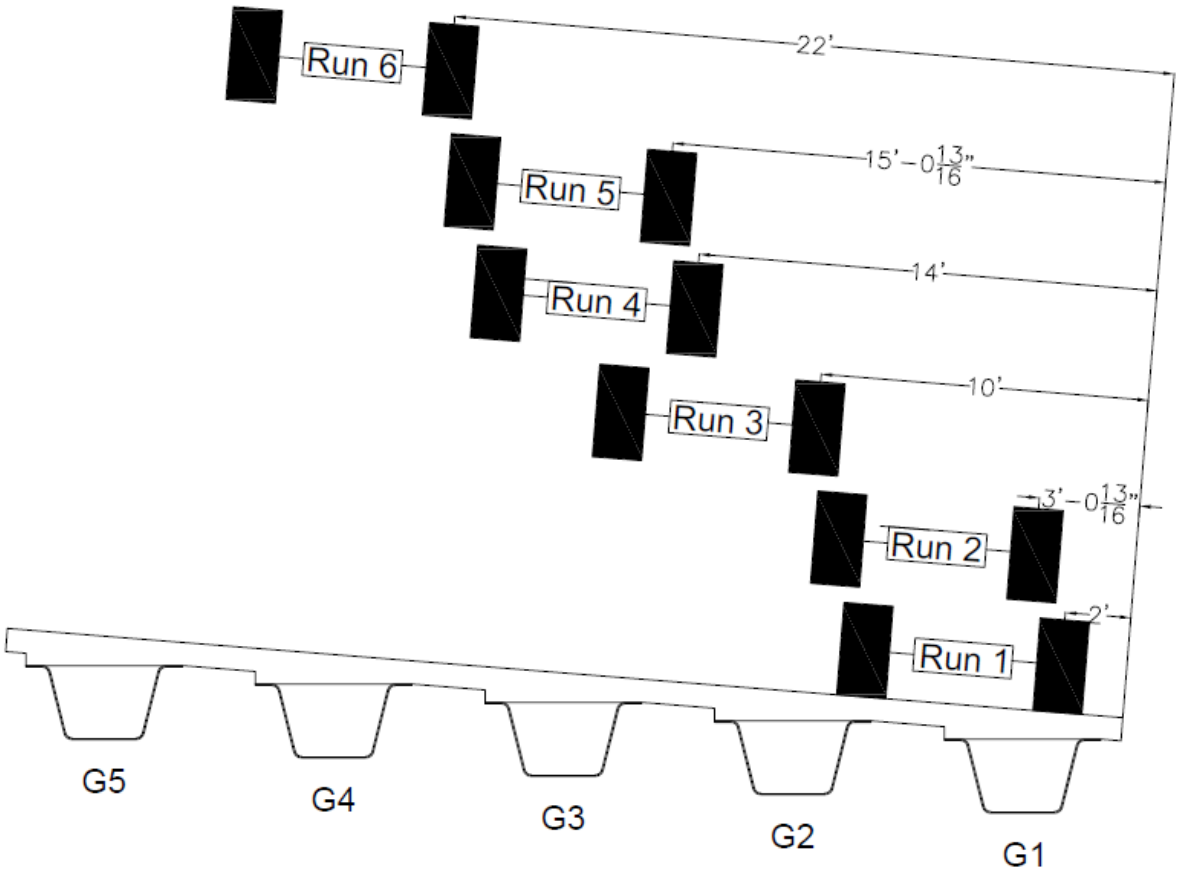

Figure 2.11 Live load truck placement (Roh, 2019)

For live load field testing, a tandem axle truck resembling the HS-20 design load truck from the AASHTO LRFD BDS was employed. The truck's location across the bridge was systematically orchestrated, ensuring it aligned perfectly with the marked grid, maximizing strain on targeted girders. As the truck traversed the bridge, the BDI Software recorded strain values at a sample rate of 10 Hz, with data captured both before loading and after the bridge returned to a static condition post-loading. The weight of each wheel of the truck was also documented along with the axle geometries. This on-site testing, combined with the analytical data, provided invaluable insights into the bridge's performance under live loading conditions.

The readings from the three strain gauges on each bottom flange were averaged, compensating for the torsion that arose during the field tests. Such an approach ensured that the data extracted was representative of the overall strain experienced by the bridge's girders. These averaged strains were then used in conjunction with multiple presence factors to compute LLDFs

in the same way as Gibbs (2017). The truck's position at midspan was specifically chosen for this evaluation, given its maximum impact on the girders. To provide a comparative analysis, the field test results were contrasted against readings derived from finite element models and the standards set by AASHTO LRFD BDS, as shown in Figure 2.12. The analytical modeling results closely mirrored the outcomes of the field tests, reinforcing the precision of both methodologies.

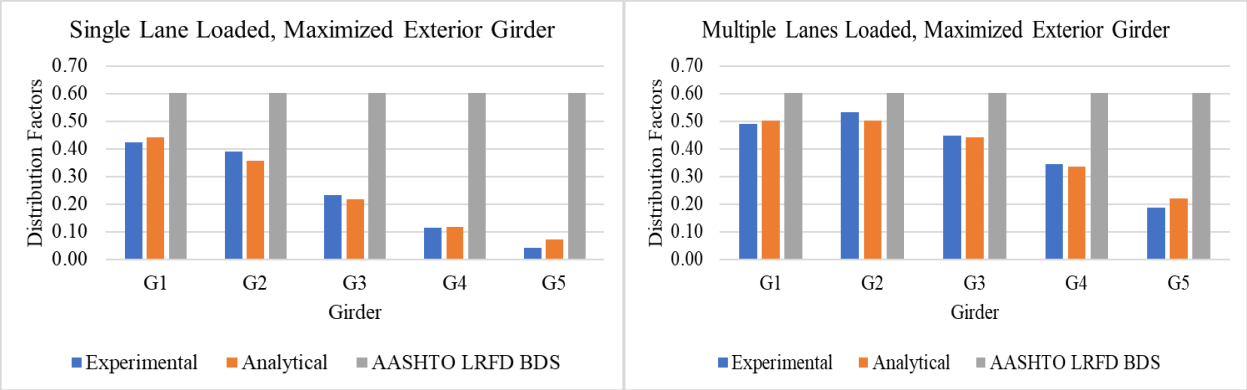

Figure 2.12 Comparison of analytical, experimental, and AASHTO results (Roh, 2020)

In the same case as Gibbs (2017), while the experimental and finite element model outcomes were largely in alignment, the AASHTO LRFD BDS standards were found to be more conservative. Specifically, the AASHTO equations predicted notably higher distribution factors, especially for the single-lane loaded condition. Even though the AASHTO standards were found to be more conservative, it was evident in this study that the performance of PBFTGs remains a safe and reliable solution.

2.3 Development and Assessment of Live Load Distribution Factors

2.3.1 Lateral Distribution of Load in Composite Box Girder Bridges

The LLDF provision available for multiple box sections is based on the studies by Johnston and Mattock (1967). The researchers calculated LLDFs on simple, straight-box girder bridges. A computer program was developed utilizing folded plate theory to analyze a matrix of 24 composite welded steel box girder bridges with span lengths ranging from 50 ft to 150 ft. The program was utilized to study the lateral distribution of load in simple span composite box girder bridges that do not have transverse diaphragms or internal stiffeners. The accuracy of the analysis was confirmed through tests of a quarter-scale model of a two-lane, 80-ft span bridge supported by three box girders. Figure 2.13 shows the bridge and girder cross-sections.

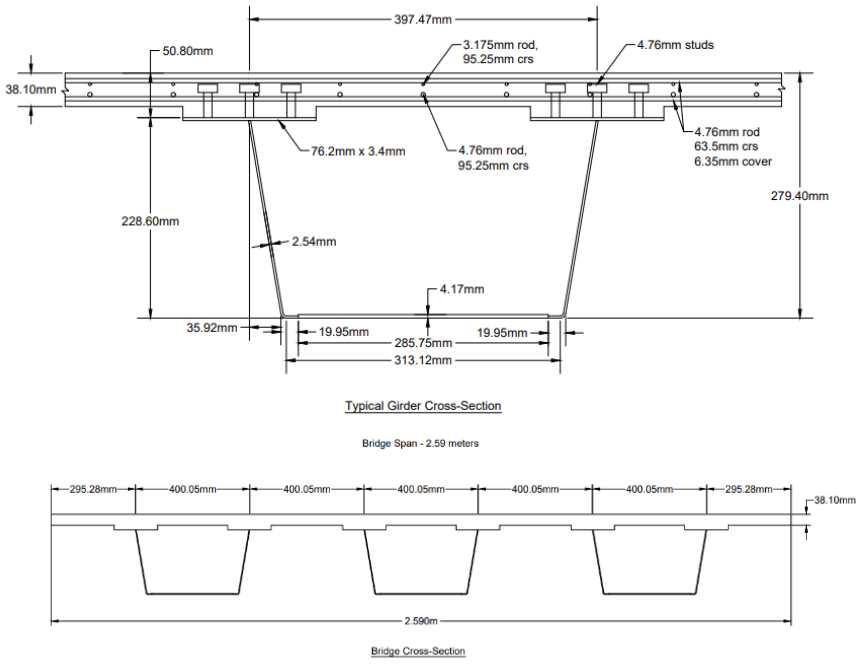

Figure 2.13 Girder cross-section used for the experimental study

The current distribution factor in the AASHTO Standard Specifications for box-girder bridges was developed through the works of Johnson and Mattock (1967). The researchers proposed the following equations:

$$W_i = 0.42 + 2.08R - 0.002S \qquad (Eq. 2-1)$$

$$W_e = \frac{1.69 - 1.23R}{1.22 - R} \qquad (Eq. 2-2)$$

Where $R = 0.5 \leq \frac{Number\ of\ Lanes}{Number\ of\ Box\ Girders} \leq 1.5$ and S is the spacing in feet.

2.3.2 Distribution of Wheel Load on Highway Bridges

The AASHTO Standard Specifications for Highway Bridges have provided empirical distribution factors since 1931. However, Zokaie et al. suggested the need to revise these specifications since the first edition of the AASHTO LRFD BDS was published in 1994, with the new LRFD bridge design method necessitating the revision of live load distribution. To address the issues with the AASHTO Standard Specifications, the National Cooperative Highway Research Program (NCHRP) Project 12-26 was conducted.

The study evaluated the wheel load distribution methods for various bridge types, including beam and slab, box girder, slab, multi-box beam, and spread box beam bridges. A significant part of the objective was to develop consistent and complete sets of equations for wheel load distribution for integration into AASHTO LRFD BDS specifications. The study also addresses the application of modern computer technology, like finite element techniques, for bridge analysis. However, it acknowledges the continued need for simplified load distribution methods. For each general bridge type, three separate levels of analysis were proposed. The analysis was divided into three levels:

- Level one – simplified methods using formulas to predict lateral load distribution.
- Level two – methods including graphical approaches, influence surfaces, or specific computer programs.
- Level three - detailed modeling of the bridge deck with a full finite element analysis.

The current LLDF equations specified in AASHTO originated from a study of 365 diverse bridges across various states. These bridges were primarily constructed from three distinctive superstructural materials: prestressed T-beams, concrete I-girders, and steel I-girders. To gauge the impact of different parameters on lateral load distribution, a prototype "average bridge" was constructed, integrating the mean characteristics of the studied bridges. This representative model was then tweaked, varying one parameter at a time to discern the specific influence of each parameter.

The sensitivity study examined the following set of parameters to investigate their effect on LLDF:

- girder spacing/number of girders,
- span length,
- girder stiffness,
- slab thickness,
- number of loaded lanes,
- deck overhang,
- skew,
- load configuration,

- support condition, and
- end diaphragms.

From this sensitivity analysis, parameters greatly influencing the LLDF of beam and slab bridges were found to be girder spacing, span length, girder rigidity, and deck thickness. The authors recommended that no revisions were proposed for bridges with a concrete deck on multiple steel box girders.

Zokaie et al. also suggested that the systematical derivation of a formula needed certain assumptions to be made. Firstly, it is assumed that each parameter's effect can be expressed as an exponential function ax^b, where x is the parameter value, and a and b are constants determined by x's variation. Secondly, the effects of different parameters are assumed to be independent, allowing for individual consideration. The resulting distribution factor formula is:

$$g = aS^{b_1}L^{b_2}t^{b_3}\cdots \qquad (\text{Eq. } 2-3)$$

- g is the wheel load distribution factor,
- S, L, and t are parameters included
- a is the scale factor,
- b_1, b_2, and b_3 are derived from the variations in S, L, and t.

Throughout the research, this method was consistently applied to develop the formulas. Where an exponential function did not fit a parameter's effect, minor alterations to the process were made. However, this method was generally effective, yielding highly accurate formulas.

2.3.3 Wheel Load Distribution in I-Girder Highway Bridges

The study by Tarhini and Fredrick (1992) examines the finite element analyses and modeling techniques of I-girder highway bridges, leading to the development of a wheel load distribution formula. The authors systematically varied specific parameters – notably the size and spacing of steel girders, the presence of cross bracing, the thickness of the concrete slab, span length, and the distinctions between single/continuous spans and composite/noncomposite behaviors. Their findings suggest that their formula aligns closely with existing AASHTO specifications but crucially emphasizes the role of span length in determining wheel load distribution factors. Notably, while AASHTO's design specifications are known for their

simplicity and conservative nature, this study finds potential limitations. The paper underscores the importance of perceiving the bridge superstructure as an integral entity rather than a mere aggregation of individual structural components.

Tarhini and Fredrick's study proposed a new wheel load distribution formula, which correlates with both span length and girder spacing, that emerged from the FEA and offers an alternative to the conventional AASHTO expression. The distribution factor was calculated by dividing the maximum moment in a girder found using FEA by the maximum moment in a girder found using LGA.

2.3.4 Live Load Distribution Factors for Exterior Girders in Steel I-Girder Bridges

Michaelson (2010) performed a comprehensive exploration of the live load distribution factors for exterior girders in steel I-girder bridges. Recognizing the pivotal role of live loads in bridge design and the evolution of vehicular loads and configurations, the study focused on the need for accurate and precise load distribution estimation methodologies for ensuring the safety and longevity of bridge structures. While the equations and methods found in AASHTO LRFD BDS provide a foundation, Michaelson identified potential gaps and limitations, especially when applied to exterior girders, which often experience different loading characteristics compared to interior girders. The study emphasized that these exterior girders, being directly exposed to traffic lanes and often lacking the symmetry of load distribution seen in interior girders, necessitate a unique and tailored approach.

Michaelson (2010) performed a comprehensive literature review to explore the impact of various parameters on live load distribution, with a specific focus on the NCHRP Report 12-26. This report played a pivotal role in formulating the empirical distribution factors that continue to be a part of the current AASHTO LRFD Specifications. Following this, a highly precise finite element modeling technique was evaluated, which would subsequently be utilized to ascertain live load distribution factors. This evaluation involved a comparison of the modeling results with empirical data gathered from the 2002 load testing of Missouri Bridge A6101 (Wu, 2003). A sensitivity matrix was constructed to gauge the influence of specific parameters on the live load distribution of exterior girders. The bridges under consideration were then examined using the previously mentioned modeling technique with the aid of a commercial finite element software package from Dassault Systèmes (2009).

The ensuing analysis of the sensitivity study's results brought to light the parameters that exerted the most substantial influence on exterior girder live load distribution. In response, an expanded parametric matrix covering a broader spectrum of bridges was formulated and analyzed using the same finite element modeling technique. Live load distribution factors were again calculated from the finite element results of this expanded study. To bring the research to fruition, the results of the comprehensive parametric study were input into a commercial data correlation software tool from Oakdale Engineering (2008). This process facilitated the development of empirical distribution factors specifically tailored for exterior girders, finishing the extensive investigation into live load distribution influences.

2.3.5 Live Load Distribution Factors for Skewed Composite I-Girder Bridges

The introduction of a skew angle adds a layer of complexity to the analysis of composite slab-on-girder bridges, particularly due to the twisting of steel I-girders placed over skewed supports. This phenomenon, more pronounced at the obtuse corners of the bridge, challenges engineers due to the non-uniform distribution of loads across the bridge's superstructure. The resulting structural implications include increased lateral flange bending stresses, heightened shear and end reactions at the obtuse corners, and potential uplift in girders at acute corners. In recent years, North American bridge code specifications have been updated to include considerations for the angle of skew in slab-on-girder bridges. However, the design parameter ranges specified in these provisions are often too restrictive, leading to frequent exceedances during routine design checks. This necessitates the use of more refined analysis techniques, a skill set that many engineers may not possess. Additionally, the analysis equations provided in the current guidelines are derived from grillage analysis results and do not always suit skewed bridges. These guidelines also tend to neglect the role of diaphragms in such structures, potentially leading to inaccurate load distribution predictions.

In his 2017 study, Razzaq formulated empirical equations to evaluate LLDFs in skewed slab-on-steel I-girder bridges. This involved a detailed parametric analysis of a composite bridge structure, examining its behavior under various loads (dead, live, and those pertinent to ultimate, serviceability, and fatigue limit states). Key factors such as the bridge's skew angle, girder stiffness, layout of cross-frames, span length, spacing between girders, the total number of girders, and the number of design lanes were taken into account in developing these equations for

calculating moment and shear LLDFs. The findings were then juxtaposed with the equations provided in the Canadian Highway Bridge Design Code (CHBDC). These new equations have shown strong alignment with finite element analysis results for both straight and skewed bridges, highlighting their potential for improving design accuracy. However, it is noted that existing CHBDC equations may not always provide reliable results, especially for straight bridges and certain skewed configurations.

From the findings of the current research, several key insights can be highlighted from Razzaq (2017):

- The outcomes from the Finite Element Analysis (FEA) indicated a shift in reactions toward the obtuse corners of the girders and away from the acute corners as the skew angle increased. This shift was relatively minor when the skew angle was below 30° but became markedly pronounced for skew angles exceeding 30°.
- An increase in the number of lanes led to heightened moment and shear distribution factors at the obtuse corners for exterior girders. This was particularly noticeable in bridges with:
    i. Skew angles greater than 30° coupled with long spans ($L \geq 25$ m) and
    ii. Higher girder count but reduced spacing between them.
- Exterior girders exhibited less susceptibility to skew angle effects compared to interior girders. This trend was more evident in bridge structures featuring larger skew angles and extended spans.

The research also delved into the applicability of the proposed equations for multi-span continuous bridges, identifying scenarios where both the new equations and the CHBDC guidelines could lead to unsafe or overly conservative estimates. This led to the development of new design equations tailored for skewed continuous bridges, ensuring closer conformity with finite element analysis outcomes. The study concludes with the proposal of design guidelines that encourage treating skewed bridges similarly to straight bridges, a paradigm shift expected to bolster the reliability and cost-effectiveness of bridge design practices.

2.3.6 Straight Skewed I-Girder Bridges

White's (2020) study offers an elaborate exploration of straight-skewed I-girder bridges, with a focus on understanding the impacts of skew angles on load distribution and structural

performance. The paper identifies the skew index, I_g, as a crucial parameter in assessing the effects of skewness, with a particular emphasis on bridges having skew indices up to and slightly beyond 0.3. The research underscores a transition in bridge design practices, noting a shift towards more refined methods of analysis such as 3D FEA, especially for bridges with significant skewness. However, the study also acknowledges the prevalent use of one-dimensional line girder analysis (LGA) in the design of many straight skewed I-girder bridges, highlighting a potential area for simplification in design workflows.

$$I_s = \frac{w_g \tan(\theta)}{L_s} \qquad (Eq. 2-4)$$

- w_g is the framing width between the fascia girders,
- θ is the angle of skew, and
- L_s is the span length under consideration.

The study conducts comparative parametric analyses using both 3D FEA and LGA across a suite of 26 bridges, aiming to examine the adequacy of LGA in capturing the bridge responses under various conditions. The bridges under study exhibit a range of characteristics, including varying span designs, skew angles, and girder arrangements. The research meticulously examines a spectrum of response quantities, from bending moments and shear forces to vertical displacements and live load effects, providing a comprehensive understanding of the bridges' behavior. The findings revealed that the accuracy of LGA is intricately linked to a combination of structural attributes, including the skew index, the skew angle of the bearing lines, and the framing arrangement of the cross-frames or diaphragms. Building on these insights, White's paper categorizes bridges into three distinct categories, each with tailored design recommendations to account for the unique challenges posed by skew angles. The study highlights that while LGA provides a fast and sufficient solution for a substantial range of straight skewed I-girder bridges, its accuracy diminishes as skewness and transverse load path effects intensify. The paper presents a set of refined design guidelines, emphasizing the need for additional correction factors and adjustments in certain scenarios to ensure the reliability of LGA results.

The study also ventures into practical application and design improvements. It offers a suite of recommendations aimed at improving the calculation of girder flange lateral bending stresses,

cross-frame forces, and other critical response quantities; by refining current design practices and introducing new calculation methodologies, the research endeavors to enhance the precision and reliability of straight skewed I-girder bridge design.

2.3.7 Expanding the Applicability of Press-Brake-Formed Tub Girders through the Extension of the Maximum Span Length and the Evaluation of Pier Continuity

Tennant (2022) investigated the expansion of the applicability of PBFTGs thorough analytical and laboratory experiments, particularly focusing on the integration of link slabs with modular PBFTGs in continuous span configurations and thoroughly examining the constraints applied to box-section flexural members in relation to PBFTGs. A comprehensive literature review was carried out on PBFTGs, link slab details, live load distribution, and the impact of compactness on flexural capacity. Additionally, analytical tools were developed to examine the behavior and capacity of PBFTGs, considering varying dimensions, properties, and parameters. This was complemented by conducting behavioral and parametric studies aimed at identifying critical parameters influencing the computation of live load distribution factors for PBFTGs, alongside behavioral studies to evaluate the impact of skew on the ultimate capacity of PBFTGs. Practical insights and supporting data for the analytical work were obtained through flexural testing on modular units that are transversely joined by a link slab, ensuring a comprehensive understanding and evaluation of PBFTGs in various applications and validating or revising existing restrictions as necessary.

When developing the analytical framework, Tennat (2022) benchmarked against several laboratory experiments and two live-load field tests – one of which is the field tests performed by Roh (2020). Both the Stallings/Yoo and Tarhini/Frederick methods were employed to calculate the LLDFs, with the latter being a specific addition for this research. The comparative analysis between the field data and the analytical model, focusing on Girder 1 with one design lane loaded, demonstrated negligible differences between the two LLDF calculation methods and the live load field test. This result underscores the validity of the analytical modeling techniques employed for determining LLDFs in PBFTG bridges.

For this literature review, the research involving generating and analyzing a matrix of bridge models via finite element software, aiming to discern the sensitivity of various parameters on live load distribution, is examined closely. A modified matrix is created, narrowing down on

parameters identified as significantly influential. Four standard PBFTG bridge scenarios were generated and analyzed, focusing on understanding how specific parameters influence live load distribution in PBFTG bridges. This is achieved through a detailed analysis of a matrix of bridges using Abaqus/CAE, where parameters are either held constant or varied to observe their impacts. The dimensions of the standard bridges are given in Table 2-1.

Table 2-1 Standard bridge dimensions for the sensitivity study

Bridge Number	Plate Size (in)	Span Length (ft)	Number of Girders	Girder Spacing (ft)	Deck Thickness (in)	Overhang Width (ft)
1	72 x 1/2	30	3	6	8	2.22
2	84 x 1/2	40	4	8	8	2.11
3	96 x 1/2	60	5	8	8	1.8
4	120 x 5/8	80	6	10	8	1.29

The constant parameters include dimensions related to the bridge's structural elements, material properties of concrete and steel, and certain boundary conditions. The varied parameters encompass a wide range of possibilities, including different span lengths, number of girders, individual PBFTG cross-sections, girder spacings, deck thicknesses, overhang ratios, and load placements. These varied parameters provide a comprehensive view of how different aspects of bridge design can influence live load distribution. Figure 2.14 shows the cross-section of the standard bridge 3.

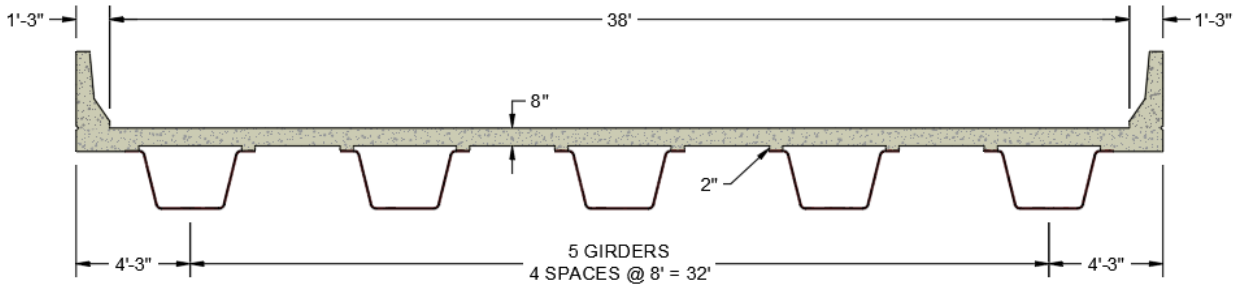

Figure 2.14: Sensitivity Bridge Cross-Section

The sensitivity study yielded extensive results, showcasing the influence of each varied parameter on live load distribution. It is observed that the LLDFs derived from analytical modeling generally tend to be lower than those calculated using empirical equations from AASHTO LRFD

BDS, with specific trends noted for one-lane and two-lane loaded scenarios. The study provides a granular view of how parameters such as span length, number of beams, PBFTG size, girder spacing, deck thickness, and overhang ratio impact LLDFs. For instance, span length and girder spacing are found to have a significant effect on LLDFs, whereas deck thickness has a negligible impact. The overhang ratio, while having a minimal effect on interior girder LLDFs, shows a noticeable influence on exterior girder LLDFs. Figure 2.15 presents a sample of graphs used in the sensitivity study.

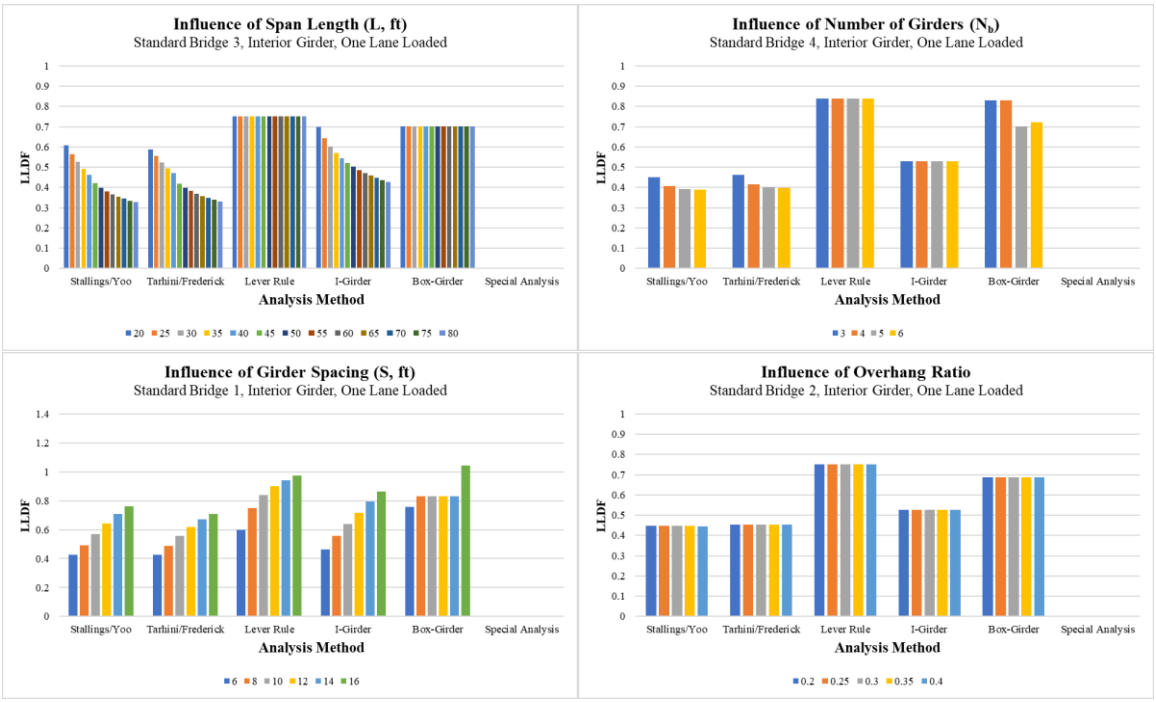

Figure 2.15 Results of the sensitivity analysis performed to assess the influence of several parameters.

The extensive sensitivity study and subsequent analysis provided a reliable tool for further study of the LLDF for PBFTGs.

2.4 SUMMARY

The comprehensive study by Michaelson (2014) presented an innovative modular design of PBFTGs, primarily substituting traditional concrete box beams for short-span bridges up to 90 feet. This innovation, involving the cold bending of standard steel plates into a trapezoidal box girder, encourages faster bridge construction and reduces traffic disruptions, which is attributed to its composite modular unit design that can accommodate various deck options. On the other hand,

Kelly (2014) explored the structural behavior of noncomposite PBFTGs, focusing on stability and torsional behavior through experimental tests, highlighting the critical construction stage for cast-in-place decks. Gibbs (2017) and Roh (2020) further extended the application of PBFTGs to real-world scenarios, investigating their on-field performance and construction methodologies, respectively, with an emphasis on accelerated bridge construction strategies and quality assurance through controlled environments.

Studies by Johnston and Mattock (1967), Tarhini and Fredrick (1992), and Michaelson (2010) delved into the live load distribution in bridges, developing various analytical tools and formulas for a better understanding of load distribution in different types of bridges. The National Cooperative Highway Research Program (NCHRP) and Razzaq highlighted the need to revise live load distribution specifications and address challenges in the analysis of skewed bridges, respectively. White (2020) further contributed to this domain by exploring the impact of skew angles on load distribution in straight skewed I-girder bridges, and Tennant (2022) expanded the applicability of PBFTGs in various configurations, ensuring a comprehensive understanding of these structural systems.

CHAPTER 3: OVERVIEW OF CURRENT AASHTO LRFD BDS

3.1 SPECIFICATIONS RELATED TO THE DESIGN AND ANALYSIS OF PBFTGS

This chapter provides guidelines available for the design and analysis of PBFTGs set forth in AASHTO LRFD BDS (2020).

3.1.1 Introduction

The AASHTO LRFD BDS (2020) sets the standards for highway bridge design in the United States. Within this document, Section 6 contains guidelines for designing steel structures. Specifically, Chapter 6.11 outlines the requirements for designing box section (tub girder) flexural members. However, these specifications may not fully align with the requirements for cold-bent press-brake-formed tub girders. Therefore, it's important to review these provisions to determine their suitability for such systems. This review is a step towards adapting and proposing specific standards for these types of girders within the framework of the AASHTO LRFD BDS.

3.1.2 Structural Loads

Bridge structures are subject to varying types of loads, which can be primarily classified into two broad categories: permanent loads and transient loads. This distinction is essential for the design, analysis, and safety assurance of bridges. Permanent loads encompass both dead loads and earth loads. Dead loads are essentially the unchanging, constant loads attributed to the structure itself, including all its integral and attached components. This includes the weight of the bridge girders, deck, and other structural elements, along with any permanent fixtures like utilities, the wearing surface, and provisions for future expansion such as planned bridge widening. AASHTO provides a useful reference for approximating these loads through stipulated unit weights of various materials, aiding in the calculation of the total dead load, especially when the exact weights of components are not known. (see Table 3-1).

The dead loads are further categorized into non-composite and composite loads based on the phase of construction. Non-composite dead loads, designated as DC1, encompass loads during the construction phase before the completion of the composite action. Examples of DC1 loads include the self-weight of girders, wet concrete deck, stay-in-place metal formwork, concrete haunches, overhang tapers, and other miscellaneous weights that are present before the concrete

deck achieves composite action with the girder. Until the concrete attains 75% of its designated compressive strength, it is assumed that the load is supported solely by the girders.

Table 3-1 Unit Weights (AASHTO, 2020)

Material		Unit Weight (kcf)
Aluminum Alloys		0.175
Bituminous Wearing Surfaces		0.140
Cast Iron		0.450
Cinder Filling		0.060
Compacted Sand, Silt, or Clay		0.120
Concrete	Lightweight	0.110
	Sand-Lightweight	0.120
	Normal Weight with $f'_c \leq 5.0$ ksi	0.145
	Normal Weight with $5.0 < f'_c \leq 15.0$ ksi	$0.140 + 0.001\, f'_c$
Loose Sand, Silt, or Gravel		0.100
Soft Clay		0.100
Rolled Gravel, Macadam, or Ballast		0.140
Steel		0.490
Stone Masonry		0.170
Wood	Hard	0.060
	Soft	0.050
Water	Fresh	0.0624
	Salt	0.0640
Item		Weight per Unit Length (klf)
Transit Rails, Ties, and Fastening per Track		0.200

After the concrete sets achieve the requisite compressive strength, a full composite action is generated between the concrete deck and the steel girder. This phase marks the transition to composite dead loads, categorized as DC2 and DW. The composite loads, DC2, include the weight of curbs, barriers, sidewalks, and pedestrian hand railings, which now act in unison with the girders and deck to resist applied loads. Additionally, DW represents the anticipated future wearing surface loads due to planned enhancements or modifications to the wearing surface of the bridge.

For the scope of this study, the focus will be narrowed down to an analysis of dead loads and live loads (vehicular traffic), which are pivotal in the Strength I, Service II, and Fatigue load combinations, essential for ensuring the bridge's safety and serviceability. These load combinations are crucial for understanding and preparing for the structural demands the bridge will encounter, thereby enabling a more robust and resilient design.

According to the AASHTO Specifications, the designated vehicular live load (LL) to be applied on structures is known as HL-93. This load model is a combination of a uniform lane load

and specific axle loads. It includes a lane load of 0.64 kips per foot, used in conjunction with either a design truck or a design tandem. The design truck is characterized by a three-axle configuration: an 8-kip front axle followed by two 32-kip rear axles (see Figure 3.1). The distance between these rear axles can vary from 14 to 30 feet, a range specifically chosen to simulate the most demanding load scenarios. On the other hand, the design tandem comprises two axles, each bearing 25 kips and spaced 4 feet apart. Furthermore, engineers are tasked with strategically positioning these loads longitudinally on the structure. This placement is crucial as it determines the maximum live load response of the structure, ensuring that the design accounts for the most critical loading conditions.

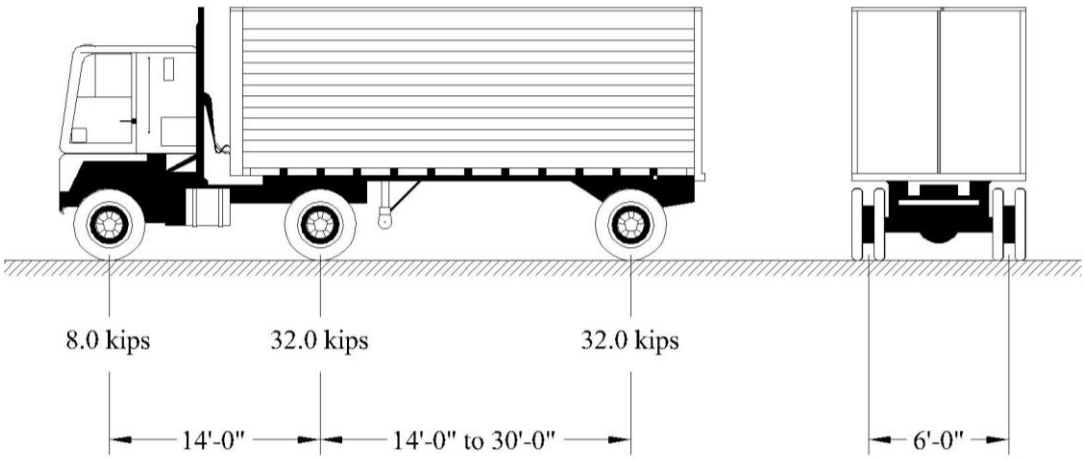

Figure 3.1 HL-93 truck vehicular live load (AASHTO, 2020)

Conversely, the design tandem consists of a pair of 25 kip axles with a fixed spacing of 4 feet apart (see Figure 3.2). It represents another facet of vehicular loading, expanding the representation of real-life track loadings and the versatility of the HL-93 load model in encompassing various vehicular loading configurations.

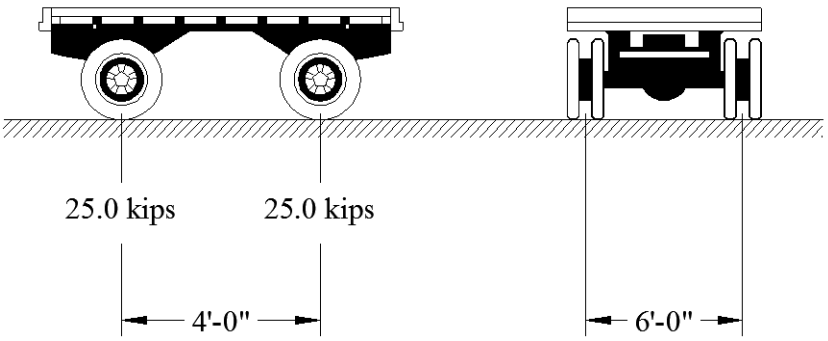

Figure 3.2 HL-93 tandem vehicular live load (AASHTO, 2020)

Dynamic load allowances (IM) are also factored into account for the dynamic impacts of the design vehicle, such as the vehicle's interaction with the driving surface. The dynamic effects are integrated by enhancing the effects of the design truck and design tandem. Specifically, the vehicular live load is augmented by 33% for all limit states, except in the cases of fatigue evaluation and deck joint assessment. In the fatigue limit state, the live load sees a 15% increment, while a substantial 75% increment is applied for evaluating deck joints. These allowances ensure a more realistic and safe approximation of the live loads, considering the dynamic nature of vehicular traffic.

Additionally, beyond the finished state of the bridge, loads applied during the construction phase necessitate additional thorough evaluation. These construction loads encompass various elements. Moreover, the deck casting sequences, particularly in multiple-span bridges, introduce an added layer of complexity. Typically, the deck is cast in the positive bending regions initially to mitigate the risk of cracking over the piers, demanding a strategic and well-considered approach to ensure structural integrity during and post-construction.

3.1.3 Limit State Summary

To accommodate the statistical likelihood of various loads occurring simultaneously, engineering design typically involves the use of multiple load combinations or limit states. These limit states are essential in ensuring that structures can withstand different scenarios of loading, whether they occur individually or in combination. Each limit state must adhere to a general equation. This equation serves as a foundational guideline, ensuring that the structure's design is robust enough to handle the specified load combinations. The specifics of this general equation usually encompass factors like dead loads (permanent static loads), live loads (variable or dynamic loads), environmental loads (like wind or earthquake forces), and other relevant factors.

$$\sum \eta_i \gamma_i Q_i \leq \phi R_n = R_r \qquad (Eq. 3-1)$$

- γ_i is a load factor: a statically based multiplier applied to force effects,
- ϕ is a resistance factor: a statistically based multiplier applied to nominal resistance,
- η_i is a load modifier: a factor relating to ductility, redundancy, and operational classification,
- Q_i is force effect,
- R_n is nominal resistance, and
- R_r is factored resistance.

The equation is structured to ensure that, under all probable loading conditions, the structure remains safe and functional. It's a crucial aspect of structural engineering design, providing a mathematical framework to evaluate and validate the safety and stability of the proposed structure under various loading scenarios. To comprehensively address the durability and safety of bridges, engineering design employs a multifaceted approach that includes various load modifiers and limit states:

1. Load Modifiers: These are applied to account for the ductility, redundancy, and operational importance of the bridge, collectively forming the ηi term.
    a. Ductility Load Modifier: Ensures that visible inelastic deformations occur before structural failure, enhancing safety.
    b. Redundancy Load Modifier: Increases the resilience of the bridge system, preventing total collapse in case one member fails.
    c. Operational Importance Load Modifier: Assigns higher resistance to bridges that are crucial for emergency roadways or have national security implications. For most bridges, this modifier is set to one.
2. Strength Limit States: These are designed to ensure the bridge's strength and stability over its lifetime, taking into account both local and global components and connections.
    a. Strength I: Considers basic load combinations under normal vehicular use, excluding wind loads.
    b. Strength II: Accounts for Owner-specified vehicles or evaluation permit vehicles without wind loads.

    c. Strength III: For bridges in areas with wind velocities over 55 mph.
    d. Strength IV: When there's a significant ratio of dead load to live load force effects.
    e. Strength V: Considers normal vehicular use with wind velocities of 55 mph.
3. Extreme Event Limit States: These cover rare but significant loads like earthquakes and vehicle collisions.
    a. Extreme Event I: Earthquake loads.
    b. Extreme Event II: Ice loads, collisions, floods, and other hydraulic events.
4. Service Limit States: Focused on preventing excessive stress, deformation, and cracking under regular service conditions.
    a. Service I: Normal bridge use with 55-mph wind, typically for checking deflection and concrete deck cracking.
    b. Service II: Controls steel yielding and slip-in connections due to vehicular live load.
    c. Service III: Crack control in prestressed concrete superstructure and girder members.
    d. Service IV: Crack control in prestressed concrete columns.
5. Fatigue and Fracture Limit States: Aimed at limiting stress range and preventing crack growth and fracture under repetitive loads.
    a. Fatigue I: For infinite load-induced fatigue life.
    b. Fatigue II: Related to finite load-induced fatigue life.

Each of these limit states plays a critical role in ensuring that bridges are designed to withstand a variety of stressors over their lifetime, maintaining safety and functionality.

3.1.4 Structural Analysis Provisions

Multiple presence factors are employed to account for the probability of multiple design lanes being loaded simultaneously. The extreme live load force effect is determined by considering each possible combination of the number of lanes loaded multiplied by the corresponding multiple presence factor. It should be noted that these factors are not to be used when considering the fatigue truck; when assessing fatigue, one design truck is used, regardless of the number of design lanes. AASHTO's multiple presence factors are listed in Table 3-2.

Table 3-2 Multiple Presence Factors (AASHTO, 2014)

Number of Loaded Lanes	Multiple Presence Factors, *m*
1	1.20
2	1.00
3	0.85
>3	0.65

3.1.5 Strength Limit State

The strength limit state, as outlined in AASHTO (2020), is crucial in ensuring that a bridge possesses the necessary capacity to withstand the moments and shears applied throughout its entire lifespan. This is especially pertinent to box girders, which are covered in Article 6.11.6 and divided into four main sections.

For bridges with a straight alignment, there are specific requirements regarding the yield strength of the structural components:

- The minimum yield strength for both the flanges and the web of the box girders is capped at 70 ksi (kilo-pounds per square inch). This limit is set to ensure that the materials used have the requisite strength while maintaining some level of flexibility to handle stress and strain effectively.

Additionally, the web of the box girder must adhere to the specifications laid out in AASHTO (2020) Article 6.11.2.1.2. This article deals with the cross-section proportion limits for webs that do not have longitudinal stiffeners. The guidelines in this section are important for maintaining the structural integrity of the web, as they dictate the optimal proportions and configurations to prevent issues like buckling or excessive deformation under load.

- Web Slenderness Limit: The slenderness of the web (a key structural component of a bridge) is checked using an equation that relates the depth of the web in compression, the steel's modulus of elasticity, the minimum yield strength of the compression flange, and the web thickness.
- Compact and Noncompact Sections: Bridge sections are classified as either compact or noncompact based on specific criteria set out in AASHTO articles. Compact sections

must satisfy certain ductility requirements, ensuring that the section can deform under stress without breaking.

- Strength Limit State for Compact Sections: At this limit state, the bending moment caused by applied loads must be less than or equal to the product of a resistance factor for flexure and the nominal flexural resistance of the section. The nominal flexural resistance is calculated differently depending on whether the beam is simply supported or continuous-span.
- Strength Limit State for Noncompact Sections: For noncompact sections, the longitudinal flange stress must not exceed the product of the resistance factor for flexure and the nominal flexural resistance of the compression flange. The nominal flexural resistance of the compression flange is calculated using the specified minimum yield strength of the compression flange, a web load shedding factor, and a hybrid factor.

These criteria are essential for ensuring that bridge structures can safely support the loads they are subjected to, taking into account factors like material properties, structural configuration, and load distribution. The requirements are part of a broader set of design principles aimed at ensuring that bridges are not only strong enough to carry the loads they are subjected to but also resilient enough to endure these stresses over a prolonged period. The strength limit state is a critical component of bridge design, ensuring that all elements of the bridge work in harmony to provide a safe and durable structure.

3.2 LIVE LOAD DISTRIBUTION FACTOR

One of the fundamental concepts in simplified bridge design and analysis is the LLDF. Understanding and accurately determining live load distribution is crucial for engineers to design bridges that are both economical and safe. LLDF is a percentage that represents how live loads, such as vehicular traffic, are distributed among the structural elements of a bridge, primarily the girders. This factor is essential in bridge design as it helps engineers estimate the portion of live loads carried by each structural component, allowing for a more accurate analysis of stress and deflection.

The AASHTO LRFD BDS provides guidelines on calculating LLDFs, which take into account various bridge parameters like span length, girder spacing, and the number of lanes, among others. In lieu of a complex three-dimensional analysis, LLDF equations are commonly employed by engineers to simplify the analysis of a bridge system. Specifically, instead of analyzing the three-dimensional bridge system as a whole, these factors allow the engineer to consider bridge girders individually. Some of the methods specified in AASHTO LRFD BDS that are used to find moment LLDFs are discussed in this section.

3.2.1 I-girder

The applicable distribution factors found in AASHTO LRFD BDS Table 4.6.2.2.2b-1for moment is an interior girder of an I girder with concrete deck is as follows,

One lane loaded,

$$0.06 + \left(\frac{S}{14}\right)^{0.4}\left(\frac{S}{L}\right)^{0.3}\left(\frac{K_g}{12Lt_s^3}\right)^{0.1} \qquad (Eq\ 3-10)$$

Two lanes loaded,

$$0.075 + \left(\frac{S}{9.5}\right)^{0.6}\left(\frac{S}{L}\right)^{0.2}\left(\frac{K_g}{12Lt_s^3}\right)^{0.1} \qquad (Eq\ 3-11)$$

- S is the spacing between girders,
- L is the span length,
- K_g is the longitudinal stiffness parameter, and
- t_s is the deck thickness.

The longitudinal stiffness parameter, K_g, can be computed using,

$$K_g = n\left(I + Ae_g^2\right) \qquad (Eq\ 3-12)$$

$$n = \frac{E_B}{E_D} \qquad (Eq\ 3-13)$$

- n is the modular ratio between the beam and deck,
- I is the moment of inertia of the beam,

- A is the area of a stringer, beam, or component,
- e_g is the distance between the centers of gravity of the basic beam and deck,
- E_B is the modulus of elasticity of beam material and
- E_D is the modulus of elasticity of the deck material.

For the number of beams less than three, the code recommends the use of the minimum value obtained from the above equations or the lever rule, which is discussed herein.

3.2.2 Lever Rule

AASHTO LRFD BDS provides guidelines on the usage of the lever rule to determine the distribution of moment and shear under certain scenarios. Tables found in article 4.6.2.2.2 of the AASHTO Specifications advocate the use of the Lever Rule that satisfies certain conditions. In order to use the Lever Rule, the slab functions as a beam, which is simply supported by the girders. At the interior girder adjacent to the exterior girder, an internal hinge is presumed to exist, serving as a pivotal point for analyzing the load distribution, as illustrated in Figure 3.3. Following this, a design vehicle is positioned on the bridge – adhering to the guidelines specified in AASHTO Section 3.6.1.3.1 and setting the stage for examining the load effects. The stipulation here is that the center of any wheel load must maintain a distance of no less than 2.0 feet from the edge of the design lane. This ensures a realistic scenario for assessing the load effects.

To determine the distribution factor, a summation of moments is carried out at the assumed hinge, which enables the calculation of the percentage of load borne by the exterior girder. This deduced percentage becomes a cornerstone for evaluating both moment and shear in the exterior girders under a one-lane loaded scenario. The derived percentage is then subjected to multiplication by the appropriate multiple presence factor. As mentioned in Section 3.1.4, for a one-lane loaded condition, the applicable multiple presence factor stands at 1.20. Thus, to obtain the moment and shear exterior girder distribution factor for one loaded lane, a multiplication of the derived percentage by 1.20 is executed. However, the designer should follow the AASHTO LRFD BDS recommendation on the use of the Lever Rule since there are limitations on its applicability.

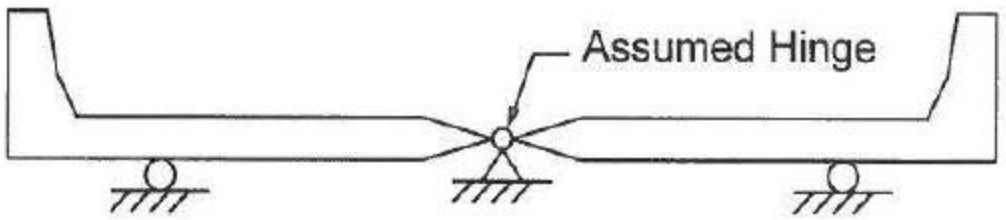

Figure 3.3: Notional model for applying lever rule to three-girder bridges (AASHTO, 2020)

3.2.3 Exterior Girder and Skew Correction Factors

To determine accurate LLDFs of the moment in exterior beams, specifically under scenarios where two or more lanes are loaded, the AASHTO LRFD BDS recommends the adoption of correction factors. This approach, akin to the application of correction factors for addressing skew, enhances the precision of load distribution analysis. The correction factor for exterior girder is utilized to adjust the distribution factors originally computed for interior girders, thereby extending the analysis to exterior beams under multi-lane loading conditions. For a one-lane loading scenario, the specification recommends the use of the lever rule to determine exterior girder LLDF.

The applicable distribution factors found in AASHTO LRFD BDS Table 4.6.2.2.2d-1for moment is an exterior girder of an I girder with concrete deck with two of more design lanes is as follows,

$$\left(0.77 + \frac{d_e}{9.1}\right) g_{interior} \qquad (Eq. 3-14)$$

- d_e is the distance between the interior edge of the parapet and the centerline of the exterior web, and
- $g_{interior}$ is the LLDF for the interior girder.

The orientation of the exterior web in relation to the interior face of the traffic railing significantly influences the value of LLDF in the exterior girder. Specifically, the value of d_e is regarded as positive if the exterior web is located inboard of the interior face of the traffic railing, with the stipulation that it must be less than or equal to 5.5 feet. Conversely, the value of d_e is considered negative if the exterior web is positioned outboard of the curb or traffic barrier, and in this scenario, it must be greater than or equal to 1.0 feet.

The applicable distribution factors found in AASHTO LRFD BDS Table 4.6.2.2.2e-1for moment reduction of an I girder with concrete deck with any number of design lanes is as follows,

$$1 - c_1(\tan\theta)^{1.5} \qquad (Eq. 3-15)$$

$$c_1 = 0.25\left(\frac{K_g}{12Lt_s^3}\right)^{0.25}\left(\frac{S}{L}\right)^{0.5} \qquad (Eq. 3-16)$$

- $\theta\ is\ the\ skew\ angle.$

3.2.4 Multiple Steel Box Girders

The applicable distribution factors for moment in a concrete deck on multiple steel box girders are as follows, regardless of the number of lanes loaded (AASHTO Table 4.6.2.2.2b-1):

$$0.05 + 0.85\frac{N_L}{N_b} + \frac{0.425}{N_L} \qquad (Eq. -3.17)$$

The use of Equation 3.14 has a condition outlined in Eq. 3.15.

$$0.5 \le \frac{N_L}{N_b} \le 1.5 \qquad (Eq. 3-18)$$

- N_L is the number of design lanes as specified in Article 3.6.1.1.1
- N_b is the number of girders

When designing bridges with multiple tub girders, there are specific restrictions related to the live load distribution factor to ensure structural integrity and safety. These restrictions include:

- Bearing Lines: The bearing lines of the girders must not be skewed. This means they should be aligned perpendicularly to the direction of the traffic flow, ensuring even distribution of loads.
- Web Plate Inclination: The inclination of the web plates (the vertical elements of the box girder) relative to a plane normal (perpendicular) to the bottom flange should not exceed a slope of 1:4. This restriction is important for maintaining the structural effectiveness of the girder.
- Cantilevered Overhang Limits: The overhang of the concrete deck, which includes elements like the curb and parapet, is restricted. It should not exceed 60% of the average

distance between the centers of the top steel flanges of adjacent box sections (see Figure 3.4), or 6.0 feet, whichever is lesser. This limitation helps in managing the balance and load distribution of the overhanging section.

- Midspan Distance: The distance 'a' taken at midspan must be within a specific range – neither more than 120% nor less than 80% of the distance from center-to-center of the flanges of each adjacent box (see Figure 3.4). This stipulation helps in ensuring that the girders are spaced optimally for load distribution.
- Nonparallel Box Section Limits: In cases where nonparallel box sections are used, the center-to-center distance of the flanges of each adjacent tub girder must be within a specified range – not exceeding 135% and not less than 65%. This guideline is crucial for bridges with varying girder alignments to ensure stability and appropriate load distribution.

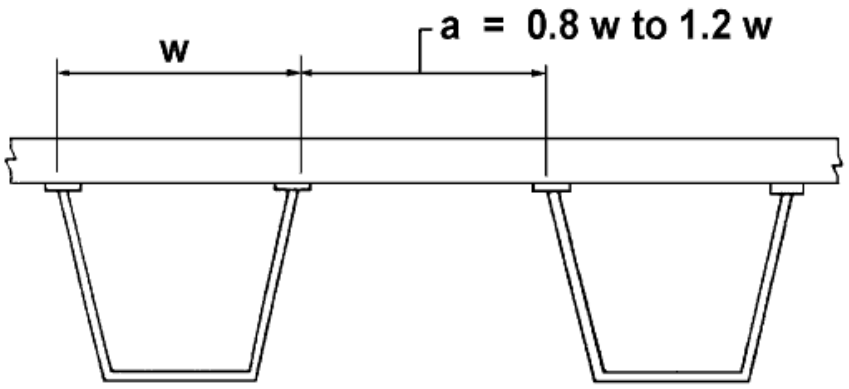

Figure 3.4 Center-to-Center flange distance (AASHTO, 2020)

The preceding chapter provides an overview of the current AASHTO LRFD BDS guidelines on the design and analysis of Box Sections.

CHAPTER 4: FINITE ELEMENT MODELING TECHNIQUES AND ANALYTICAL METHODS

4.1 INTRODUCTION

This chapter provides a comprehensive overview of the finite element modeling methods applied in this research. It covers various aspects, including the selection of elements, the definition of materials, the process of mesh discretization, the application of boundary conditions, and how loads are applied.

4.2 FINITE ELEMENT MODELING TECHNIQUES

Finite element analysis was conducted in this study using the commercial finite element software package Abaqus/CAE (Dassault Systèmes, 2020). Discussed in this chapter are the specific provisions used to carry out analyses for this project. In addition, loads and loading methods are presented.

4.2.1 Element Selection

Abaqus offers a wide array of element choices for three-dimensional stress analysis, necessitating an initial evaluation of the most suitable element type for each specific issue. Previous studies (Barth, 1996; Yang, 2004; Roberts, 2004; Righman, 2005) have shown that general-purpose shell elements are highly effective in simulating the behavior of both composite and noncomposite steel plate girders. The S4R element in Abaqus, a 3D, 4-node shell element, is designed for accurate modeling of both thin and thick shell structures, accommodating finite strains and rotational movements. This feature is particularly beneficial in scenarios where understanding the deformation history of the shell is crucial. Additionally, these elements account for variations in shell thickness related to membrane strain and include considerations for transverse shear deformation.

S4R elements employ reduced integration schemes; that is, for a four-noded element, only one Gauss integration point is used to form the element stiffness matrix. This integration scheme yields several advantages over traditional shell elements. For example, reduced integration computes strains and stresses at the locations known to provide optimal accuracy; thus, reduced integration usually produces more accurate results, provided the elements are not disturbed or

loaded in in-plane bending. The use of fewer integration points also benefits the user by resulting in reduced computing time and storage requirements. The primary disadvantage of using reduced integration is that deformation modes that cause no strain at the integration points may develop.

S4R elements were employed to simulate the girder, deck, and bearing stiffeners in all models for this project. Additionally, S3R elements were used on the bearing stiffeners. The formulation of the S3R element is derived through the degeneration of a quadrilateral element known as S4R. Thus, all the appealing properties of S4R formulation are applicable to S3R elements. To model the composite action between both the girders and the deck, node-to-node multiple-point constraints (MPC) were used such that the degrees of freedom between nodes were restrained. MPCs are employed to model the interaction between the girders and the deck accurately, ensuring that they function as a singular unit as opposed to isolated entities. This is achieved by establishing a precise relationship or constraint between the nodes belonging to the girders and the deck.

4.2.2 Material Model

The materials involved, steel and concrete, were assumed to adhere to a linear, elastic, and isotropic behavior, which simplifies the analysis by reducing the complexity associated with material non-linearities. This assumption was grounded on research by Barth et al. (2018, Vol. 4), who found a linear response in the in-service behavior of such girders, affirming the validity of treating the materials as linear elastic mediums in the analysis. After conducting the analysis, it was observed that the maximum stress levels in both the steel and concrete components of all the models remained significantly below the yield stress of steel and the compressive strength of concrete, respectively. This outcome validates the decision to model these materials as linear elastic mediums in the study, demonstrating that this approach accurately captured the behavior of the materials under the applied loads without reaching their respective yield or failure points. A study by Eom and Nowak (2001), after testing 17 steel I-girder bridges in Michigan, also concluded that the linear, elastic, and isotropic modeling assumptions are valid under live load applications throughout their investigation.

In the study, specific material properties were used for reinforced concrete and steel, in line with the provisions of the AASHTO LRFD:

1. Reinforced Concrete:
    a. Compressive Strength: Set at 4.0 ksi, as per AASHTO LRFD Section 5.4.2.4.
    b. Modulus of Elasticity: Determined to be 3640 ksi.
    c. Poisson's Ratio: Taken as 0.2, following AASHTO LRFD Section 5.4.2.5.
2. Steel:
    a. Yield Strength: Assumed to be 50 ksi, in accordance with AASHTO LRFD Section 6.4.1.
    b. Modulus of Elasticity: Set at 29000 ksi.
    c. Poisson's Ratio: Taken as 0.3.

These material properties were integral in ensuring that the modeling and analysis were conducted in compliance with recognized engineering standards and reflected realistic behavior under applied loads.

4.2.3 Mesh Discretization

AASHTO LRFD Section 4.6.3.3 sets forth specific guidelines for modeling beam-slab bridges, which were carefully followed in the study's mesh discretization for finite element models. Key among these guidelines is the aspect ratio of finite elements and avoiding abrupt changes in element shape. The aspect ratio, which is the ratio of the length to the width of the elements, should not exceed 5.0. This restriction helps in maintaining a balance between computational efficiency and the accuracy of the model. The design of the elements should be such that there are no sudden changes in their shape. This approach ensures a more uniform and accurate representation of the bridge structure in the model. The mesh discretization was designed to not only yield precise results but also to comply with the specifications outlined in the AASHTO LRFD.

Additionally, the chosen mesh densities were validated by previous research conducted by Michaelson (2010 and 2014), which demonstrated their effectiveness in accurately capturing the load response of composite steel bridges. This adherence to established guidelines and proven research methodologies underscores the reliability and accuracy of the finite element modeling conducted in the study. For the bridges in this study, the mesh discretization protocols utilized were as follows:

- Two elements were used along the widths of the top flanges.
- Three elements were used along the bend regions.
- Two elements were used along the flat portions of the webs.
- Two elements were used along the widths of the bottom flanges.
- Longitudinally, elements were discretized to be approximately 8 in. long.
- For the deck, transverse element widths were computed to generate elements with a target aspect ratio of 1.0.

4.2.4 Boundary Conditions and Multi-Point Constraints

In the models, the boundary conditions were set to mirror typical pin-roller conditions commonly used in bridge construction. Additionally, to reflect real-world scenarios, the ends of the girders were also restricted from lateral movement. These conditions were applied to the nodes located along the edges of the bottom flange of each girder, ensuring that the model accurately represented the physical constraints of an actual bridge. Figure 4.1 in the study illustrates a typical modeled bridge, highlighting the applied boundary conditions (marked in orange) and showcasing the mesh discretization. For the sake of clarity and ease of understanding, the MPC Beams, which are used to model the interaction between different components of the bridge, were omitted from this representation. This visual representation aids in understanding how the boundary conditions are applied in the model and how they interact with the overall structure.

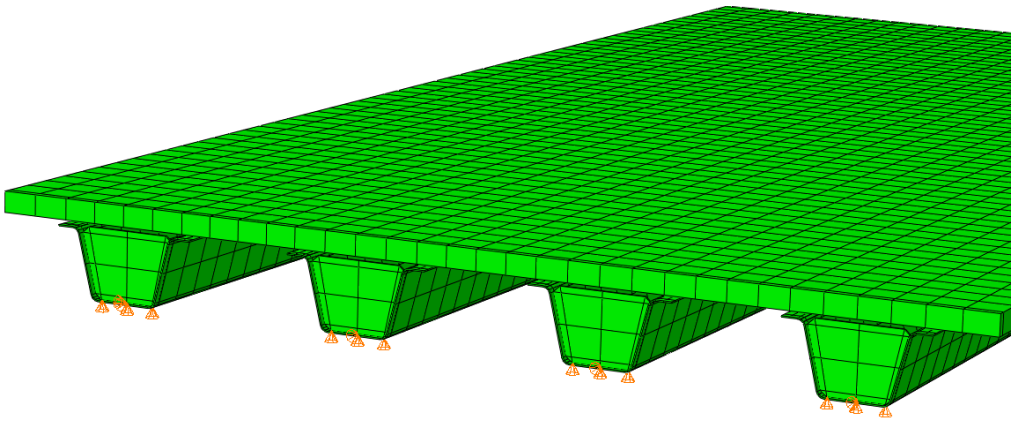

Figure 4.1 Abaqus model of the Flat Run bridge

4.3 LOAD APPLICATION

To compute live load distribution factors or to assess live load deflection characteristics, the bridges were loaded with the AASHTO LRFD BDS design truck to determine the distribution of this truck to exterior and interior girders, respectively. This section will provide a brief description of the design truck and the methodology behind loading the truck on the finite element models.

4.3.1 Live Load Applications

4.3.2 Description of HL-93 Truck Loading

The HL-93 is defined in AASHTO LRFD Section 3.6.1.2. Specifically, the load model consists of a combination of the following:

- The design lane load is a uniformly distributed load of 0.64 kips per foot of the bridge.
- The design truck – commonly referred to as HS 20-44 – is described in section 3.2 of this document.

4.3.3 Placement of AASHTO Truck Loading

When determining the placement of design trucks on bridges for maximum force effect analysis, AASHTO provides specific guidelines, particularly for simply supported bridges. These rules, along with their corresponding AASHTO references, are summarized as follows:

1. 3.6.1.1.1 - Determination of Design Lanes:
    a. The number of design lanes is calculated as the integer part of the clear roadway width divided by 12 feet (since the width of a design lane is 12 feet).
    b. For roadway widths between 20.0 and 24.0 feet, two design lanes are required, each being half of the clear roadway width.
2. 3.6.1.1.2 - Rear Axle Spacing:
    a. The rear axle spacing on the design truck should vary between 14 and 30 feet to produce extreme force effects, as depicted in the previous figure.
3. 3.6.1.3.1 - Transverse Placement of Design Trucks:
    a. Each design truck should be placed transversely within its design lane, which has a transverse width of 10 feet.

b. The center of the wheel of the design truck must be no closer than 2 feet from the edge of the design lane.

For studying the live load distribution on exterior girders, the design trucks were positioned as close to the edge of the bridge as allowable. In scenarios with a single lane loaded, this meant placing the truck 2 feet from the edge of the barrier. For multiple lane loadings, in compliance with the rules mentioned, the trucks were placed 6 feet apart laterally. The total number of trucks applied to each bridge model corresponded to the number of design lanes as determined by AASHTO Section 3.6.1.1.1. This approach was also replicated for the investigation of interior girder live load distribution, with the difference being the positioning of the first truck line directly over the girder line under study.

For the skewed bridges, an extra measure was taken to place the live load on the bridge. Figure 4.2 presents the aerial views of finite element models developed in Abaqus for analyzing the structural behavior of bridges with skew angles at -30 degrees and 30 degrees, respectively. These models are particularly useful for studying the effect of skew angles on the distribution of forces within the bridge structure.

As shown in Figure 4.3, the LLDF across a cross-section of both an exterior (left) and an interior girder. The graphs show the variation of LLDF for skew angles of -30 degrees and 30 degrees across five girders. The comparison between the two skew angles suggests that the orientation of the skew angle has a noticeable effect on the load distribution among the girders. Notably, the girders closer to the acute angle of the skew tend to have higher LLDF values, highlighting the impact of bridge geometry on load distribution.

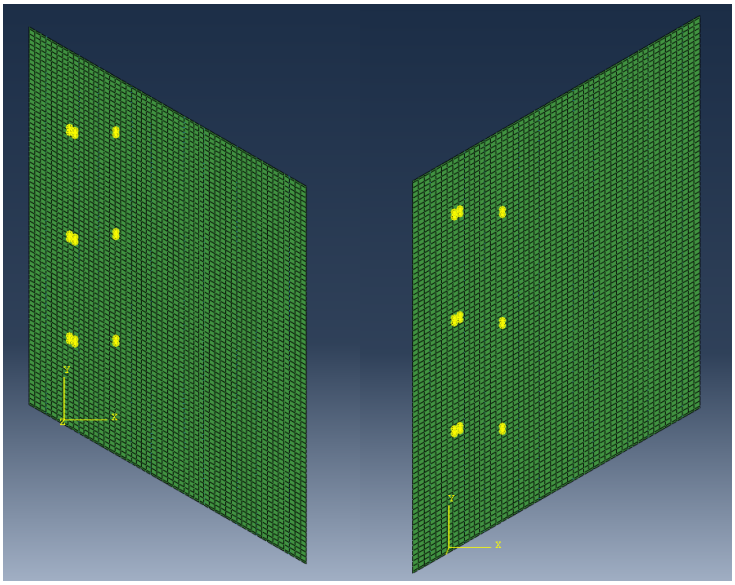

Figure 4.2 Abaqus model ariel view of skew angles at -30 degrees (left) and 30 degrees (right)

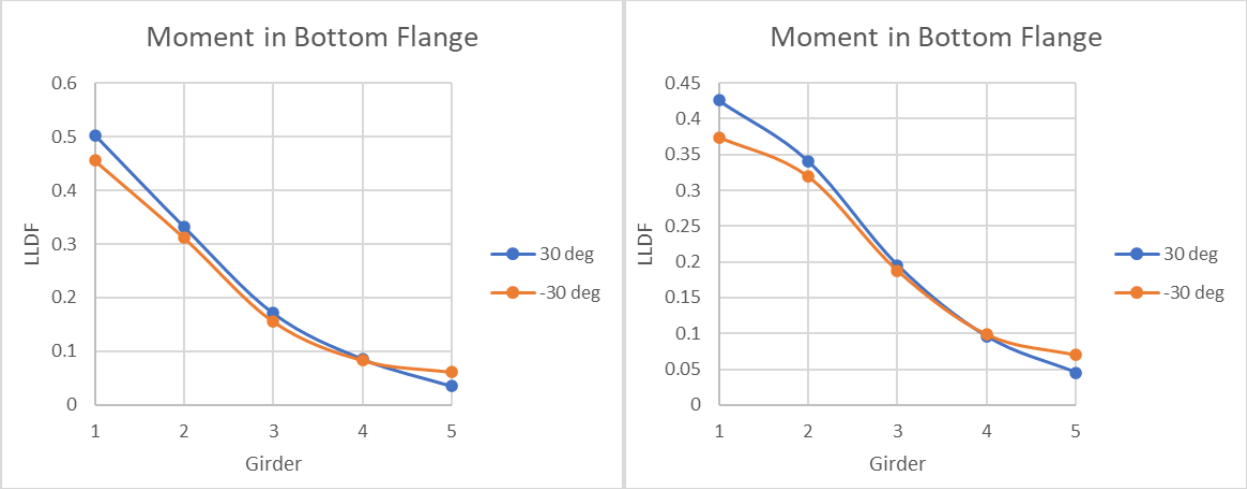

Figure 4.3 Live load distribution across a cross-section of an exterior (left) and interior girder in PBFTG bridge.

As for the longitudinal placement of the live loads on bridges, the theory of influence lines was used to place the trucks longitudinally (McCormac 2007). After investigation, the maximum moment in simple-span beams was determined to occur when rear axle spacing was at its minimum specified value of 14 ft. Once the load truck placement was determined, the wheel point loads on the elements were linearly distributed to the neighboring node.

4.3.4 Nodal Placement of Load

Once the load truck placement position was determined, the wheel point loads on the elements were linearly distributed to the neighboring nodes. A schematic of this loading is shown in Figure 4.4. Also, the following four equations describe the nodal loads shown in this figure. According to AASHTO LRFD Section 4.6.3.3.1, nodal loads shall be statically equivalent to the actual loads being applied. It can be easily shown that the equations corresponding to the following figure, once summed, will equal the applied point load.

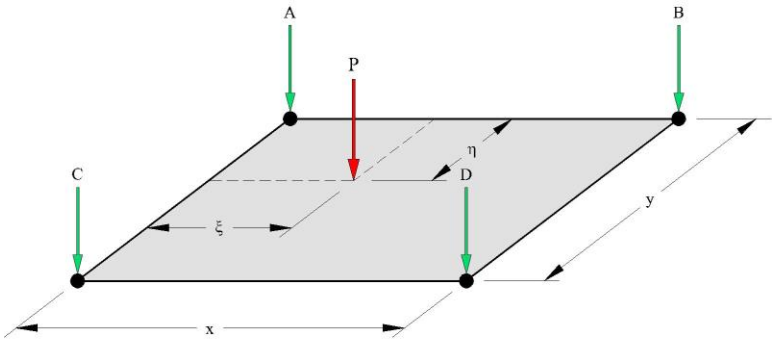

Figure 4.4 Nodal distribution of wheel loads

$$A = P\left(1 - \frac{\xi}{x}\right)\left(1 - \frac{\eta}{y}\right) \qquad (Eq. 4-1)$$

$$B = P\left(\frac{\xi}{x}\right)\left(1 - \frac{\eta}{y}\right) \qquad (Eq. 4-2)$$

$$C = P\left(1 - \frac{\xi}{x}\right)\left(\frac{\eta}{y}\right) \qquad (Eq. 4-3)$$

$$D = P\left(\frac{\xi}{x}\right)\left(\frac{\eta}{y}\right) \qquad (Eq. 4-4)$$

4.4 Computation of Live Load Distribution Factors

For calculating distribution factors from finite element data, two predominant methodologies are recognized. The first, known as the Stallings/Yoo method, calculates the distribution factor by dividing the moment in the beam under study by the sum of moments in all

beams, a technique detailed in research by Stallings and Yoo in 1993. The second approach termed the Tarhini/Frederick method, involves dividing the moment in the targeted beam by the moment derived from a line-girder analysis, which utilizes the same loads as the finite element model. This method was introduced by Tarhini and Frederick in their 1992 research. Each method provides a distinct perspective on analyzing and interpreting finite element data to determine distribution factors, highlighting different aspects of beam behavior under load. Previous research by Tennant (2022) has shown that the Tarhini/Frederick method gives appropriate results when computing live load distribution factors; therefore, this method was used exclusively for this research. Also, since the section moduli for each of the girders in the proposed system are identical, the computation of distribution factors is simplified by the equation below:

$$DF_i = \frac{M_i}{M_{LGA}} = \frac{\sigma_i S_i}{\sigma_{LGA} S_i} = \frac{\sigma_i}{\sigma_{LGA}} \qquad (Eq. 4-5)$$

- DF_i = distribution factor of ith girder
- M_{LGA} = bending moment computed using line girder analysis
- σ_i = longitudinal bending stress of ith girder
- S_i = section modulus of ith girder

4.5 Validation of Finite Element Modeling Techniques

Benchmarking FEA is a crucial step in validating computational models by comparing them against experimental results. This process ensures that the FEA tool generated is capable of predicting real-world behavior under various conditions. Several Researchers (Michelson, 2014; Kelly, 2014; Roh, 2019; Tennat, 2022) developed FEA tools and benchmarked them against field and laboratory experiments. For this study, three field experiments were chosen to be benchmarked against analytical modeling. The goal was to determine the degree of correlation and to fine-tune the FEA modeling techniques for better accuracy. The comparison was carried out using a matched pair t-test.

The matched pair t-test, also known as the paired sample or dependent sample t-test, is a statistical method designed to compare two related samples. It is instrumental in situations where

the same subjects are tested under two different conditions. The essence of the test lies in examining the mean difference between these pairs to test the null hypothesis, which posits no difference in the group means. The t-statistic is calculated based on this mean difference, considering the sample size and the standard deviation of the differences. The significance of the test result is determined by comparing the t-statistic to a critical value from the t-distribution, helping to ascertain whether the observed differences are statistically significant or likely due to chance.

4.5.1 Amish Sawmill Bridge

Gibbs (2017) utilized live load field testing with an HS-20 equivalent loading – a standard measure for highway loadings – to assess the live load distribution. This empirical data provided a basis to verify the accuracy of the computational model. Figure 4.5 depicts the comparison between experimental and analytical values.

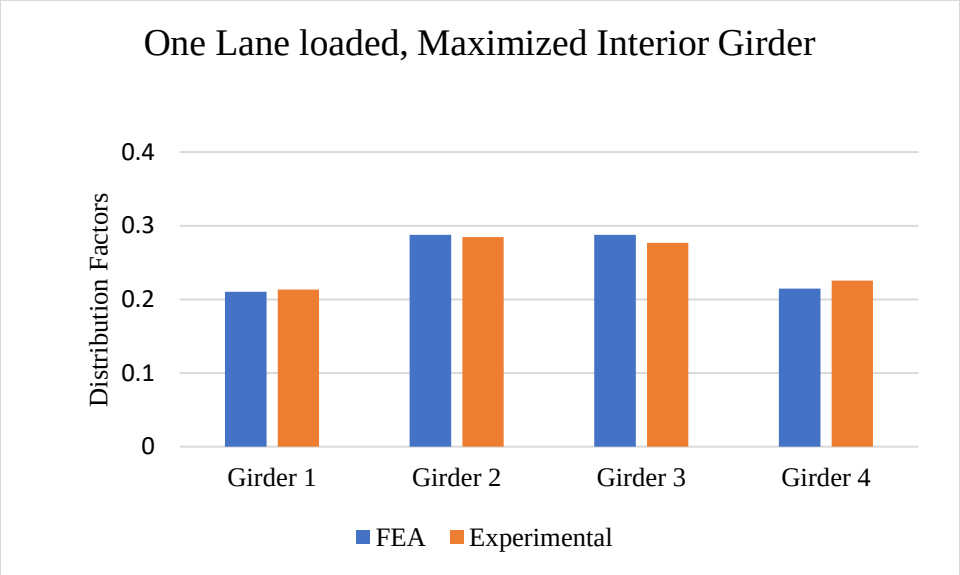

Figure 4.5 Amish Sawmill Bridge analytical vs. experimental LLDFs

In the matched pairs t-test conducted to compare the experimental and FEA LLDFs, the results indicate a negligible difference between the two methodologies, as shown in Table 4-1. The mean difference between the experimental and FEA results was extremely small, measured at 2.5e-10, suggesting an almost identical value between the two methods. The t-ratio was a low value of 2.854e-8, which when considered alongside the high probability values (Prob > |t| = 1.0000), indicates that the observed differences could largely be attributed to random variability rather than

systematic discrepancies between the experimental and FEA methods. The sample, comprising four matched pairs (N = 4), yielded a high correlation coefficient of 0.99344, reinforcing the strong positive relationship between the two sets of measurements. The conclusion is that there is no significant difference between the experimental and FEA live load distribution factors. This analysis underscores the reliability of FEA as a predictive tool in this context, aligning closely with experimental outcomes and demonstrating its robustness for practical applications.

Table 4-1 Matched pair t-test result for Amish Sawmill Bridge

LLDF - FEA	0.25
LLDF - Exp	0.25
Mean Difference	2.5e-10
Std Error	0.00876
Correlation	0.99344
t-Ratio	2.854e-8
DF	3
Prob > |t|	1.0000

4.5.2 Flat Run Bridge

The Flat Run Bridge is a 56 ft long, single-span PBFTG bridge in Marion County, West Virginia. The bridge consisted of four fully composite modular components, each brought to the site by truck and lifted into place by crane. A 96-inch wide by 0.5-inch thick plate of AASHTO M270 was used for the PBFTGs. Experimental live load field testing was performed with the goal of comparing measured strains due to physical loading to strains determined from analytical modeling to assess the performance of the structure. The BDI STS Wi-Fi Data Acquisition System was used to instrument the structure and record results. Twenty strain gauge locations were identified for this field test; three gauges were located on the bottom of each girder (12 total), and two gauges were located on each web (8 total). Gauges were placed at 0.3L to allow for easier access for preparation and removal. The bridge deck was systematically marked, creating a grid that identified panel points, which subsequently determined the precise locations for truck placements during testing. The truck passes, which refer to the transverse spacing of the truck path, and panel points, indicating the truck's longitudinal position, were identified to maximize loading on specific girders. Strain values from multiple passes were superimposed for each girder to simulate various multi-lane-loaded scenarios. The AASHTO LRFD BDS were found to be

conservative, with the field performance exceeding the performance expected using the empirical equations. Figure 4.6 shows the comparison of LLDFs obtained from FEA.

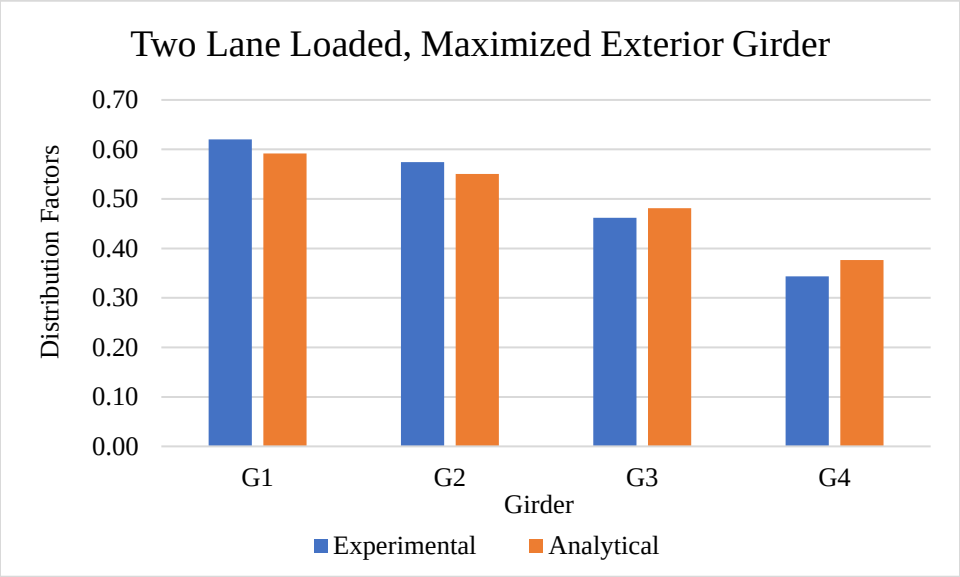

Figure 4.6 Flat Run bridge analytical vs. experimental LLDFs

Similar to the results for the Amish Sawmill Bridge, the results for the Flat Run bridge strongly indicate the consistency between the experimental and FEA LLDFs, demonstrating their close alignment and suggesting that they are likely predicting the same value. The result is summarized in Table 4-2.

Table 4-2 Matched pair t-test result for Flat Run Bridge

LLDF - FEA	0.5
LLDF - Exp	0.5
Mean Difference	-3e-10
Std Error	0.01512
Correlation	0.99593
t-Ratio	-1.65e-8
DF	3
Prob > |t|	1.0000

4.5.3 Fourteen Mile Bridge

The Fourteen Mile Bridge presented an ideal specimen for benchmarking due to its distinctive design features. The bridge's skew angle of 10° and superelevation of 8% introduce

complexities in structural behavior that are more common in standard bridge designs, thus providing a variety of features, such as skew, for testing the accuracy of FEA modeling techniques. Figure 4.7 illustrates the comparison of LLDFs obtained from FEA.

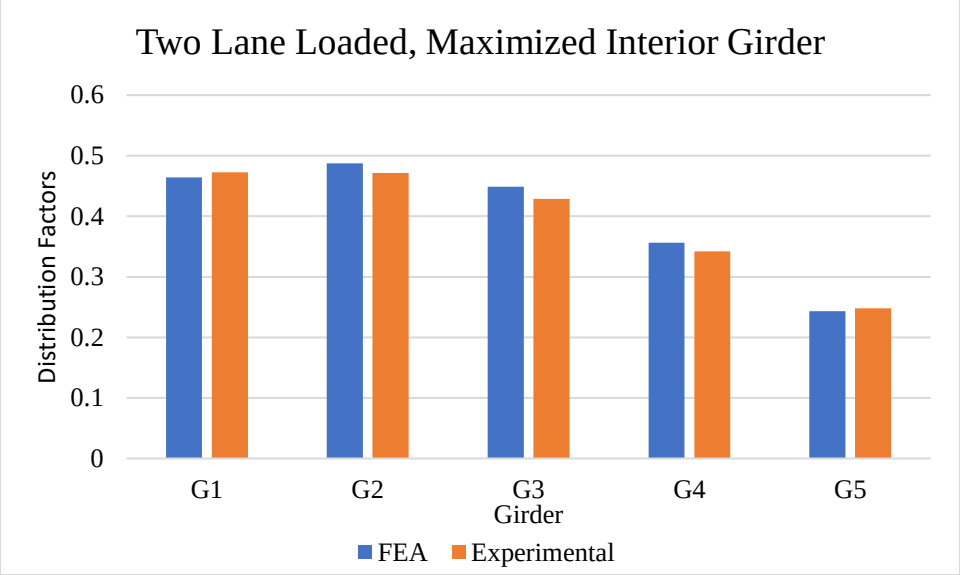

Figure 4.7 Fourteen Mile bridge analytical vs. experimental LLDFs

The matched pairs t-test results for the Fourteen Mile Bridge reveal a subtle, yet not statistically significant, difference between the experimental and FEA LLDFs. The mean difference between the two LLDFs stands at -0.0074, indicating that experimental values are marginally lower than those computed using FEA. The t-ratio of -1.26869, while negative, is not substantial enough to denote a significant deviation from the null hypothesis, which posits no difference. Additionally, a high correlation coefficient of 0.99206 reinforces the strong positive relationship between them. Therefore, these findings collectively indicate a negligible, statistically non-significant difference between the experimental and FEA LLDF values.

Table 4-3 Matched pair t-test result for Fourteen Mile Bridge

LLDF - FEA	0.39258
LLDF - Exp	0.4
Mean Difference	-0.0074
Std Error	0.00585
Correlation	0.99206
t-Ratio	-1.26869
DF	4
Prob > |t|	0.2734

4.6 SUMMARY

The previous chapter provided a detailed overview of the finite element modeling techniques employed in this research project. It comprehensively covered various critical aspects, including the selection of elements, definitions of materials used, the process of mesh discretization, the boundary conditions applied, and the methods of load application.

CHAPTER 5: LIVE LOAD DISTRIBUTION FACTOR FOR MOMENT IN INTERIOR GIRDER

5.1 DATA DESCRIPTION

The two comprehensive studies, NCHRP 12-26 (1991) and Tarhini and Frederick (1992) served as the basis for creating a data set by varying crucial design parameters. The following parameters were varied throughout the matrix to determine their influence on interior girder live load distribution:

1. Four PBFTG plate sizes:
    i. 72 inches wide by 0.5 inches thick, with a span length from 20 feet to 45 feet in 5-foot increments. I = 1635 in^4, 5432 bridges,
    ii. 84 inches wide by 0.4375 inches thick, with a span length from 40 feet to 55 feet in 5-foot increments. I = 4781 in^4, 3888 bridges,
    iii. 96 inches wide by 0.5 inches thick, with a span length from 45 feet to 60 feet in 5-foot increments. I = 4781 in^4, 3888 bridges, and
    iv. 120 inches wide by 0.625 inches thick with a span length from 60 feet to 90 feet in 5-foot increments. I = 12285 in^4, 4760 bridges.
2. Four numbers of girders in the cross-section: 4, 5, 6, 7, and 8 girders.
3. Five girder spacings: 5 feet to 9 feet in 1-foot increments.
4. Five deck thicknesses: 8 inches to 9.5 inches in 0.5-inch increments.
5. Five overhang ratios: 0 inches to 24 inches in 6-inch increments.
6. One-lane and two-lane loading scenarios.

The dataset for this project includes the analysis of the 19,152 PBFTG bridges using three-dimensional finite element analysis that provided crucial insights into the live load distribution behavior. This data is used to produce simplified empirical equations that better predict live load moment distribution in PBFTGs, considering the impact of uncertainty in designing PBFTG bridges.

5.2 EXPLORATORY DATA ANALYSIS

The Exploratory Data Analysis (EDA) of this study was performed to gain a deeper understanding of the data produced from the FEA of the 19,152 PBFTG bridges. The data was

split into two-lane loading scenarios: 9800 one-lane loaded and 9352 two-lane loaded. EDA is an essential step in data analysis as it facilitates the visualization, identification of patterns, and extraction of qualitative insights from the data. Descriptive statistics, graphical representations, and correlation analysis were used to summarize and visualize the data and explore the interaction of dependent and potential independent variables.

The descriptive statistics of the dependent variable, LLDF, were calculated. For this dataset, descriptive statistics of the dependent variables were not performed since the data comes from a “rigged” variable matrix. (i.e., the dependent variables were chosen, and the independent variable was obtained from analysis). The descriptive statistics on LLDF include measures of central tendency (mean), measures of dispersion (standard deviation and range), and the shape of the data distribution (skewness and kurtosis). These metrics give us an overall picture of the data distribution and variability, which are essential in identifying patterns, outliers, and possible data issues.

Table 5-1: Summary of Descriptive Statistics for interior girder LLDF

Statistics Measures	One Lane Loaded	Two Lanes Loaded
Mean	0.3697054	0.4914331
Std Dev	0.0524329	0.0615760
Skewness	0.9561108	0.2339199
Kurtosis	1.1898239	-0.4416540
Range	0.3103144	0.3151386

As shown in Table 5-1, under the one-lane loaded condition, the mean LLDF is approximately 0.370, indicating that, on average, about 37.0% of the vehicle loading is distributed to an individual girder. The standard deviation of 0.0524 suggests a moderate dispersion in LLDF values, reflecting variations in the distribution of live loads across different girder bridges. The skewness value of 0.9561 implies a more pronounced positive skew in the data, suggesting that the distribution is skewed towards lower values, with some higher-value outliers. Kurtosis, which gauges the "tailedness" of the data distribution, stands at 1.1898, indicating a distribution with tails that are less extreme than a normal distribution but with a sharper peak.

For the condition of two lanes loaded, the mean LLDF value rises slightly to 0.4914, which is expected to be higher than the one-lane loaded case since the bridge is loaded with two vehicles. The standard deviation is higher at 0.0616, suggesting a moderately wider distribution of LLDF values compared to the one-lane loaded scenario. The skewness drops significantly to 0.2339, indicating a distribution closer to symmetry around the mean. The kurtosis is negative at -0.4417, signifying a distribution that is flatter than a normal distribution, indicating less extreme values in the tails. This data depicts the nuances in live load distribution between one-lane and two-lane loaded scenarios, providing a general understanding of the load distribution dynamics in these varying conditions. Figure 5.1 provides the distribution of the LLDFs for one-lane and two-lane loaded scenarios for interior girders.

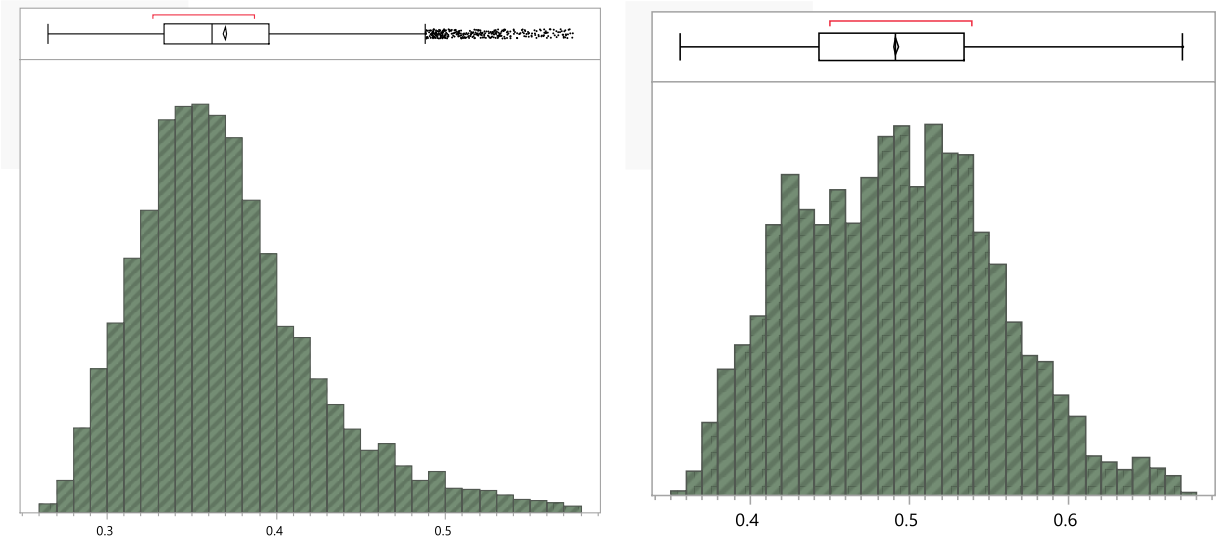

Figure 5.1. LLDF Distribution for (a) one-lane loaded and (b) Two-lane loaded scenarios.

Graphical representations, including histograms, box plots, and scatter plots, were utilized to visualize the data. Histograms and box plots allowed for the understanding of the distribution of LLDFs identified outliers, and visualized data spread. After careful consideration, the outliers were not excluded from the analysis because the outlier bridges represented a potential bridge to be built on the field. Scatter plots, on the other hand, enabled the visualization of the relationships between the different variables in the dataset and served as a basis for the development of the empirical equations. For instance, Figure 5.2 illustrates a positive correlation between Spacing and LLDF, indicating that as the spacing increases, the LLDF value also tends to rise, irrespective of the span length. This consistent upward trend is observed across all span lengths, suggesting that

the relationship between spacing and LLDF remains stable regardless of variations in span length. However, upon closer inspection, the steepness of the correlation, represented by the slope of the blue lines, appears to differ among the sections. The section for the span length range "20 - 40" shows the steepest slope, implying that in this specific range, LLDF - FEA values exhibit a more pronounced sensitivity to changes in spacing. Meanwhile, the overall y-axis range for LLDF is confined between approximately 0.30 and 0.50, highlighting a specific interval of change. Dividing the graph based on span length offers a granular perspective on how the relationship between spacing and LLDF might be consistent or divergent across different span lengths. Such insights could be pivotal for design or engineering decisions, especially when fine-tuning for span lengths and spacings. It was identified throughout the EDA that there are potential relationships or patterns between exterior LLDFs and Overhang distance and interior LLDFs.

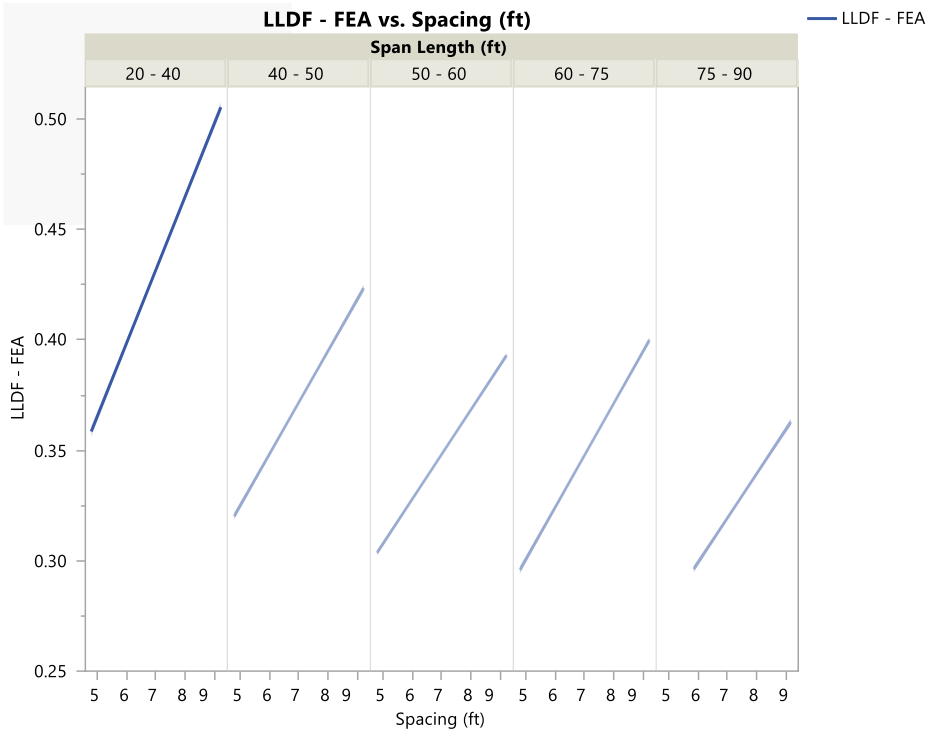

Figure 5.2. Line of Fit Plot of Interior Girder LLDFs grouped by span length and spacing.

A correlation matrix was also utilized to determine the correlation coefficients of exterior girder LLDF with all other variables. Each cell in Table 5-2 shows the correlation between two variables for one lane loaded scenario. A correlation coefficient ranges from -1 to 1, with -1

indicating a perfect negative correlation, +1 indicating a perfect positive correlation, and 0 indicating no correlation.

Table 5-2: Multivariate Correlation Coefficients for one lane loaded scenario in Interior Girders.

	Number of Beams	Spacing (ft)	Plate Size (in)	Deck Thickness (in)	Span Length (ft)	LLDF-FEA
Number of Beams	1.0000	0.0000	-0.0000	-0.0000	-0.0000	-0.1233
Spacing (ft)	0.0000	1.0000	0.1493	0.0000	0.1336	0.5657
Plate Size (in)	-0.0000	0.1493	1.0000	0.0000	0.8941	-0.4370
Deck Thickness (in)	-0.0000	0.0000	0.0000	1.0000	0.0000	-0.1032
Span Length (ft)	-0.0000	0.1336	0.8941	0.0000	1.0000	-0.6210
LLDF - FEA	-0.1233	0.5657	-0.4370	-0.1032	-0.6210	1.0000

The correlation matrix explains the relationships among various design parameters and the LLDF - FEA. The number of beams exhibits no discernible correlation (correlation coefficient = 0) with other variables such as spacing, plate size, deck thickness, and span length, yet has a slight negative correlation with LLDF - FEA), showing a minor decrease in LLDF - FEA as the number of beams increases. Spacing shows a moderate positive correlation with LLDF – FEA, indicating that an increment in the spacing between beams is associated with an increase in LLDF - FEA. A mild positive correlation is also observed with plate size and span length. Plate size displays a positive correlation with span length, confirming the obvious that there is a tendency for larger plates to be associated with longer spans, while a moderate negative correlation with LLDF - FEA is indicative of a decrease in LLDF - FEA as the plate size enlarges. Deck thickness portrays no correlation with other variables and a slight negative correlation with LLDF – FEA, indicating a marginal decrease in LLDF - FEA with increasing deck thickness. Span length, apart from its substantial correlation with plate size, shows a moderate negative correlation with LLDF - FEA, signaling a tendency for LLDF - FEA to decrease as the span length increases. The correlation coefficient of 1.0000 along the diagonal for LLDF - FEA is a standard characteristic of correlation matrices, representing a perfect positive correlation of a variable with itself, which confirms the reliability of the correlation matrix. The correlation coefficient matrix for the two-lane loaded scenario is shown in Table 5-3.

Table 5-3: Multivariate Correlation Coefficients for two lanes loaded scenario In Interior Girders.

	Number of Beams	Spacing (ft)	Plate Size (in)	Deck Thickness (in)	Span Length (ft)	LLDF - FEA
Number of Bea	1.0000	-0.0973	-0.0231	0.0000	-0.0207	-0.2980
Spacing (ft)	-0.0973	1.0000	0.1324	-0.0000	0.1185	0.8213
Plate Size (in)	0.0231	0.1324	1.0000	0.0000	0.8946	-0.1875
Deck Thickness (in)	0.0000	-0.0000	0.0000	1.0000	0.0000	-0.0645
Span Length (ft)	-0.0207	0.1185	0.8946	0.0000	1.0000	-0.3114
LDF - FEA	-0.2980	0.8213	-0.1875	-0.0645	-0.3114	1.0000

The results from the EDA are purely descriptive and do not imply causality. It is beneficial to investigate these relationships further with regression analysis to account for the interactions between variables. Furthermore, high correlations between the independent variables, which indicate multicollinearity, were found not to be a significant issue in the data. The relationships identified in this phase will be formally tested in the subsequent analysis using inferential statistics and model fitting.

5.3 EMPIRICAL EQUATION DEVELOPMENT

This study developed simplified empirical equations by modeling the LLDFs obtained from the parametric study for the 9,800 and 8,168 one-lane and two-lane loaded PBFTG bridges, respectively. The recommendation of the literature is followed to identify a suitable equation function structure and use the insights of the sensitivity analysis to identify potential independent variables. The NCHRP 12-26 study concluded that the relationship between the varied parameters and the LLDF can be captured and represented with a power function model (Zokei et al.1991), as shown in Eq. 4.

$$\boldsymbol{LLDF = c_0 x_1^{c_1}\, x_2^{c_2} \cdots x_k^{c_k}} \qquad (\boldsymbol{Eq.\, 5-1})$$

- DF is the distribution factor,
- c_i's are constants,
- x_i's are varied parameters, and
- k is the number of varied parameters.

Thus, the structure of the models developed were multiple log-log linear regression models (Eq. 5). Several other potential transformations were tested for the dependent and independent variables. The results corroborated the suggestions of NCHRP Report 12-26 (1991) and confirmed that a logarithmic transformation of the dependent variable (LLDF) and the independent variables provides the best fit.

$$\boldsymbol{log\,(LLDF)\;=\;log\,(c_0)+c_1 log\,(x_1)+c_2 log\,(x_2)+\cdots+c_k log\,(x_k)+\varepsilon} \qquad \boldsymbol{(Eq.\,5-2)}$$

- ε is the error term.

The qualitative assessment from the sensitivity analysis (Tennant, 2022) and the multivariate correlations identified the following potentially influential variables: spacing, span length, and girder size were identified as having a strong relationship with LLDF, and the number of beams and deck thickness as having a moderate relationship with LLDF. For statistical modeling, the longitudinal stiffness parameter was used to represent girder size. A series of models was developed aiming to maximize prediction power and ensure that the models are accurately specified to the extent possible, and the estimators are unbiased. Variations in bridge geometry and load placement are hypothesized to affect live load distribution in an unobservable manner that impacts the load-resisting mechanisms of a bridge. While the live load distribution can be predicted with a certain level of confidence, the three-dimensional interaction of load and resistance makes it challenging to observe this distribution precisely due to the complexities of load-resistance interactions. The model parameters were estimated using Ordinary Least Squares (OLS).

The Ordinary Least Squares (OLS) method was utilized to estimate the model parameters. OLS is a popular technique in linear regression used by several researchers (Michaelson 2010, Zoakie 1991), which assumes:

1. Linearity – the relationship between the independent and dependent variables is linear. This means that the line of best fit through the data points is a straight line rather than some grouping factor.
2. Independence – the residuals are independent. There is no correlation between consecutive residuals in time series data.

3. Homoscedasticity – the residuals have constant variance at every level of the independent variables. In other words, the spread of the residuals should be the same across all levels of the independent variables.
4. Normality – the residuals of the model are normally distributed.
5. No Multicollinearity – regression assumes that the independent variables are not perfectly linear functions of each other. If this condition is not met, it can be difficult to determine the independent effect of each variable on the dependent variable.
6. No Endogeneity – the error term should not be correlated with the independent variables. In other words, there should not be any omitted variables that are correlated with both the dependent variable and one or more independent variables.

Violations of these assumptions can lead to biased or inefficient estimates. Therefore, it is important to check these assumptions when using linear regression models. For this study, depending on the severity of the violation, decisions were influenced by a trade-off between addressing violations and maintaining the simplicity and usability of the prediction equations.

5.4 Regression Analysis

The development of predictive models is imperative to ensure safe and economical design; thus, several models were carefully produced to ensure accuracy, unbiased estimators, and maximized prediction power. The coefficient of determination (R^2) and other goodness-of-fit measures were used to evaluate the models, ensuring that they accurately represent the data's underlying patterns. Variations in the specificity of bridge geometry and load placement were theorized to affect live load distribution in a manner that's not directly observable but impacts the bridge's load-resisting mechanisms.

Four models for each lane loading scenario using the two functional forms mentioned above were compared for the goodness of fit measures, such as R^2 (shown in Table 5-4). These measures were only utilized to compare models that fit the same dataset. The functional form in Equation 5 – 1 was deemed appropriate for both one-lane loaded and two-lane loaded scenarios, confirming the suggestions of NCHRP Report 12-26 (1991) to be appropriate. For this study, only two models are discussed in depth.

Table 5-4: Summary of Goodness of Fit for both one-lane and two lanes loaded scenarios, respectively

RSquare	0.952518	0.934813
RSquare Adj	0.952494	0.934778
Root Mean Square Error	0.029675	0.03203
Mean of Response	-1.00454	-0.71828
Observations	9800	9352

Table 5-5 and Table 5-6 provide the estimates of the one-lane loaded and two-lane loaded models, respectively. The model aims to predict the dependent variable, interior girder LLDF, based on several independent variables. The table reflects a statistical analysis where the coefficients for each independent variable, number of beams, spacing, deck thickness, span length, and moment of inertia, are assessed for their impact on a dependent variable. Starting with the intercept at -0.561415, it signifies the expected value of the dependent variable when all predictors are at their baseline level (log-transformed baseline is 1). Its standard error is relatively low at 0.01168, and an extremely high t Ratio of -48.07 suggests the intercept is significantly different from zero. The coefficient for the log-transformed number of beams is -0.080814, again with a very low standard error, indicating a precise estimate and a significant negative impact on the dependent variable. Its t Ratio of -66.03 further confirms its significance, and a VIF of 1 implies no multicollinearity. Spacing has a positive coefficient of 0.4506969 with an exceptionally high t Ratio, indicating a strong positive effect on the dependent variable and a VIF of 1.0270791, pointing to minimal multicollinearity.

Table 5-5: Ordinary Least Squares regression models parameter estimates for one-lane loaded scenario

Term	Estimate	Std Error	t Ratio	Prob>|t|	VIF
Intercept	-0.561415	0.01168	-48.07	<.0001*	
Log(Number of Beams)	-0.080814	0.001224	-66.03	<.0001*	1
Log(Spacing (ft))	0.4506969	0.001546	291.54	<.0001*	1.0270791
Log(Deck Thickness (in))	-0.245094	0.00469	-52.26	<.0001*	1.0041591
Log(Span Length (ft))	-0.380623	0.001516	-251.1	<.0001*	3.7230019
Log(Kg (in^4))	0.0689717	0.000794	86.91	<.0001*	3.7631765

Deck thickness presents a negative coefficient (-0.245094) with a standard error that maintains the estimate's precision and a significant t Ratio, denoting a substantial impact on the dependent variable while exhibiting almost no multicollinearity (VIF of 1.0041591). The span length's coefficient is also negative (-0.380623), with a high t Ratio, implying a pronounced effect, but with a VIF of 3.7230019, there is a moderate suggestion of multicollinearity. Lastly, the moment of inertia has a positive relationship with the dependent variable, indicated by a coefficient of 0.0689717 and an exceptionally low p-value; however, its VIF of 3.7631765, like span length, indicates a moderate level of multicollinearity that is expected since the longer the span, the higher longitudinal stiffness needed to resist loads.

Table 5-6 Ordinary Least Squares regression models parameter estimates for two-lane loaded scenario

Term	Estimate	Std Error	t Ratio	Prob>|t|	VIF
Intercept	-0.961192	0.013053	-73.63	<.0001*	
Log(Number of Beams)	-0.125922	0.001412	-89.19	<.0001*	1.0129996
Log(Spacing (ft))	0.5530908	0.001764	313.53	<.0001*	1.0339962
Log(Deck Thickness (in))	-0.134614	0.005182	-25.98	<.0001*	1.0041231
Log(Span Length (ft))	-0.199111	0.00168	-118.5	<.0001*	3.7586292
Log(Kg (in4))	0.0372239	0.000876	42.51	<.0001*	3.7912726

5.5 DIAGNOSTIC TESTS

5.5.1 Linearity

The linearity assumption was checked visually by plotting the observed vs. predicted values or residuals vs. predicted values, as shown in Figure 5.3. A non-random pattern might indicate a problem with linearity. For both loading scenarios, no systematic observable deviation was noticed.

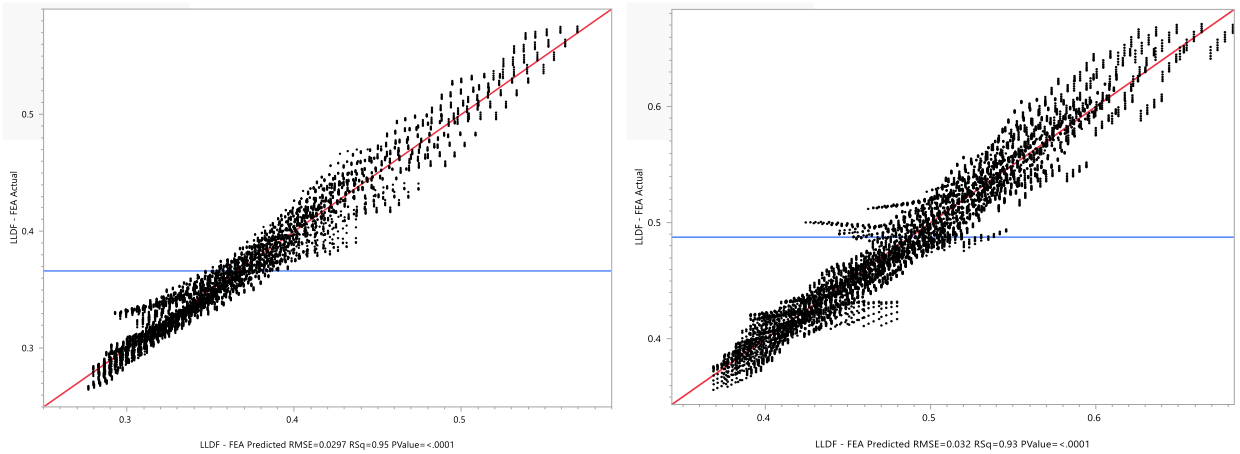

Figure 5.3. Predicted by Actual plots for (a) one-lane loaded and (b) two-lane loaded scenarios.

5.5.2 Independence

Independence was tested using the Durbin-Watson test, which tests for autocorrelation in the residuals. Durbin-Watson values range from 0 to 4. A value around 2 indicates no first-order autocorrelation, while values below one or above 3 indicate positive and negative first-order autocorrelation, respectively. For both loading scenarios, as shown in Figure 5.4, no serial autocorrelation was detected (a Durbin-Watson value of 2.01 was computed for both scenarios). This was expected, given the nature of the data.

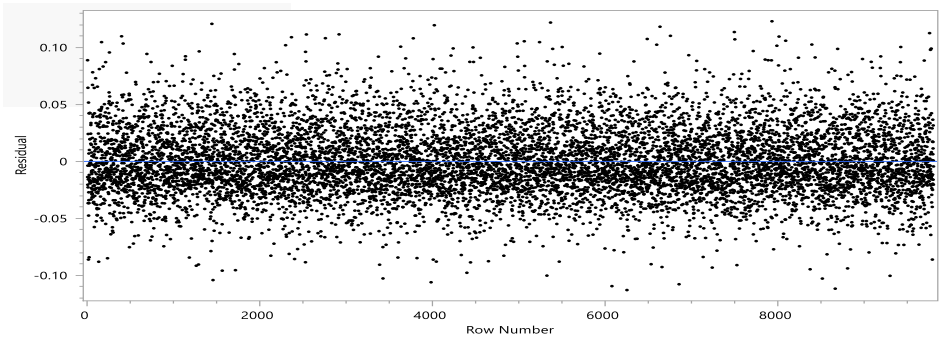

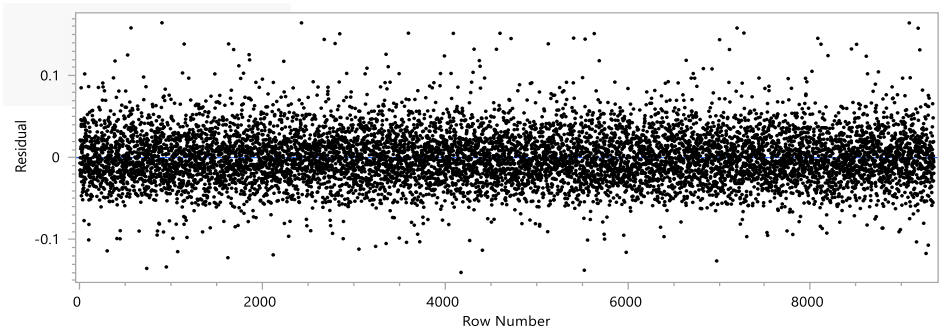

Figure 5.4. Residuals by Row Plots for (a) one-lane loaded and (b) two-lane loaded scenarios.

5.5.3 Equality of Error Variance

The equality of error variance was visually inspected by looking at a plot of the residuals vs. predicted values – the spread of residuals should be constant across all levels of the predicted values, as illustrated in Figure 5.5. A more formal test for homoscedasticity is the Breusch-Pagan test, but JMP does not have the functionality to do the test.

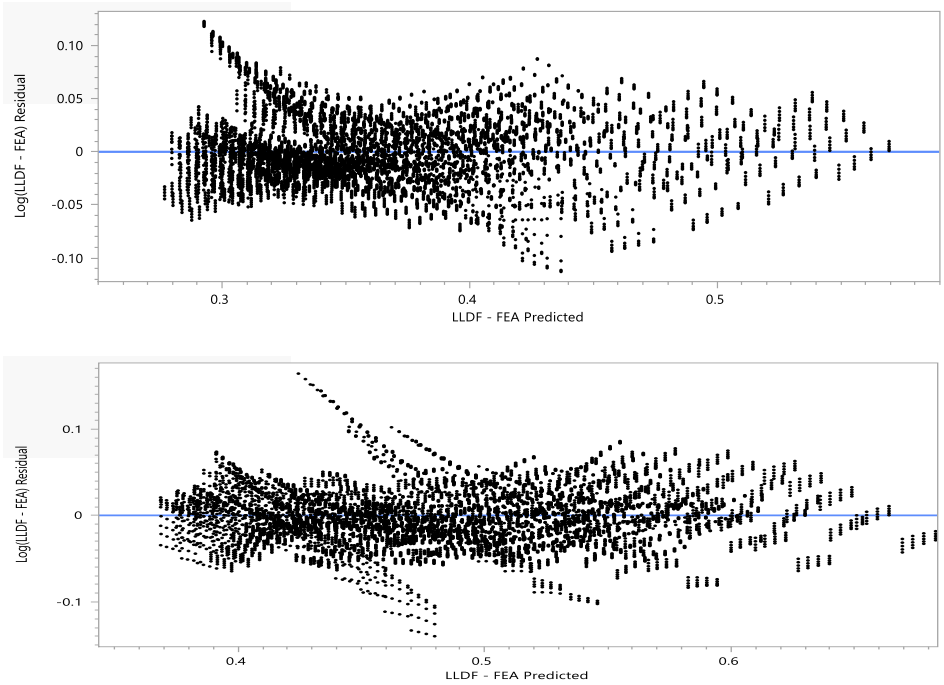

Figure 5.5. Residuals by Predicted Plots for (a) one-lane loaded and (b) two-lane loaded scenarios.

A test of variance for a split sample was performed in the absence of the Breusch-Pagan test in JMP. To quantify the variance equality, the sample was split based on the median value of the prediction, and the variance of the two groups was compared. If the variances in the two groups are substantially different, it could be an indication of heteroscedasticity. This approach provided some insight into the homoscedasticity of the error terms, which is parallel to Levene's test, where whether the variance is the same across different groups is checked.

The test resulted in rejecting the null hypothesis that the variances are equal. However, this method does have its limitations. The data is split into only two groups, and heteroscedasticity could potentially be more complex, with the variance of the errors changing in a non-linear way across the range of the independent variables. It is worth mentioning that Levene's test is sensitive to departures from normality. Thus, if the data are not normally distributed, Levene's test might be significant even if the variances are equal. In the presence of heteroscedasticity, the estimates of the regression coefficients themselves remain unbiased. The main problem with heteroscedasticity is that it can lead to inefficient estimates (i.e., estimates with larger standard errors than necessary).

5.5.4 Normality of Error

Normality can be checked visually by looking at a histogram of the residuals or a QQ plot - the points should fall roughly along a straight line, as depicted in Figure 5.6. More formal tests, such as the Shapiro-Wilk test, are sensitive to the number of observations and result in significance that the residuals are not normally distributed. For this project, the distribution of the errors was accepted to be a normal distribution. If the errors are not normally distributed, it can affect the validity of certain statistical tests, like the t-test or F-test, that are used to determine the significance of coefficients.

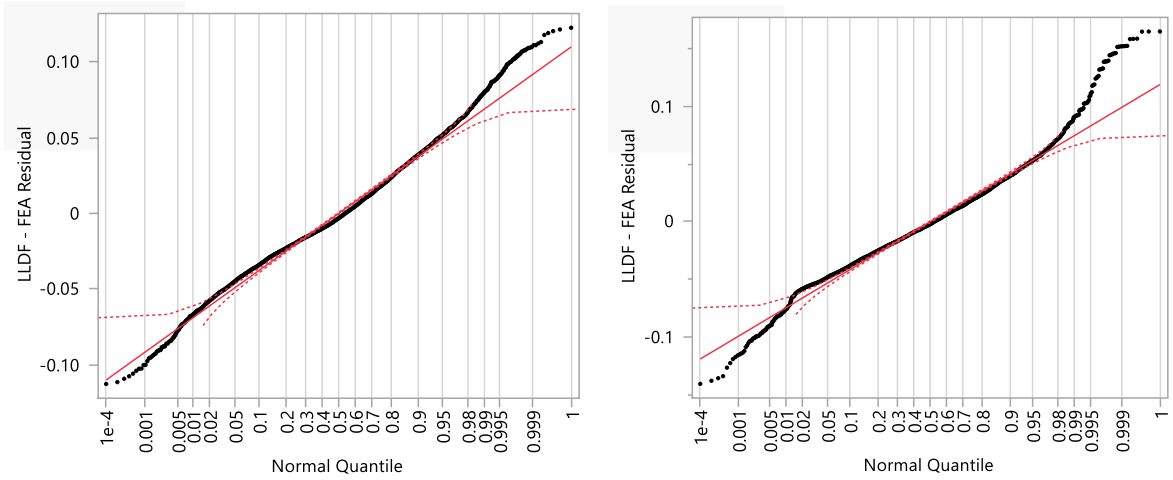

Figure 5.6. Histogram of the residuals and a QQ plot for (a) one lane loaded and (b) two lanes loaded scenarios.

5.5.5 Multicollinearity

When multicollinearity is present, it can make it difficult to determine the effect of each predictor variable on the response variable independently of the others. This can lead to unstable estimates of the regression coefficients (they can change erratically in response to small changes in the data or the model), and it can make the estimates very sensitive to small changes in the model. The Variance Inflation Factor (VIF) quantifies how much the variance of the estimated regression coefficients is increased due to multicollinearity. VIF is always greater than or equal to 1. A VIF of 1 indicates that there is no correlation among the k^{th} predictor and the other predictors. As a rule of thumb, a VIF value that exceeds 5 or 10 indicates a problematic amount of multicollinearity.

For one lane loaded, both variables had a VIF of approximately 1.04, which suggests that multicollinearity is not a problem in the data. For a two-lane loaded case, Spacing and Computed interior LLDF have a VIF of approximately 2.7. Though higher, it is still well below the threshold of 5 or 10, often used as a benchmark, suggesting that the predictor associated with this VIF is only moderately correlated with the other predictors. This outcome is expected since spacing was one of the independent variables in the computed interior LLDF. Based on these VIF scores, the assumption of the absence of multicollinearity is satisfied for the model, i.e., each variable brings some unique information to the model.

5.5.6 Endogeneity

A correlation test was performed between residuals and independent variables. No correlation was found statistically significant, as shown in Table 5-7; this suggests no endogeneity.

Table 5-7: Correlation test between Residuals and independent variables

	Residual	Number of Beams	Spacing (ft)	Deck Thickness (in)	Span Length (ft)	Kg (in4)
One-Lane Loaded LLDF Residual	1.0000	0.0273	0.0188	-0.0001	-0.0370	0.0024
Two-Lane Loaded LLDF Residual	1.0000	0.0368	0.0034	-0.0002	-0.0567	-0.0186

The models were found free of any severe problems, suggesting that they meet the assumptions of the linear regression to an acceptable extent and can provide reliable, unbiased estimates for predicting live load distribution factors.

5.6 PROPOSED EQUATIONS

The models explained approximately 95.2% and 93.4% of the data variability for the one-lane loaded bridges and for the two-lane loaded bridges, respectively.

Following the determination of the coefficients, c_i's the coefficients were rounded to two or three decimal places, according to the industry practices. Subsequently, each equation was multiplied by a modification factor, 1.20 for Eq. 5 – 3 and 1.16 for Eq. 5 – 4, to ensure conservative predictions. By definition, the OLS estimation technique minimizes the sum of squares of errors (i.e., the differences between the actual LLDFs and the predicted LLDFs), and thus, the resulting equations are expected to roughly underestimate half and overestimate the other half of the LLDFs. The modification factors were estimated with the goal of accurately predicting or overpredicting 100% of the LLDFs, using a 95% prediction interval (PI) for the individual predicted LLDFs based on the existing bridge sample. This prediction interval corresponds to approximately 98% confidence interval (CI) for the average expected LLDFs based on the sample.

Eq. 5 – 3 and 5 – 4 are the final equations proposed to calculate LLDFs for PBFTG bridges.

For interior girders with one-lane loaded:

$$\boldsymbol{LLDF = 0.685\frac{S^{0.45}}{L^{0.38}}\left(\frac{K_g^{0.7}}{N_b t_s^{2.5}}\right)^{0.1}} \qquad (\boldsymbol{Eq. 5-3})$$

For interior girders with two-lane loaded:

$$\boldsymbol{LLDF = 0.455\frac{S^{0.55}}{L^{0.2}}\left(\frac{K_g^{0.4}}{N_b t_s^{1.5}}\right)^{0.1}} \qquad (\boldsymbol{Eq. 5-4})$$

- $LLDF$ is the live load distribution for the corresponding number of loaded lanes,
- S is girder spacing in feet,
- L is the span length in feet,
- N_b is the number of girders, and
- t_s is the deck thickness in inches.

5.7 SUMMARY

The preceding chapter discusses the development of LLDFs for the moment in an interior girder of PBFTGs and gives a statistical assessment of the method of developing the equation through an empirical equation.

CHAPTER 6: LIVE LOAD DISTRIBUTION MODIFICATION FACTORS FOR EXTERIOR GIRDER AND SKEW

6.1 EXTERIOR GIRDER LLDF MODIFICATION FACTOR

This Section focuses on the development of LLDF modification factors applicable to exterior girders, aligning with the AASHTO LRFD BDS. The approach resembles the established equations for Steel I-girders, ensuring that the LLDF Modification factor is built upon a robust and widely accepted analytical foundation and familiarity to the user.

6.1.1 Data Description

The same parameters were varied as the interior ones since the difference between the two cases is the truck potion and the girder of interest to determine their influence on exterior girder live load distribution.

6.1.2 Exploratory Data Analysis

EDA was performed on the 19,152 PBFTG bridges. The data was split into two-lane loading scenarios: 9800 one-lane loaded and 9352 two-lane loaded. The earlier section elaborates on the need for EDA and its different elements.

Table 6-1: Summary of Descriptive Statistics for exterior girder LLDF

Statistics Measures	One Lane Loaded	Two Lanes Loaded
Mean	0.5024179	0.5541429
Std Dev	0.0795031	0.0737135
Skewness	0.4056825	-0.050883
Kurtosis	-0.072914	-0.592824
Range	0.4641174	0.3809963

Descriptive statistics for the dependent variable, which is the LLDF for the exterior girder, is given in Table 6-1; for one lane loaded condition, the mean LLDF is approximately 0.502, indicating that, on average, about 50.2% of vehicle loading is distributed to an exterior girder when the load is applied to be maximized on an exterior girder. The standard deviation of 0.0795 signifies a moderate dispersion in LLDF values. The skewness value of 0.4057 indicates a slight positive skew in the data, implying that the distribution is slightly skewed toward lower values, with a few higher-value outliers. Kurtosis is slightly negative at -0.0729, indicating a distribution

slightly flatter than a normal distribution. For the two lanes loaded condition, the mean LLDF value is 0.5541, which is expected to be higher than the one-lane loaded case since two trucks are on the bridge. The standard deviation is lower at 0.0737, indicating a slightly tighter distribution of LLDF values compared to the one-lane loaded scenario. The skewness is approximately zero (-0.0508), suggesting a nearly symmetric data distribution around the mean. The kurtosis is negative (-0.5928), implying a distribution that is flatter than a normal distribution; Figure 3 depicts the distribution of the LLDFs for one-lane and two-lane loaded scenarios.

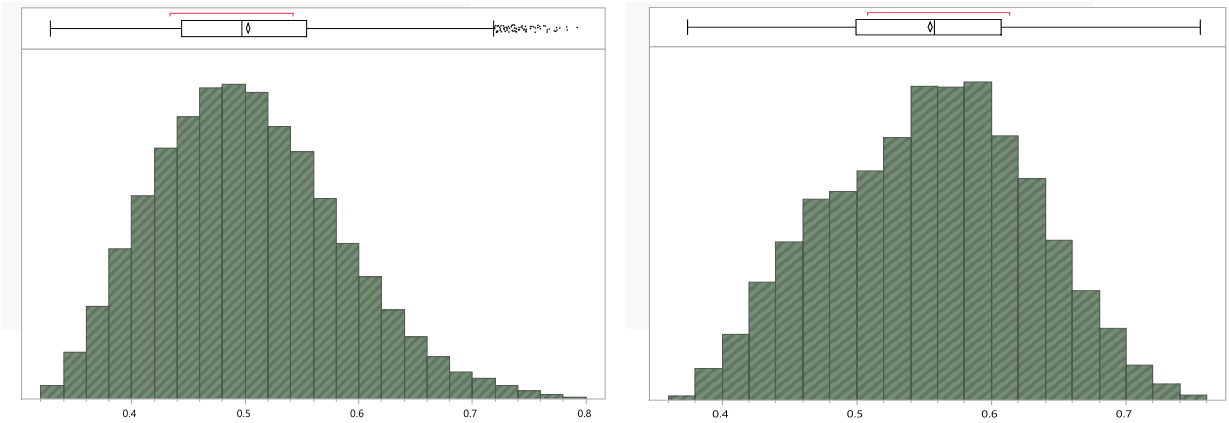

Figure 6.1. LLDF Distribution for (a) One lane loaded and (b) Two lanes loaded scenarios.

Following the descriptive statistics, several visual representations of the data were assessed; scatter plots of exterior LLDFs against interior LLDFs are presented as a sample in Figure 6.1. It can be seen in the figure that there is a positive correlation between those two variables. It was identified throughout the EDA that there are potential relationships or patterns between exterior LLDFs and Overhang distance and interior LLDFs.

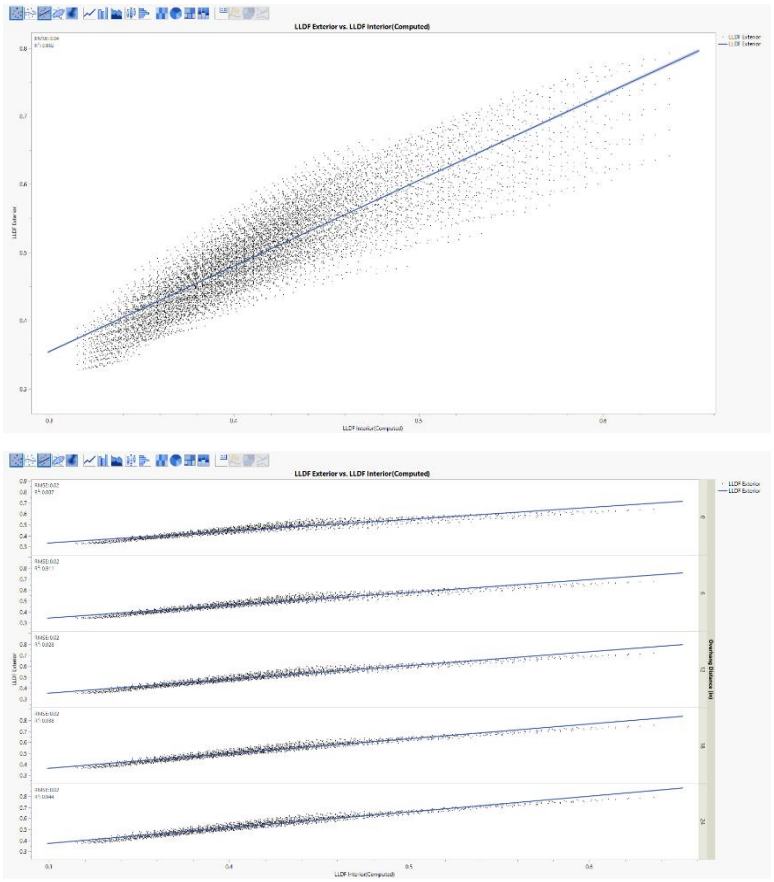

Figure 6.2. Scatter plot of exterior LLDFs plotted against (a) computed interior LLDF and (b) computed interior LLDF and overhang distance.

Table 6-2 provides the multivariate correlation matric. The correlation between the Number of Beams and the LLDF Exterior is -0.0609, which indicates a very weak negative correlation. This suggests that as the number of beams increases, the LLDF Exterior might slightly decrease, but this relationship is quite weak. The correlation between Spacing and LLDF Exterior is 0.5972, which indicates a moderately strong positive correlation. This suggests that as the spacing increases, the LLDF Exterior also tends to increase. Lastly, the correlation between LLDF Interior (Computed) and LLDF Exterior is very strong at 0.8956. This suggests that these two variables move together closely. Table 6-3 shows the correlation matrix for the two-lane loaded scenario.

Table 6-2: Multivariate Correlation Coefficients for one lane loaded scenario.

	Number of Beams	Spacing (ft)	Overhang Distance (in)	Deck Thickness (in)	Span Length (ft)	LLDF Exterior	LLDF Interior (Computed)
Number of Beams	1.0000	0.0000	-0.0000	-0.0000	-0.0000	-0.0609	-0.1799
Spacing (ft)	0.0000	1.0000	-0.0000	0.0000	0.1336	0.5972	0.5531
Overhang Distance (in)	-0.0000	-0.0000	1.0000	0.0000	-0.0000	0.3522	0.0000
Deck Thickness (in)	-0.0000	0.0000	0.0000	1.0000	0.0000	-0.0693	-0.0944
Span Length (ft)	-0.0000	0.1336	-0.0000	0.0000	1.0000	-0.5261	-0.6235
LLDF Exterior	-0.0609	0.5972	0.3522	-0.0693	-0.5261	1.0000	0.8956
LLDF Interior (Computed)	-0.1799	0.5531	0.0000	-0.0944	-0.6235	0.8956	1.0000

In Table 6-3, the correlation between Spacing and LLDF Exterior is 0.8205, which is noteworthy since it indicates a strong positive correlation, which was not the case for the one-lane loaded case. This is the strongest correlation we observe in the matrix, suggesting that spacing is a significant factor impacting the LLDF Exterior for the two-lane loaded scenario. As expected, the correlation between LLDF Interior (Computed) and LLDF Exterior is 0.8472, showing a very strong positive correlation.

Table 6-3: Multivariate Correlation Coefficients for two lanes loaded scenario.

	Number of Beams	Spacing (ft)	Overhang Distance (in)	Deck Thickness (in)	Span Length (ft)	LLDF Exterior	LLDF Interior (Computed)
Number of Beams	1.0000	-0.1036	-0.0298	-0.0000	0.0056	-0.2308	-0.4417
Spacing (ft)	-0.1036	1.0000	-0.0179	-0.0000	0.1044	0.8205	0.7943
Overhang Distance (in)	-0.0298	-0.0179	1.0000	-0.0000	-0.0004	0.4225	0.0034
Deck Thickness (in)	-0.0000	-0.0000	-0.0000	1.0000	-0.0000	-0.0313	-0.0573
Span Length (ft)	0.0056	0.1044	-0.0004	-0.0000	1.0000	-0.1608	-0.3190
LLDF Exterior	-0.2308	0.8205	0.4225	-0.0313	-0.1608	1.0000	0.8472
LLDF Interior (Computed)	-0.4417	0.7943	0.0034	-0.0573	-0.3190	0.8472	1.0000

In this case, multicollinearity was found not to be a major issue in the data. The relationships identified in this phase will be formally tested in the subsequent analysis using inferential statistics and model fitting.

6.1.3 Empirical Equation Development

This study developed simplified empirical equations by modeling the LLDFs obtained from the parametric study for the 9,800 and 8,168 one-lane and two-lane loaded PBFTG bridges, respectively. An initial basic model was first estimated. The development followed the AASHTO specification for LLDF of the exterior girder of an I-beam to identify a suitable equation function structure and used the results of the exploratory data analysis to identify potential independent variables. After several iterations of testing functional structures, two linear functions were deemed appropriate and modeled for the purpose of this project, which is shown in Eq. 5 – 5 and 5 – 6.

$$\boldsymbol{LLDF_{exterior} = \beta_0 + (\beta_1 + \beta_2 d_e)\widehat{LLDF_{interior}} + \varepsilon} \qquad (\boldsymbol{Eq. 5-5})$$

$$\boldsymbol{LLDF_{exterior} = \beta_0 + (\beta_1 + \beta_2 d_e)\widehat{LLDF_{interior}} + \beta_3 S + \varepsilon} \qquad (\boldsymbol{Eq. 5-6})$$

- $LLDF_{exterior}$ is the predicted exterior girder LLDF,
- $\beta_i's$ the estimators,
- d_e the overhang distance,
- $\widehat{LLDF_{interior}}$ is the interior girder LLDF computed using the proposed equations,
- S the spacing, and
- ε the error term.

Since $\widehat{LLDF_{interior}}$ did not have the variable d_e, it is justified to multiply two of them together to estimate the coefficients. This can be observed from the multivariate analysis as well – overhang distance and interior LLDF have no correlation. This section will be expanded with steps taken to estimate the models and interpretation of results.

6.1.4 Regression Analysis

The development of predictive models is imperative to ensure safe and economical design; thus, several models were carefully produced to ensure accuracy, unbiased estimators, and maximized prediction power. The R^2 and other goodness-of-fit measures were used to evaluate the models, ensuring that they accurately represent the data's underlying patterns. Variations in

the specificity of bridge geometry and load placement were theorized to affect live load distribution in a manner that's not directly observable but impacts the bridge's load-resisting mechanisms.

Four models for each lane loading scenario using the two functional forms mentioned above were compared for the goodness of fit measures, such as R^2 (shown in Table 6-4) and Root Mean Square Error (RMSE). These measures were only utilized to compare models that fit the same dataset. Of the four models, the functional form the functional form presented in Equation 5 – 6 was deemed appropriate for both one-lane loaded and two-lane loaded scenarios. For this project, only two models are discussed in depth.

Table 6-4: Summary of Goodness of Fit for both one-lane and two lanes loaded scenarios, respectively

RSquare	0.932529	0.963247
RSquare Adj	0.932516	0.963234
Root Mean Square Error	0.020653	0.014134
Mean of Response	0.502418	0.554143
Observations	9800	9352

Table 6-5 provides the results of two OLS regression models, one for one loaded lane and the other for two loaded lanes. Each model aims to predict the dependent variable, Exterior LLDF, based on different independent variables.

Table 6-5: Ordinary Least Squares regression models parameter estimates

Term	Estimate	Std Error	t Ratio	Prob>|t|	VIF
One Lane Loaded					
Intercept	-0.022219	0.001551	-14.32	<.0001*	
LLDF Interior*Overhang Distance	0.0080244	5.833e-5	137.58	<.0001*	1.036172
LLDF Interior (Computed)	1.1596853	0.003746	309.58	<.0001*	1.036172
Two Lanes Loaded					
Intercept	0.0851699	0.001283	66.37	<.0001*	
LLDF Interior*Overhang Distance	0.0067533	3.318e-5	203.56	<.0001*	1.033604
LLDF Interior (Computed)	0.4602045	0.003755	122.55	<.0001*	2.760589
Spacing (ft)	0.0234428	0.000193	121.54	<.0001*	2.712993

Marginal effects can be interpreted directly from the coefficients in a linear regression model. In this case, each coefficient represents the change in the dependent variable for a one-unit change in the respective independent variable, holding all other variables constant. For instance,

the marginal effect of 'LLDF Interior (Computed)' in the one-lane loaded model is 1.1596853. This means that a one-unit increase in 'LLDF Interior (Computed)' would lead to a 1.1596853 unit increase in the predicted Exterior LLDF, all else being equal. Similarly, for the two-lane loaded model, the coefficient for 'Spacing (ft)' is 0.0234428, which implies that a one-foot increase in spacing increases the predicted Exterior LLDF by 0.0234428 units, holding all other variables constant. However, the interpretation of interaction terms in linear regression models can be more complex as the effect of one variable depends on the level of the other.

Elasticities can be calculated for each variable by multiplying the estimated coefficients by the ratio of the average of the independent variable to the average of the dependent variable. Elasticity measures the percentage change in the dependent variable given a one percent change in an independent variable, holding all other variables constant. All the coefficients are statistically significant at any conventional level as their p-values are all less than 0.05, and most are less than 0.0001.

6.2 SKEW GIRDER LLDF REDUCTION FACTOR

The development of LLDFs for bridges often involves consideration of the skew angle. This section discusses the formulation of a reduction factor for moment LLDF for use in bridge design, adhering closely to the current guidelines outlined in the AASHTO LRFD BDS. The methodology employed in this chapter reflects the effort to mirror existing equations designated for Steel I-girders; thus, the reduction factor is both relevant and consistent with established practices.

6.2.1 Data Description

Skew was introduced into the analysis for LLDFs in this study, varying skew angle from 0 to 45 degrees in 5-degree increments to provide a comprehensive range for observing the influence of skew on load distribution of routine bridge design. For bridges with a skew index greater than 0.3, the skew's impact on the load path becomes increasingly significant, thus altering the method used to obtain LLDFs. A study by White (2020) suggests that higher skew indexes can substantially alter the load path in bridges, prompting a need to consider these effects in LLDF development. In this context, load path refers to the route by which loads travel through the bridge structure. Skew can change the effectiveness of load distribution across the bridge elements,

potentially leading to an overestimation of LLDFs for skewed bridges. Thus, for this study, bridges that have skew indices less than 0.3 were excluded from the analysis.

6.2.2 Exploratory Data Analysis

In the EDA of LLDF for skewed girders from 169,392 PBFTG bridges, the average LLDF was found to be approximately 0.464, as shown in Table 6-6, indicating a common central tendency across the dataset. The standard deviation, relatively small at 0.0978, suggests a tight clustering of data points around the mean, indicating consistency in LLDF values among the bridges studied. The positive skewness value hints at a distribution with a tail extending towards higher LLDFs, although the flatness indicated by the negative kurtosis suggests a broader range of LLDFs than a bell curve would typically show.

Table 6-6: Summary of Descriptive Statistics for skewed girder LLDF

Statistics Measures	Values
Mean	0.4636433
Std Dev	0.0978472
Skewness	0.2269559
Kurtosis	-0.575218
Range	0.5539566

Further statistical inquiry into the distribution of LLDFs for skewed PBFTG bridges is visually represented in Figure 6.3. This analysis provides a detailed depiction of how the LLDFs are spread across the dataset, highlighting tendencies and patterns that are critical for understanding structural behaviors and informing design decisions.

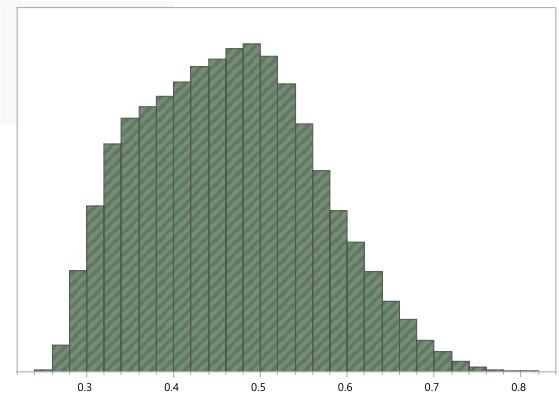

Figure 6.3. LLDF Distribution for skewed girder

Scatter plots of skew LLDFs against skew are presented in Figure 6.4 as a sample. The graph provides a visual analysis of the relationship between the skew angle of bridge girders and their corresponding LLDF as part of the EDA on skew girder LLDF reduction factors. It can be seen in the figure that there is a negative correlation between those two variables.

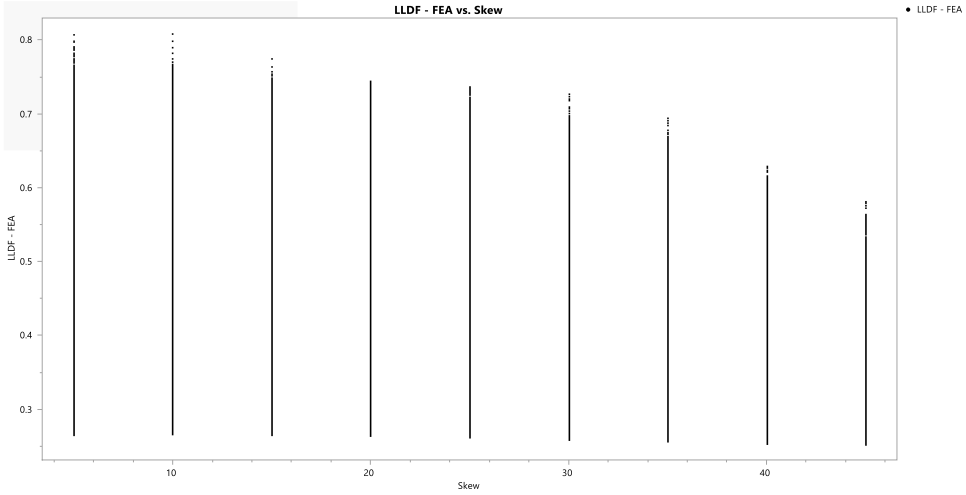

Figure 6.4. Scatter plot of exterior LLDFs plotted against skew angle

A correlation matrix was also utilized to determine the correlation coefficients of exterior girder LLDF with all other variables. Table 6-7: Multivariate Correlation Coefficients for one lane loaded scenario. shows the multivariate correlation coefficients between three variables: LLDF as computed using FEA, bridge skew angle, and LLDF for the interior girder of a straight bridge (0-degree skew). The LLDF-FEA has a strong positive correlation of 0.9697 with the LLDF for the interior. The negative correlation between LLDF-FEA and skew (-0.2306) and between skew and LLDF is moderate, suggesting only a slight tendency for the LLDF values to decrease as the skew

angle increases. Additionally, the correlation between LLDF - FEA and LLDF- Interior (-0.1227) is relatively weak, suggesting slight multicollinearity. However, this correlation is not strong enough to imply a substantial direct relationship.

Table 6-7: Multivariate Correlation Coefficients for one lane loaded scenario.

	LLDF - FEA	Skew	LLDF - Interior
LLDF - FEA	1.0000	-0.2306	0.9697
Skew	-0.2306	1.0000	-0.1227
LLDF - Interior	0.9697	-0.1227	1.0000

6.2.3 Empirical Equation Development

The empirical equation development aimed to devise equations that can accurately predict LLDF values, with a particular focus on skewed PBFTG bridges. The approach was to base the model on the parameters derived from the parametric study, incorporating the insights gained into how the LLDFs behave under different skew conditions. The study adhered to the guidelines laid out by the AASHTO LRFD BDS for reducing moment LLDF values in bridges with skewed girders I-beam bridges. This basic model served as the foundation upon which further models were iteratively developed and refined. Through this process of iteration, the most fitting relationship to describe the skewed LLDFs was developed. Eventually, a linear model, as described in Eq. 6 – 1, was found to be the most appropriate.

$$\boldsymbol{LLDF_{skew} = \beta_0 + (\beta_1 + \beta_2\, tan\,(\theta)^{1.75})\widehat{LLDF_{interior}} + \varepsilon} \qquad (\boldsymbol{Eq.\,6-1})$$

- $LLDF_{skew}$ is the predicted exterior girder LLDF,
- $\beta_i's$ the estimators,
- θ is the skew angle,
- $\widehat{LLDF_{interior}}$ is the interior girder LLDF computed using proposed equations and
- ε the error term.

Since $\widehat{LLDF_{interior}}$ did not have a skew angle as a variable, it is justified to multiply two of them together to estimate the coefficients. This can be observed from the multivariate analysis as well.

6.2.4 Regression Analysis

The development of this model followed the interior and exterior girder LLDF development. Several models were carefully produced to ensure accuracy, unbiased estimators, and maximized prediction power. The coefficient R^2 and other goodness-of-fit measures were used to evaluate the models.

The statistical model presented in Table 6-8 demonstrates excellent predictive accuracy, as indicated by its summary of goodness of fit measures. With an R-square value of 0.955506, the model explains over 95% of the variance in LLDF, a figure scarcely reduced when adjusted for the number of predictors, thereby affirming the model's complexity as justified. The RMSE is 0.02064, which is significantly small relative to the mean response of 0.463643, suggesting the model's predictions are both precise and reliable. Considering the substantial sample size of 169,392 observations, these statistics collectively indicate a robust and well-fitting model that confidently predicts LLDF across a substantial range of bridge configurations.

Table 6-8: Summary of Goodness of Fit for Skewed Girder

RSquare	0.955506
RSquare Adj	0.955505
Root Mean Square Error	0.02064
Mean of Response	0.463643
Observations	169392

Table 6-9 provides the results of two OLS regression models. The table provided summarizes the estimates from an OLS regression analysis, which is used to predict the LLDFs with the effect of skew.

Table 6-9: Ordinary Least Squares regression models parameter estimates

Term	Estimate	Std Error	t Ratio	Prob>|t|	VIF
Intercept	-0.02271	0.000267	-84.93	<.0001*	
LLDF – Int	0.9020936	0.000474	1901.5	<.0001*	1.0023719
tan(skew)^1.75*LLDF – Int	-0.128115	0.000534	-239.9	<.0001*	1.0023719

The VIF for both LLDF – Int and the interaction term tan(skew)^1.75*LLDF – Int is slightly above 1. A VIF of 1 indicates no correlation among the predictors and, hence, no inflation of the variance of the β_i coefficient. For LLDF – Int, the estimate of 0.9020936 with a very low standard error of 0.000474 suggests a strong and statistically significant positive effect on the

response variable for every one-unit increase in LLDF. The t Ratio of 1901.5 and an extremely low probability denotes an extremely significant result. The term tan(skew)^1.75* LLDF – Int has a negative coefficient (-0.128115), implying that as the skewness increases, holding LLDF constant, there is a negative effect on the response variable. With a low standard error, a t Ratio of -239.9, and a Prob>|t| of less than 0.0001, this term is also statistically significant.

6.3 DIAGNOSTIC TESTS

Diagnostic tests discussed in section 5.5 were performed on the LLDFs of both exterior girders and skewed bridges. The test results for the linear regression models indicate that the assumptions for linear regression are satisfactorily met. Linearity was confirmed visually with no apparent deviations in the plots of observed vs. predicted values. The Durbin-Watson test showed no autocorrelation in the residuals; since the data is not a serial one, this was expected. Error variance equality was visually conducted. The normality of errors was accepted based on the distribution appearance in histograms and QQ plots. Multicollinearity was found to be within acceptable limits, with VIF values not exceeding the problematic threshold, suggesting that each variable contributes uniquely to the model. Lastly, no significant endogeneity was detected in the correlation tests between residuals and independent variables, confirming that the models are reliable for predicting live load distribution factors without significant bias.

6.4 PROPOSED EQUATIONS

Upon obtaining the parameter estimates (β_i's) for the models, an adjustment constant was introduced to each equation with the objective of yielding more conservative predictions. This adjustment was aimed at preserving safety by ensuring that the predicted LLDFs do not underestimate the actual values. The OLS method of estimation, which was employed in this study, works by minimizing the sum of the squared residuals. Consequently, under normal circumstances, the resulting equations from this method are designed such that they would underestimate approximately half of the LLDFs and overestimate the other half. However, considering the nature of the project and the potential risks associated with underestimation, the approach deviated from this expectation. The modification factor was calculated to achieve the goal of accurately predicting or, preferably, overpredicting 100% of the LLDFs. These factors were systematically

incorporated into the model to ensure that the predictions do not fall short of the actual LLDFs, thereby reducing the potential for underprediction errors that could compromise safety.

The same procedure was followed in section 5.6 to obtain modification factors to overestimate the predicted LLDFs. For exterior girder LLDFs, the coefficient for the one-lane loaded case was multiplied by 1.09 and the coefficient of the two-lane loaded case by 1.08. These models explained approximately 94.2% and 94.7% of the data variability for the one-lane loaded bridges and for the two-lane loaded bridges, respectively. For the skewed bridge LLDFs, the coefficient was multiplied by 1.12. The models explained approximately 95.6 of the data variability for the skewed bridges.

Once this modification was applied and the predictions were adjusted to err on the side of overestimation, the model coefficients were then rounded off. This rounding was performed to a practically suitable number of significant figures, aiming for a balance between precision and ease of use. This final step ensures that the model is not only statistically sound and conservative but also practically implementable and user-friendly.

Equations 6 – 2 and 6 – 3 are the final equations proposed to calculate LLDFs for exterior girders of PBFTG bridges.

For exterior girders with one-lane loaded:

$$LLDF_{ext} = 0.06 + \left(1.02 + \frac{d_e}{124}\right) LLDF_{int} + \frac{S}{126} \qquad (Eq. 6-2)$$

For exterior girders with two-lane loaded:

$$LLDF_{ext} = 0.15 + \left(0.52 + \frac{d_e}{146}\right) LLDF_{int} + \frac{S}{52} \qquad (Eq. 6-3)$$

Equation 6 – 4 is the final equation proposed to calculate LLDFs for skewed PBFTG bridges.

For skewed girders:

$$LLDF_{skew} = 0.09 + (0.9 - 0.13 \tan^{1.75}(\theta)) LLDF \qquad (Eq. 6-4)$$

- $LLDF_{ext}$ is the exterior girder LLDF,

- d_e the overhang distance in inches,
- $LLDF$ the computed interior or exterior girder LLDF regardless of lanes loaded,
- S is girder spacing in feet,
- $LLDF_{skew}$ is the skewed girder LLDF, and
- θ is the skew angle in degrees.

6.5 SUMMARY

The preceding chapter discusses the development of LLDF modification factors for the moment in the exterior girder of PBFTGs and skewed PBFTG bridges. It also gives a statistical assessment of the method of developing the equation through an empirical equation.

CHAPTER 7: VALIDATION AND COMPARISON AGAINST CURRENT PROVISION

7.1 STATISTICAL COMPARISON OF PROPOSED EQUATIONS WITH AASHTO LRFD BDS PROVISIONS

In assessing the performance of LLDFs calculated using a proposed empirical equation against those determined by the standards set forth in the AASHTO LRFD BDS, a two-pronged approach was employed. The LLDFs for each bridge within the scope of the parametric study were first determined using the new empirical formula. This was then compared against LLDFs calculated according to the methodologies prescribed in AASHTO's guidelines, which are contingent upon certain bridge conditions being met – conditions that preclude some PBFTGs from utilizing these AASHTO LRFD BDS equations. As stated in AASHTO Article 4.6.2.2, these factors only apply if the bridge meets specific conditions. Distribution factors for the analysis are found using Equation 7 – 1. ASHTO LRFD BDS (AASHTO 2020) LLDF is given by:

$$\text{LLDF} = 0.05 + 0.85\frac{\text{N}_\text{L}}{\text{N}_\text{b}} + \frac{0.425}{\text{N}_\text{L}} \qquad (\text{Eq. } 7-1)$$

- m is the multi-presence factor,
- N_b is the number of beams, and
- N_L is the number of lanes.

The graphical representation of these comparisons in Figure 7.1 through Figure 7.5, which plots the distribution of LLDFs, provides a visual interpretation of the effectiveness of the proposed equation against the current standard. The AASHTO equation offers a baseline for comparison.

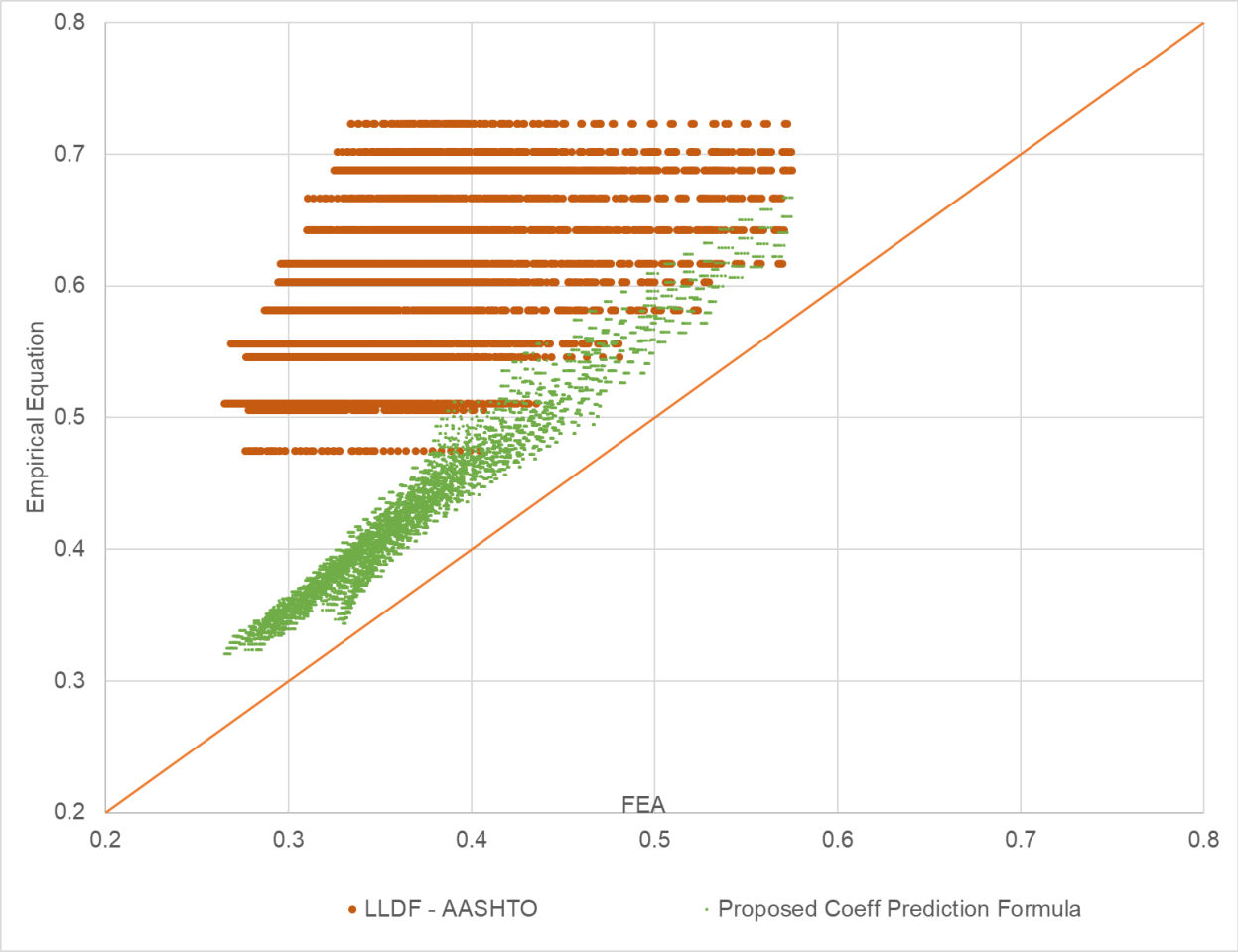

Figure 7.1 Q-Q plot of one-lane loaded LLDFs for non-skewed interior girders.

The scatter plots serve as a comparative tool, comparing LLDFs derived from field element analysis (FEA) with those predicted by empirical equations. Each data point reflects a unique instance of this comparison. Observations from the scatter plots reveal a tendency for the empirical equations to align closely with FEA results for lower LLDF values, with a divergence occurring as these values increase. Moreover, the data points form distinct bands, indicating that the empirical equations predict a limited set of discrete LLDF values that do not capture the continuous variability exhibited by FEA.

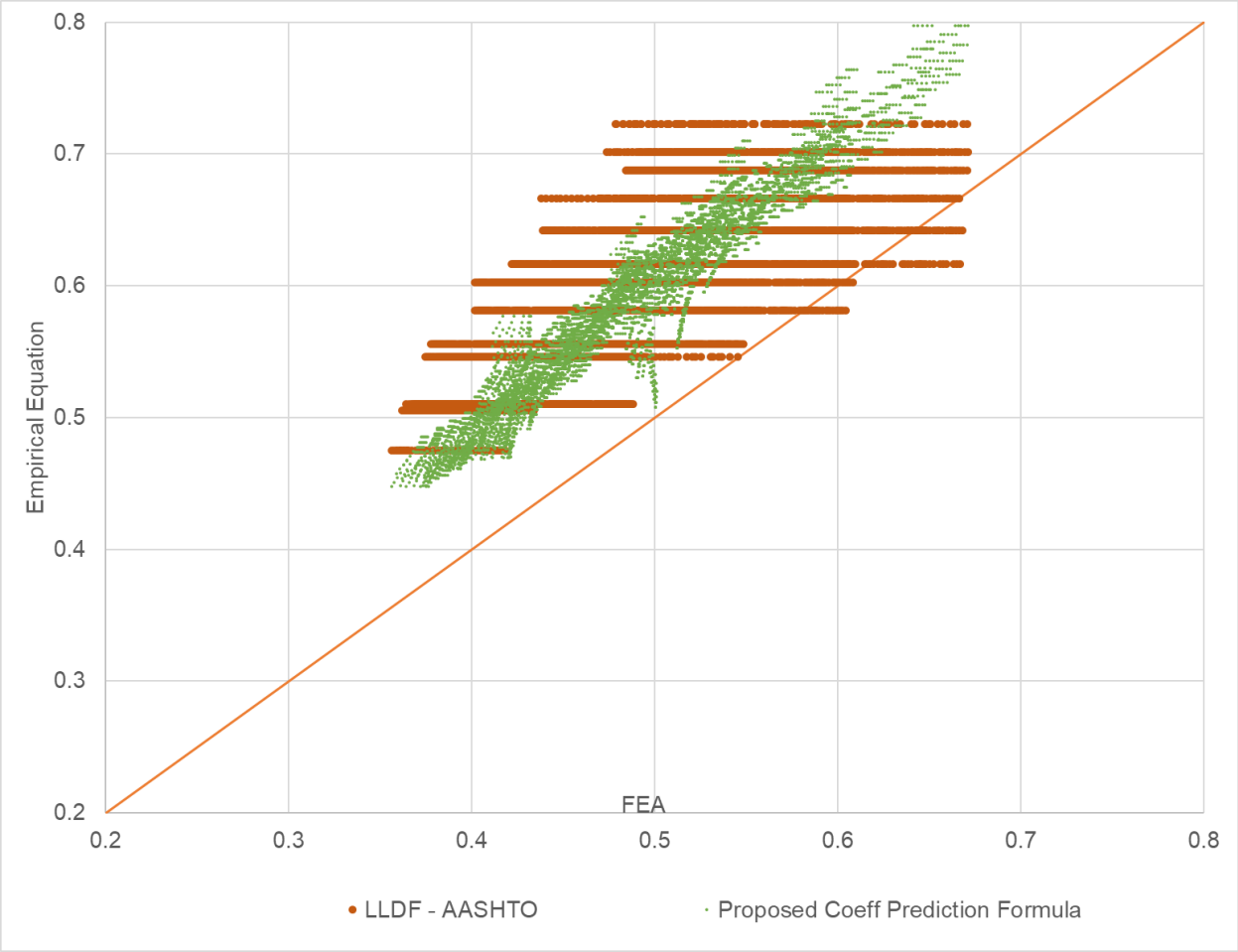

Figure 7.2 Q-Q plot of two-lane loaded LLDFs for non-skewed interior girders.

In terms of loading scenarios, the variation in data point markers suggests that the empirical equations' performance is influenced by specific conditions, such as the type of load and the number of lanes in use. A deeper statistical analysis, such as correlation coefficients or regression analysis, would be instrumental in quantifying the relationship between FEA and empirical predictions, as well as evaluating the residuals to determine the precision and potential bias of the empirical equations.

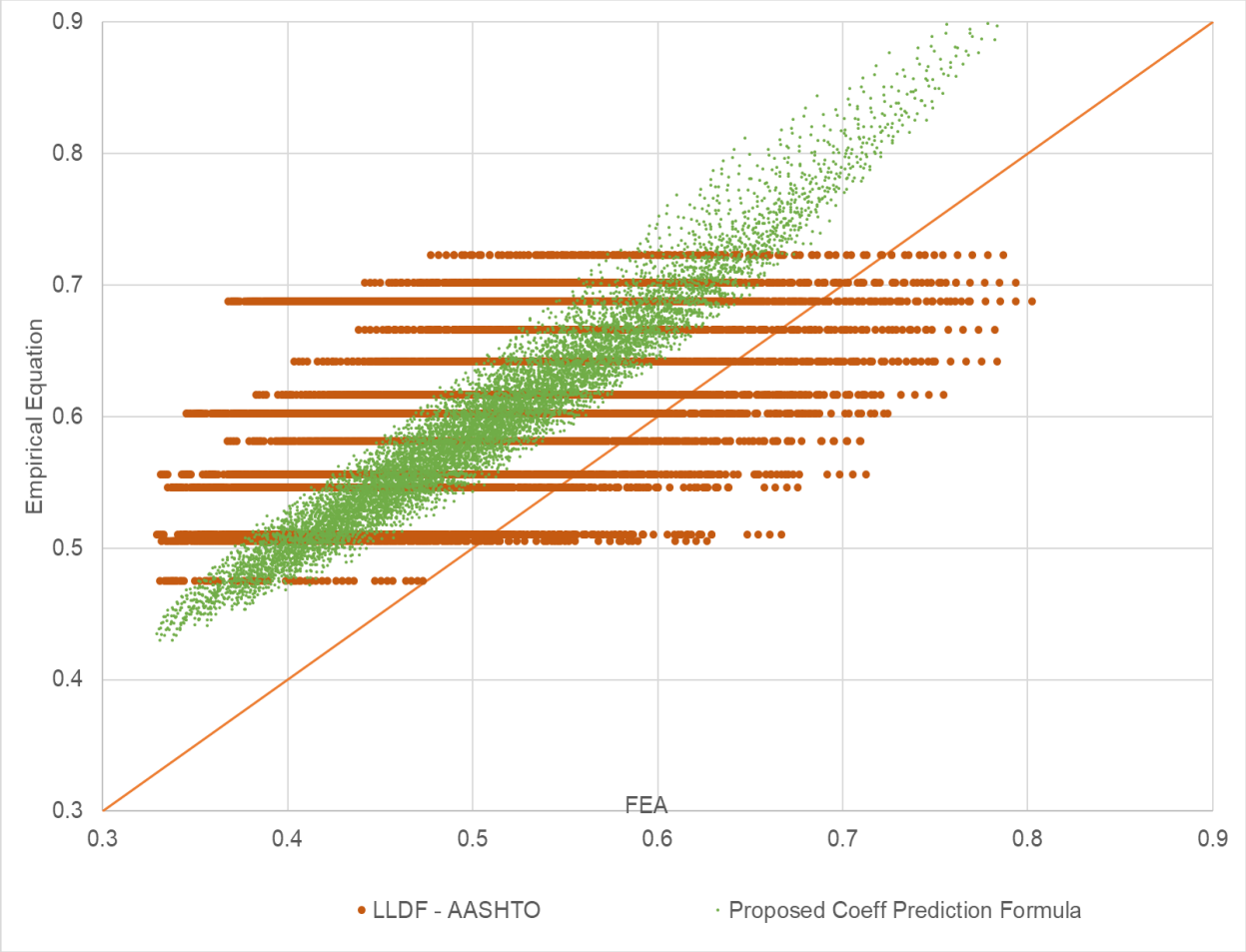

Figure 7.3 Q-Q plot of one-lane loaded LLDFs for non-skewed exterior girders.

The findings indicate that the proposed empirical equations offer a reasonable approximation of FEA-derived LLDFs far outperforming the ones computed using AASHTO LRFD BDS.

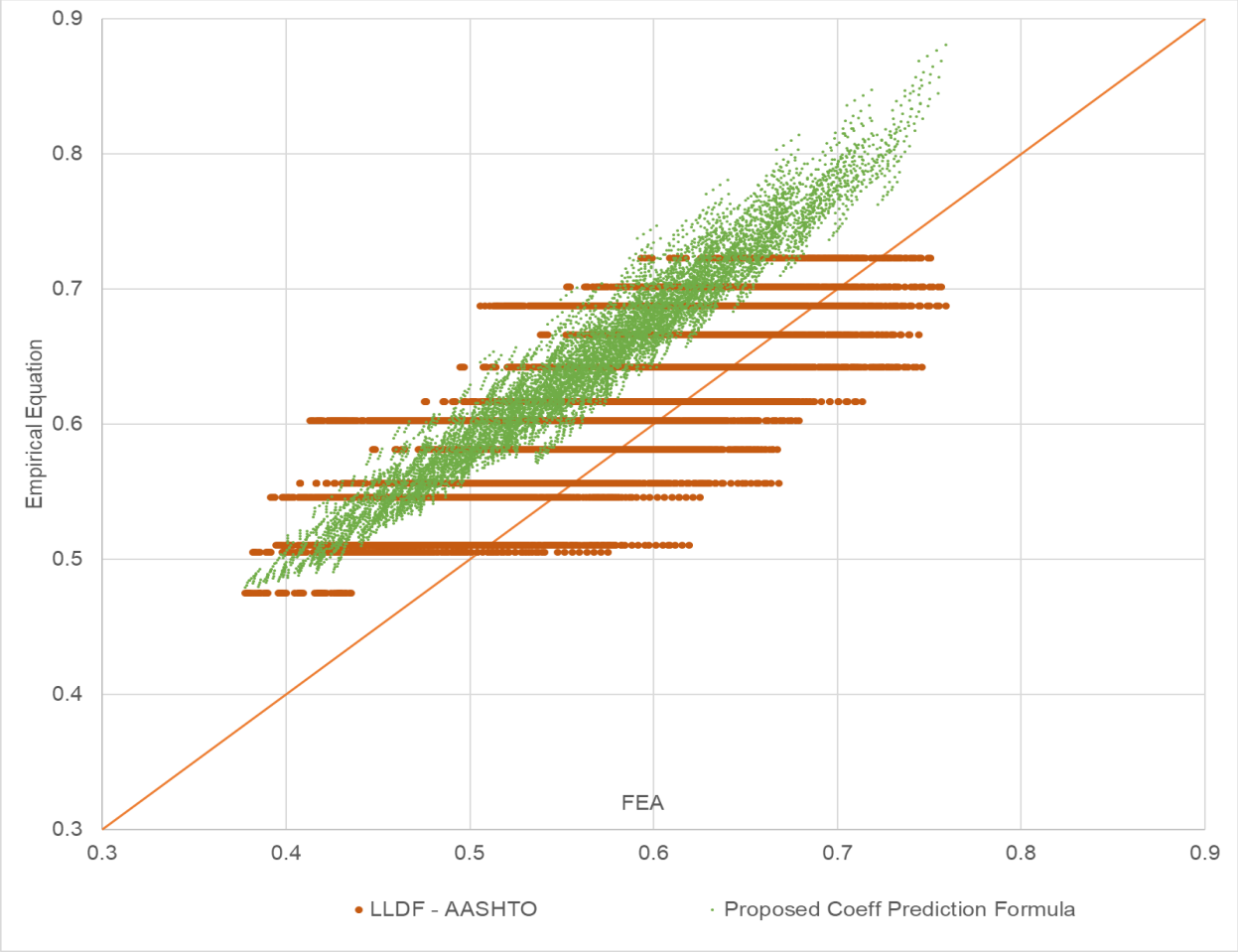

Figure 7.4 Q-Q plot of two-lane loaded LLDFs for non-skewed exterior girders.

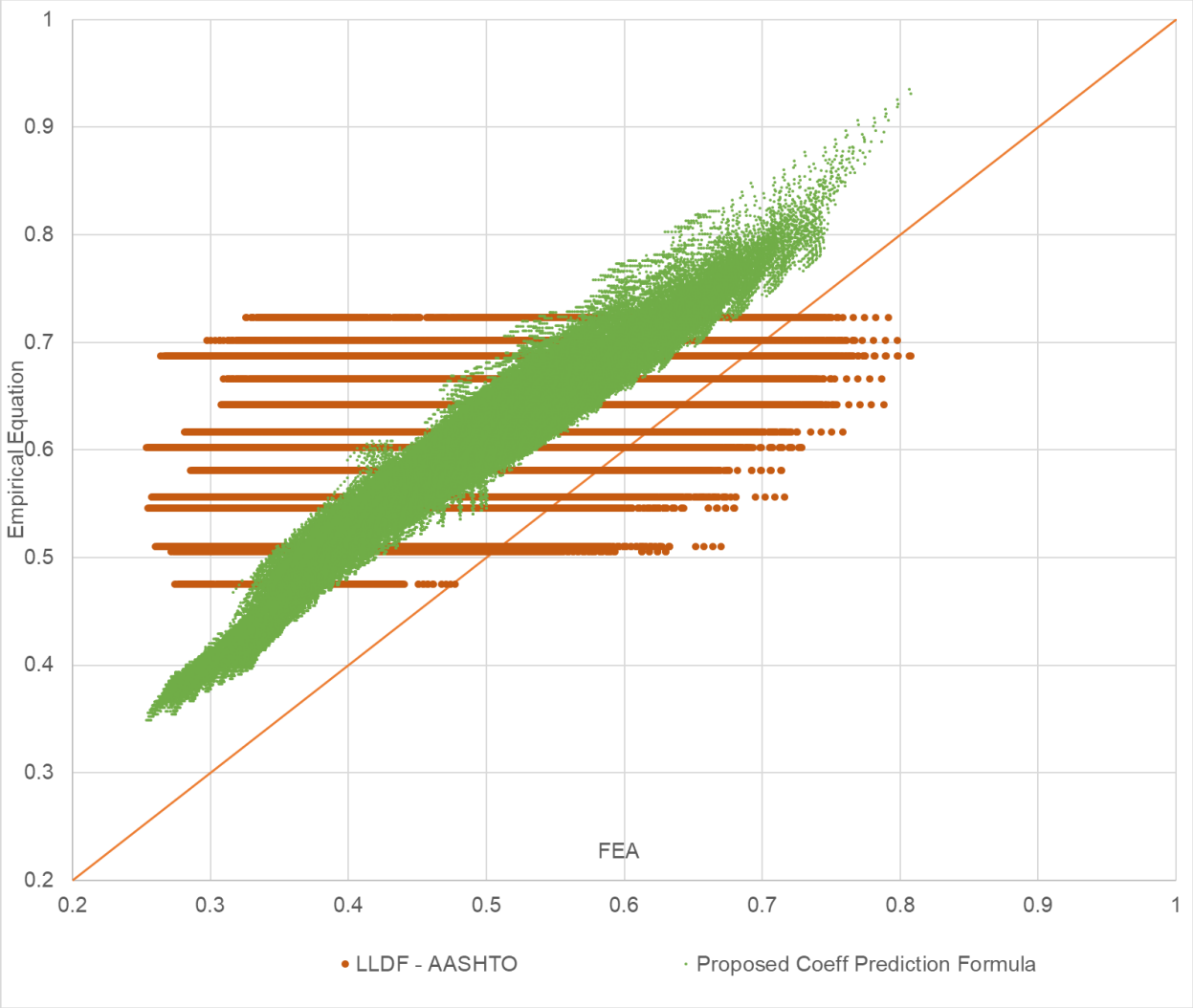

Figure 7.5 Q-Q plot of LLDFs for skewed girders

Further, the distributions of the errors of the two sets of equations were explored, and the differences between them were statistically tested. For the comparison and evaluation of the two proposed sets of equations, the prediction accuracy of the equations was assessed using the following measures.

- Root Mean Square Error (RMSE) of predictions,
- Correlation coefficients,
- Predictive Power Score (PPS), and

- Prediction bias.

This comprehensive analysis attempts to provide well-rounded insights that can support and guide future adoption decisions of the proposed simplified equations. The square root of the mean squared prediction error (or RMSE) was calculated as follows.

$$RMSE = \sqrt{\frac{\sum_{ii}^{n} \| y(i) - \hat{y}(i) \|}{n}} \qquad (\text{Eq. } 7-2)$$

- n is the number of observations,
- $y(i)$ is the i^{th} LLDF obtained from FEA and
- $\hat{y}(i)$ is the corresponding prediction from the proposed or the current AASHTO equation.

The closer the value of RMSE is to zero, the higher the accuracy of predictions. The measure essentially aggregates the magnitude of all errors in the predictions.

The Pearson product-moment captures the strength of the linear relationship between two variables. Herein, the measure was used to assess the strength of the relationship between the LLDF obtained from FEA and the corresponding predictions from the proposed or the current AASHTO equation. The equation can be written as follows.

$$r = \frac{\sum (LLDF_i - \overline{LLDF})\left(\widehat{LLDF_i} - \overline{\widehat{LLDF}}\right)}{\sqrt{\sum (LLDF_i - \overline{LLDF})^2 \sum \left(\widehat{LLDF_i} - \overline{\widehat{LLDF}}\right)^2}} \qquad (\text{Eq. } 7-3)$$

- $LLDF_i$ is the LLDF obtained from FEA,
- $\overline{LLDF}$ is the mean of the values in the sample, and
- $\widehat{LLDF_i}$ and $\overline{\widehat{LLDF}}$ are the corresponding predictions and their mean, respectively.

In addition, because, arguably, the correlation coefficient does not always detect the relationship between two variables, especially when the relationship is non-linear, the PPS was also calculated (Wetshoreck 2020). A score of 0 denotes no predictive power, while a score of 1 denotes perfect predictive power, as PPS is a normalized measure. The score was calculated using a Decision Tree Regressor and essentially corresponds to a normalized mean average error (MAE) when the minimum (lower possible value) is 0.0 (perfect prediction or no error), and the maximum possible value is the MAE of a naïve model that is empirically derived, simulated as the one that predicts the mean *y* value as the prediction of all bridges in the sample.

Finally, prediction bias (or average error) is defined as the difference between the mean of predictions from the proposed or the current AASHTO equation and the mean of LLDF obtained from FEA. A positive value denotes overprediction, and the higher the absolute value, the larger the prediction bias. All these measures, unlike R^2, can be used to assess the goodness-of-fit and the prediction accuracy of both linear and non-linear models and, thus, are more appropriate for comparing the performance of the proposed equations and the current AASHTO equation herein.

All measures suggest that the proposed equations have, by far, a higher prediction power, as summarized in Table 7-1. Further, the results showed that the proposed equations have an overall excellent fit, given the sample used to develop the equations. The difference in the performance is especially remarkable for the one-lane loaded bridges.

Table 7-1 Comparative statistics of the proposed vs. AASHTO LRFD BDS LLFDs

Equation	RMSE	Pearson Correlation*	PPS	Prediction Bias	Over-estimation	t-ratio*
			Interior One-Lane Loaded			
Proposed	0.062	0.976	0.981	0.061	100%	285.5
AASHTO	0.253	0.433	0.121	0.246	100%	
			Interior Two-Lane Loaded			
Proposed	0.103	0.966	0.966	0.101	100%	36.1
AASHTO	0.146	0.748	0.379	0.140	99.2%	
			Exterior One-Lane Loaded			
Proposed	0.092	0.971	0.855	0.090	100%	24.3
AASHTO	0.133	0.427	0.151	0.108	91.1%	
			Exterior Two-Lane Loaded			
Proposed	0.085	0.973	0.862	0.083	100%	64.1
AASHTO	0.071	0.707	0.355	0.048	81.6	
			Skewed One-Lane Loaded			
Proposed	0.113	0.978	0.912	0.111	100%	187
AASHTO	0.184	0.316	0.089	0.115	95.3	

*All values have probability < 0.0001

the one-sided paired *t-tests* that test whether the difference between the errors of the proposed equation and the current AASHTO equation is zero (null hypothesis) or greater than zero (i.e., the errors of the AASHTO equation are larger than the errors of the proposed equation).

The paired *t-test* rejected the null hypothesis that the differences are zero and, therefore, showed that the errors of the proposed equation are smaller than those of the current AASHTO equation. The difference plots below depict the difference between the errors for all bridges. As shown in the graph, the x-axis includes the average of the errors of the two equations (proposed and current AASHTO), and the y-axis includes the difference between the errors of the two equations.

Overall, the above analysis provides strong evidence that the predictive power of the proposed equations is significantly higher than the current AASHTO equation, as expected. The results indicate that, based on the sample used to develop the proposed equations, the proposed equations have a superior fit. Note that by construction, the proposed equations overestimate the LLDF for all bridges in this dataset, as this is the dataset used to develop the equations. The statistical analyses presented in the next sections evaluate the prediction accuracy of the proposed equations in comparison to the current AASHTO equations using two different datasets.

7.2 Statistical Assessment of Application of Proposed Equations to Valmont UBEAM™

The Valmont UBEAMs™ are commercialized PBFTGs currently being used in bridges in over 18 states. There is a similarity between the standard PBFTGs developed by Michaelson (2014) and the UBEAMs™ with a slight difference in the inclination of the web. A set of bridges utilizing Valmont's standard UBEAMs™ was modeled using the FEA tools developed to get analytical live load moment distribution factors. The result is then compared to LLDFs predicted by the proposed equations.

The bridges in the parametric study utilized the same constant parameters discussed in Part I. The finite element analysis performed on the UBEAMs™ contained 1896 PBFTG bridges. The following parameters were varied in the one-lane loaded scenario matrix to determine LLDFs from a varied sample:

- Five UBEAM™ girder types:
    - U12 with span lengths from 20 feet to 40 feet with 10 feet increments.
    - U18 with span lengths of 40 feet and 50 feet.
    - U24 with span lengths of 55 feet and 65 feet.

    - U30 with span lengths of 65 feet and 75 feet.
    - U33 with span lengths of 80 feet.
- Three possible numbers of girders in the cross-section: 4, 6, and 8 girders
- Three possible girder spacings: 5 feet to 9 feet in 2 feet increments
- Two possible deck thicknesses: 8 inches and 9 inches
- Two possible skews: 0-degree and 30-degree skew (*with skew index less than 0.3)

For the two-lane loaded scenario, the same variation of parameters was used, but some combinations of these variations cannot accommodate two trucks transversely. Thus, the bridges with only one design lane were not included in the finite element modeling.

To further assess the prediction accuracy of the proposed equations, like in the assessment previously presented in section 7.1 with predictions estimated using the two sets of equations (the proposed and the current AASHTO equations), the prediction errors were estimated for the two sets of equations, and differences between the predictions were tested. Table 7-2 and Figure 7.6 provide the results of the comparison.

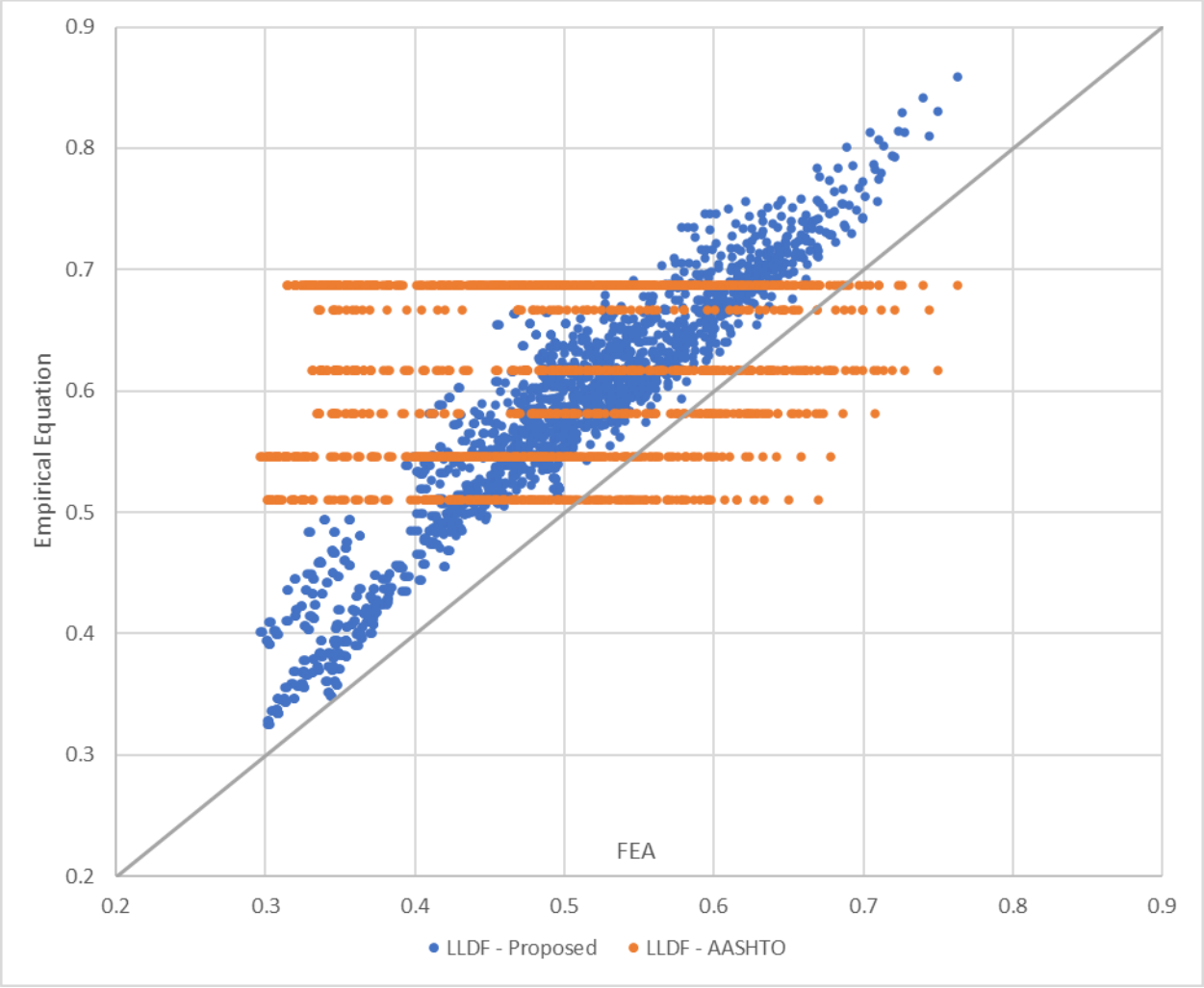

Figure 7.6 Q-Q plot of LLDFs for Valmont UBEAMs

Like with the previous analysis, the results of all measures corroborate the higher prediction accuracy of the proposed equations over the current AASHTO prediction equations. This analysis provides very similar results to the assessment of the goodness-of-fit of the proposed equations that used the initial dataset for the development of the equations. As seen in Figure 7.6, the predictions for this dataset also overall resemble the predictions for the initial dataset.

Table 7-2 Comparative statistics of the proposed vs. AASHTO LRFD BDS for Valmont UBEAMs

Equation	RMSE	Pearson Correlation*	PPS	Prediction Bias	Over-estimation	t-ratio*
Proposed	0.086	0.950	0.873	0.079	100%	21.99
AASHTO	0.174	0.179	0.050	0.135	88.6%	

*All values have probability < 0.0001

Similarly, as in the previous comparisons, the paired t-tests showed that the errors of the proposed equations are significantly lower than those of the current AASHTO ones. The results of this analysis provide further strong evidence that the proposed equation has high prediction accuracy and corroborates the assessment that the proposed equations outperform the current AASHTO equation.

7.3 Design Feasibility Assessment and Implication of Proposed Equations on The Valmont UBEAM™ System

The goal of the feasibility assessments was to assess the limit state governing span length and determine how an improved LLDF prediction can expand maximum span length applicability. The assessment was performed on the Valmont UBEAMs using AASHTO LRDF BDS provisions. The assessment was performed on all standardized Valmont UBEAMs™ that are commercially available. The design was carried out for a bridge with four beams utilizing each UBEAM™ at different spacing, as shown in Figure 7.8 and Figure 7.9. Two different methods of calculating live load distribution factors were considered in this evaluation: AASHTO LRFD Bridge Design Specifications Article 4.6.2.2. and the proposed LLDF prediction equation. The relevant limit states considered were Strength I, Service I, Service II, and Fatigue I limit states, which were evaluated at each span length increment.

The following load combinations are assessed using the permanent and transient loads mentioned previously, with values for load factors derived from AASHTO Tables 3.4.1-1 and 3.4.1-2 unless otherwise specified. The ductility factor (η_D), redundancy factor (η_R), and the operational importance factor (η_I), are taken to be 1.00 for this set of design calculations.

- Strength I: basic load combination relating to the normal vehicular use of the bridge without wind
    - 1.25DC + 1.50DW + 1.75(LL + IM)
- Service I: load combination associated with the evaluation of live load deflections (Article 3.4.2.2)
    - 1.00(LL + IM)
- Service II: load combination intended to control yielding of steel structures due to vehicular live load
    - 1.00DC + 1.00DW + 1.30(LL + IM)
- Fatigue I: fatigue load combination related to infinite load-induced fatigue life
    - 1.50(LL + IM)

Resistance for the girders in shear and flexure was computed according to AASHTO specifications. The elements resisting shear were conservatively assumed to consist only of the flat portions of the inclined web. All steel materials for this assessment were assumed to have yield stress, F_y = 50 ksi, and all concrete was assumed to be normal weight with compressive strength, f_c' = 4 ksi. It should be noted that for all limit states, according to AASHTO Article 6.5.4.2, the resistance factor for flexure (ϕ_f) and for shear (ϕ_v) are both taken to be 1.00. The hybrid factor (R_h) is taken as 1.00 since the girders are fully comprised of 50 ksi steel.

It is assumed that the deck is cast in the shop in a shored condition; therefore, no constructability checks are required because no significant loading occurs during the fabrication of the modular unit. The bridge cross-section evaluated in this analysis varied based on the plate size.

For calculating flexural resistances, the concrete deck is transformed to an equivalent area of steel using the modular ratio *n*, where *n* = 8 for this bridge. For loads applied to the short-term composite section, the concrete is transformed by dividing the concrete's effective flange width by *n*. For loads applied to the long-term composite section, the concrete is transformed by dividing the concrete's effective flange width by *3n*. AASHTO Article 4.6.2.6.1 states that the effective flange width of a concrete deck shall be taken as the tributary width to compute the effective flange width. The concrete deck attaches to the steel press-brake-formed tub girder using 6 inches-long and 7/8 inches diameter shear studs welded to the top flanges of the girder, as shown in Figure 7.7.

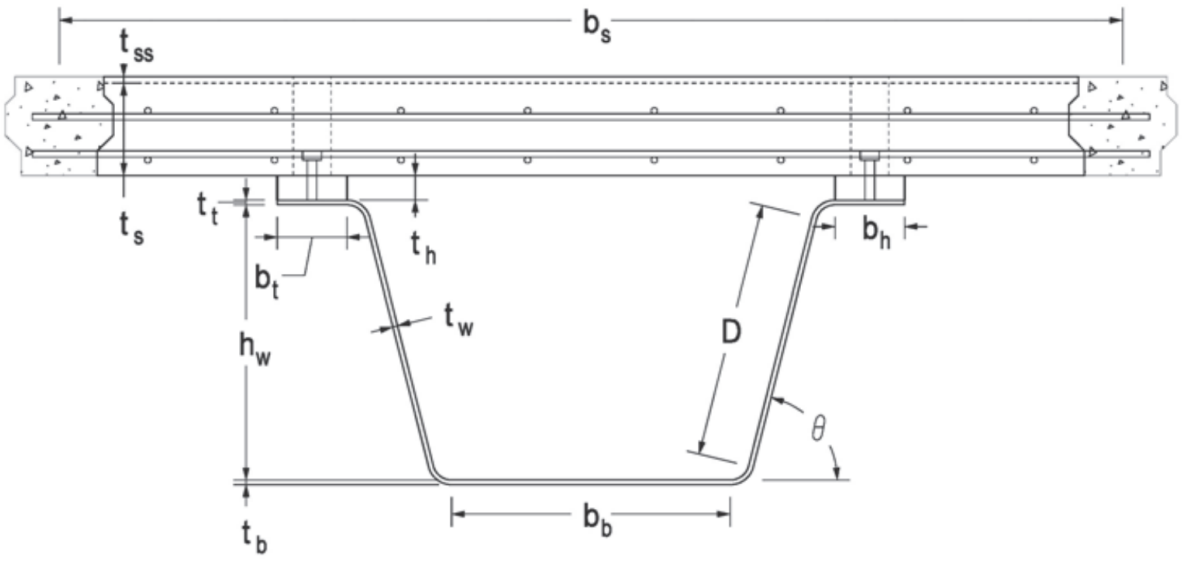

Figure 7.7 Typical Valmont's UBEAM cross-section

For this set of design evaluations, the following permanent and transient loads are used for evaluation:

- DC is the dead load of structural components and nonstructural attachments
    - Divided into two components: DC1, which is typically applied to the noncomposite section, and DC2, which is applied to the composite section
        - Note that since the concrete deck is cast in a shored manner, the DC1 loads are also applied to the long-term composite section.
- DW is a dead load of wearing surface and utilities
- IM is the vehicular dynamic load allowance
    - Serves to amplify the vehicular components of the HL-93 live load (i.e., the truck and tandem)
    - For the fatigue limit state, IM = 15% (AASHTO Table 3.6.2.1-1)
    - For all other limit states, IM = 33% (AASHTO Table 3.6.2.1-1)
- LL is the vehicular live load
    - The HL-93 vehicular live load is defined in AASHTO Article 3.6.1.2
        - Vehicular live loading on the roadways of bridges shall consist of a combination of the Design Truck + Design Lane Load -OR- Design Tandem + Design Lane Load
    - Note that the fatigue load shall be one design truck or axles but with a constant spacing of 30.0 feet between the 32.0 kip axles (AASHTO Article 3.6.1.4.1)

The following loads were taken for all calculations in this design evaluation:

- Unit weight of concrete (γc) = 0.150 kcf

- Compressive strength of concrete (f'c) = 4.0 ksi
- Modular ratio of normal weight concrete (n = 8) (AASHTO Article C6.10.1.1.1b)
- These values correspond to normal-weight concrete.
- Unit weight of steel (γ_s) =0.490 kcf
- Future wearing surface = 0.060 ksf
- Weight of a Jersey-Style Barrier = 0.304 kip/ft

DC1 loads were assumed to consist of the self-weight of the girder and the concrete deck. DC2 loads were assumed to be the guardrail system's weight, equally distributed to all girders. The DW loads, or loads of the future wearing surface, were assumed to consist of a 60 psf load applied over the clear roadway width, which varied depending on the guardrail system used.

DC1 loads are typically applied to the noncomposite section because the steel girder usually needs to resist this during erection and concrete pouring. For this feasibility assessment, it is assumed that the concrete deck is poured while the girder is completely supported in the manufacturing process, so all dead loads, including DC1, DC2, and DW loads, are applied to the long-term composite section for stress calculations. The LLDFs were computed using both AASHTO provisions and the proposed prediction equations. Eq. 7 – 4 represents the fatigue live load distribution factor.

AASHTO Fatigue Live Load Distribution Factor:

$$\mathrm{DF_{Fat}} = \frac{\mathrm{DF_{LL}}}{\mathrm{m}} \qquad (\mathrm{Eq.}\ 7-4)$$

When the proposed equations are used, the maximum feasible span length was found to be controlled by the Service I maximum live load deflection limit. However, the limit state associated

with the L/800 live load deflection limit may be overly conservative. In previous work performed by the authors (Wu, 2003), it is shown that this optional deflection limit, as provided in AASHTO, may be better characterized by the bridge's first fundamental frequency as provided for in codes such as the Canadian CSA S6-14 Canadian Highway Bridge Design Code. This specification, which is permissible to use as a substitute for the optional live load deflection limit, uses a relationship between natural frequency and maximum superstructure static deflection to evaluate the acceptability of a bridge design for the anticipated degree of pedestrian use (Ministry of Transportation, 1991; CSA International, 2000). The superstructure deflection limitations are based on the human perception of vibration. This relationship was developed from extensive field data collection and analytical models conducted by Wright and Green in 1964 (Wright & Green, 1964). For highway bridges, acceleration limits were converted to equivalent static deflection limits to simplify the design process.

Figure 7.8 and Figure 7.9 shows the extended span length applicability of U-beams. The light shade of gray is the expanded applicability of each type of U-beam, whereas the dark shade of gray shows the expanded applicability that can be generated by employing the proposed equations.

	Span Length										
Spacing	40	45	50	55	60	65	70	75	80	85	90
4' - 6"	U12	U18	U18	U24	U24	U30	U30	U33			
5' - 0"	U12	U18	U18	U24	U24	U30	U30	U33			
5' - 6"	U12	U18	U18	U24	U24	U30	U30	U33			
6' - 0"	U12	U18	U18	U24	U24	U30	U30	U33			
6' - 6"	U12	U18	U18	U24	U24	U30	U30	U33			
7' - 0"	U12	U18	U18	U24	U24	U30	U30	U33			
7' - 6"	U12	U18	U18	U24	U24	U30	U30	U33			
8' - 0"	U12	U18	U18	U24	U24	U30	U30	U33			

	Span Length										
Spacing	40	45	50	55	60	65	70	75	80	85	90
4' - 6"	U12	U12	U12	U18	U18	U24	U24	U30	U30	U33	U33
5' - 0"	U12	U12	U18	U18	U18	U24	U24	U30	U30	U33	U33
5' - 6"	U12	U12	U18	U18	U18	U24	U24	U30	U30	U33	
6' - 0"	U12	U12	U18	U18	U24	U24	U30	U30	U33		
6' - 6"	U12	U12	U18	U18	U24	U24	U30	U30	U33		
7' - 0"	U12	U12	U18	U18	U24	U24	U30	U30	U33		
7' - 6"	U12	U12	U18	U18	U24	U24	U30	U30	U33		
8' - 0"	U12	U18	U18	U24	U24	U30	U30	U33	U33		

Figure 7.8 Maximum span length applicability of Valmont UBEAMs™ for 0-degree skew

Spacing	Span Length										
	40	45	50	55	60	65	70	75	80	85	90
4' - 6"	U12	U18	U18	U18	U24	U30	U30	U33	U33		
5' - 0"	U12	U18	U18	U18	U24	U30	U30	U33	U33		
5' - 6"	U12	U18	U18	U18	U24	U30	U30	U33			
6' - 0"	U12	U18	U18	U18	U24	U30	U30	U33			
6' - 6"	U12	U18	U18	U18	U24	U30	U30	U33			
7' - 0"	U12	U18	U18	U18	U24	U30	U30	U33			
7' - 6"	U12	U12	U18	U18	U24	U30	U30	U33			
8' - 0"	U12	U12	U18	U24	U24	U30	U30	U33			

Spacing	Span Length										
	40	45	50	55	60	65	70	75	80	85	90
4' - 6"	U12	U12	U12	U18	U18	U24	U24	U30	U30	U33	U33
5' - 0"	U12	U12	U18	U18	U18	U24	U24	U30	U30	U33	U33
5' - 6"	U12	U12	U18	U18	U18	U24	U24	U30	U30	U33	
6' - 0"	U12	U12	U18	U18	U24	U24	U30	U30	U33		
6' - 6"	U12	U12	U18	U18	U24	U24	U30	U30	U33		
7' - 0"	U12	U12	U18	U18	U24	U24	U30	U30	U33		
7' - 6"	U12	U12	U18	U18	U24	U24	U30	U30	U33		
8' - 0"	U12	U18	U18	U18	U24	U24	U30	U30	U33		

Figure 7.9 Maximum span length applicability of Valmont UBEAMs™ for 30-degree skew

7.4 SUMMARY

This chapter provides a comparison of the proposed equations to the current AASHTO LRFD BDS equation and a validity assessment of the proposed LLDF equations for commercially available PBFTGs. It also discusses expanding the applicability of PBFTGs through extension of the span length.

CHAPTER 8: CONCLUDING REMARKS

8.1 PROJECT SUMMARY

The project focuses on refining design and analysis methods for PBFTGs, a type of short-span steel bridge. These girders are recognized for their efficiency and versatility and have been endorsed by the AASHTO Innovation Initiative as a key technology. The study aims to improve the prediction of the LLDF by using three-dimensional finite element analysis of an extensive matrix of PBFTG bridges. This involves the creation of more accurate empirical equations for LLDF and validating them through statistical methods. The project also compares these new equations with the existing AASHTO LRFD BDS provisions. The project is organized into chapters covering a literature review, AASHTO LRFD BDS summary, analytical modeling techniques, development and statistical assessment of LLDFs for various PBFTG bridge configurations, and a comparison with current standards. The final chapter summarizes the project and suggests directions for future research.

8.2 CONCLUSION

This study proposes moment LLDFs for use in PBFTG bridges. The comprehensive evaluation of the predictive accuracy of the proposed equations demonstrated the significantly higher predictive accuracy of the proposed equations in comparison to the current AASHTO prediction equations. These proposed equations could simplify the design process for bridge engineers using PBFTGs with line girder analysis. The current AASHTO LRFD BDS provisions for multiple box sections are conservative and highly restrictive when applied to PBFTGs. The limitation on adjacent flange spacing on the current equation is expanded to range from 12.5 to 157 percent. Meanwhile, the lower bound for the applicability that was presented in Eq. 2 is lowered to 0.25. The proposed equations have a range of applicability presented in Eq. 8.1 through 8.6.

$$\mathbf{5}\ ft \leq S \leq \mathbf{9}\ ft \qquad (Eq. 8-1)$$

$$\mathbf{20}\ ft \leq L \leq \mathbf{90}\ ft \qquad (Eq. 8-2)$$

$$\mathbf{8}\ in \leq t_S \leq \mathbf{9.5}\ in \qquad (Eq. 8-3)$$

$$\mathbf{4} \leq N_b \leq \mathbf{8} \qquad (Eq. 8-4)$$

$$\mathbf{70574.4}\ \boldsymbol{in^4} \leq \boldsymbol{k_g} \leq \mathbf{478534.6}\boldsymbol{in^4} \qquad (Eq. 8-5)$$

$$\mathbf{0}\ \boldsymbol{in} \leq \mathrm{d_e} \leq \mathbf{424}\ \boldsymbol{in} \qquad (Eq. 8-6)$$

$$\mathbf{0}^{\boldsymbol{o}} \leq \theta \leq \mathbf{30}^{\boldsymbol{o}} \qquad (Eq. 8-7)$$

Besides a higher accuracy and precision in predicting LLDFs, the proposed equations have a known statistical certainty, unlike the AASHTO LRFS BDS equation. Specifically, the proposed equation was estimated based on a 95% PI (and approximately 98% CI). Therefore, it is expected that given enough samples, future LLDF for bridges that have characteristics within the range of the characteristics of the bridge sample used for this analysis will be accurately estimated or overestimated 95% of the time with the proposed equations (with a 98% or higher probability that the predicted LLDF will overestimate the actual LLDF obtained using FEA for the average LLDF). Additionally, the implication of the proposed empirical equations and their goodness-of-fit, as well as predictive accuracy, have been assessed through statistical comparison to other commercially available shallow tub girder systems. A feasibility assessment and the impacts of adopting the proposed equations to AASHTO LRFD BDS have also been discussed. The comprehensive evaluation of the predictive accuracy of the proposed equations demonstrated the significantly higher predictive accuracy of the proposed equations in comparison to the current AASHTO prediction equations. Further, the results provided strong evidence suggesting that the proposed equations are transferable and generalizable and can accurately provide a conservative prediction of LLDF for bridges outside of the dataset used to develop them.

The proposed empirical equations offer a simplified design process for bridge engineers utilizing shallow steel tub girders and have the potential to significantly increase the span length applicability for these types of girder systems.

8.3 Continued Research and Recommendations

The author recommends the following tasks for future work and expansions to this project:

- Investigate other parameters to determine the effect on live load distribution in PBFTG bridges, specifically for bridges with skew index greater than 0.3 and those utilizing cross frame.

- Perform field testing of PBFTG bridges to determine shear stress and live load deflection characteristics.
- Perform sensitivity and parametric studies to determine the effects of key bridge and girder parameters on shear live load distribution in PBFTG bridges.
- Expand the efforts in this study to large, welded tub girder bridges and modify and validate the current equation for better statistical accuracy.

REFERENCES

American Association of State Highway and Transportation Officials. AASHTO LRFD Bridge Design Specifications, Ninth Edition. AASHTO, 2020.

Barth, K. E. "Moment-Rotation Characteristics for Inelastic Design of Steel Bridge Beams and Girders." Doctoral Dissertation, Purdue University, 1996.

Dassault Systèmes. Abaqus/CAE Version 6.14. Dassault Systèmes Simulia Corp., 2020.

Gibbs, C. L. "Field Performance Assessment of Press-Brake-Formed Steel Tub Girder Superstructures." Master's Thesis, West Virginia University, 2017. ProQuest.

Johnston, S. B., and A. H. Mattock. "Lateral Distribution of Load in Composite Box Girder Bridges." Highway Research Record: Bridges and Structures, no. 167, 1967, pp. 25-33.

Kelly, L. T. "Experimental Evaluation of Non-Composite Shallow Press-Brake-Formed Steel Tub Girders." Master's Thesis, West Virginia University, 2014. ProQuest.

Kozhokin, P. "Evaluation of Modular Press-Brake-Formed Tub Girders with UHPC Joints." Master's Thesis, West Virginia University, 2016. ProQuest.

The Mathworks, Inc. MATLAB. The Mathworks, Inc., 2021.

Michaelson, G. K. "Development and Feasibility Assessment of Shallow Press-Brake-Formed Steel Tub Girders for Short-Span Bridge Applications." Doctoral Dissertation, West Virginia University, 2014. ProQuest.

Michaelson, G. K. "Live Load Distribution Factors for Exterior Girders in Steel I-Girder Bridges." Master's Thesis, West Virginia University, 2010. ProQuest.

Nowak, A. S., J. Eom, and D. Ferrand. "Verification of Girder Distribution Factors for Continuous Steel Girder Bridges." Report No. RC-1429, Michigan Department of Transportation, 2003.

Razzaq, M. K. "Load Distribution Factors for Skewed Composite Steel I-Girder Bridges." Doctoral Dissertation, University of Windsor, 2017. ProQuest.

Righman, J. “Rotation Compatibility Approach to Moment Redistribution for Design and Rating of Steel I-Girders.” Doctoral Dissertation, West Virginia University, 2005. ProQuest.

Roberts, N. “Evaluation of the Ductility of Composite Steel I-Girders in Positive Bending.” Master’s Thesis, West Virginia University, 2005. ProQuest.

Roh, A. D. “Field Evaluation of a Modular Press-Brake-Formed Steel Tub Girder in an Application That Includes Skew and Superelevation.” Master’s Thesis, West Virginia University, 2020. ProQuest.

Tarhini, K. M., and G. R. Frederick. “Wheel Load Distribution in I-Girder Highway Bridges.” Journal of Structural Engineering, vol. 118, no. 5, 1992, pp. 1285-1294.

Tennant, R. M. “Fatigue Performance of Uncoated and Galvanized Composite Press-Brake-Formed Tub Girders.” Master’s Thesis, West Virginia University, 2018. ProQuest.

Underwood, N. M. H. “Field Performance and Rating Evaluation of a Modular Press-Brake-Formed Steel Tub Girder with a Steel Sandwich Plate Deck.” Master’s Thesis, West Virginia University, 2019. ProQuest.

Wetshoreck, F. “RIP Correlation: Introducing the Predictive Power Score.” Towards Data Science, 2020.

White, D. W., and A. Kamath. “Straight Steel I-Girder Bridges with Skew Index Approaching 0.3.” Report No. FDOT BE535, Florida Department of Transportation, 2020.

Wu, H. “Influence of Live-Load Deflections on Superstructure Performance of Slab on Steel Stringer Bridges.” Doctoral Dissertation, West Virginia University, 2003. ProQuest.

Yang, L. “Evaluation of Moment Redistribution for Hybrid HPS 70W Bridge Girders.” Master’s Thesis, West Virginia University, 2004. ProQuest.

Zokaie, T., T. A. Osterkamp, and R. A. Imbsen. “Distribution of Wheel Loads on Highway Bridges.” National Cooperative Highway Research Program